

**Protein Separation with Self-Assembled Nanoparticle Beds: Mechanism
and Separation Performance**

by

Mohammad Alaul Azim

A thesis submitted in partial fulfillment of the requirements for the degree of

Doctor of Philosophy

Department of Chemistry

University of Alberta

© Mohammad Alaul Azim, 2016

Abstract

This thesis reports the separation behavior of SDS-protein complexes in colloidal self-assembled (CSA) nanoparticle beds, and the processes of stabilization of CSA beds for high voltage separation. First, the variation of electrophoretic mobility with molecular weight (6.5-66 kDa) of SDS-protein complexes and with particle size (150-690 nm) was evaluated using a classical, modified Ogston sieving model for protein separation for a random pore gel structure, and using the modified Giddings analysis developed by Wirth for uniform pores structure. The results show improved fits ($R^2 = 0.993-0.997$) and better predictive interpolations of the molecular weight on unknowns using the Wirth/Giddings model for a uniform pore structure. The quality of fit of the single pore size model indicates that it is meaningful to characterize these structures as having a predominantly single pore size. A CSA bed of native silica nanoparticles is not stable for high voltage application. Two different approaches have been demonstrated to stabilize the CSA beds in this work. By reducing the depth of the CSA beds by half or more, three to four times the electric field stability (from ≤ 320 V/cm for 20 μm thick bed to ~ 2250 V/cm for 4 μm thick bed) is achieved. Narrowing the capillary bore greatly stabilized the particle beds, even for smaller particle assemblies. The improved separation performance of narrow bore capillaries increases the particle bed performance in protein separation. But unfortunately the narrow bore chips are still not stable for long term repetitive use. These kind of chips are suitable for up to 5-6 runs at highest stable voltage. Base catalyzed sol-gel polymerization introduces cross links between the particles to entrap them, and solves the

problem. But the acid catalyzed gel filled the pores and made the microchip unusable. The CSA bed entrapped by gel can be used for at least a week (10-15 runs /day) and the reproducibility of fabrication is high (yield = 85-90%). This study demonstrates that gel entrapped particles bed can be used for high performance SDS-protein separation up to several days without significant deviation of chip performance. The results demonstrate that this simple and inexpensive fabrication process for microchips with a CSA bed has high potential in improving protein analysis, compared to competing technologies such as conventional gels.

Preface

This thesis is an original work by Mohammad Alaul Azim. I was responsible for all of the works presented in this thesis. Parts of Chapter 2 and 5 of this thesis have been published as “Colloidal self-assembled nanoparticles sieves with orthosilicate cross linking for protein separation in microchips and retardation coefficient for on chip protein sizing”, Mohammad Azim, Abebaw B. Jemere and D. Jed Harrison, 18th International Conference on Miniaturized Systems for Chemistry and Life Sciences (MicroTAS 2014); October 26-30, San Antonio, USA; 2387-2389. Parts of Chapter 3 and 4 have been published as “Highly Stabilized Colloidal Self Assembled Nanoparticle bed in Micro-channels for High Performance Size-Based Protein Separation” Mohammad Azim, Abebaw B. Jemere and D. Jed Harrison, The 19th International Conference on Miniaturized Systems for Chemistry and Life Sciences (MicroTAS -2015) October 25-29, 2015, Gyeongju, South Korea; 1978-1980. In both of the publications, I was responsible for instrument set up, sample preparation, data collection and analysis as well as manuscript composition. Abebaw B. Jemere and D. Jed Harrison were the supervisory authors and involved with concept formation and manuscript composition.

Evaluation of Protein Separation Mechanism and Pore Size Distribution in Colloidal Self-Assembled Nanoparticle Sieves for On-Chip Protein Sizing, Mohammad Azim, Ali Malekpourkoupaei, Wenmin Ye, Abebaw B. Jemere and D. Jed Harrison; Submitted in Electrophoresis Journal. This publication is mainly from Chapter 2 of this thesis except for the pore size distribution studies, which was done by Ali Malekpourkoupaei and Wenmin Ye.

Acknowledgements

It is very difficult to fully express my sincere gratitude to all the people who supported me over the years of my PhD studies. Their support and help made this journey amazing and unforgettable in the new environment and culture.

Foremost, I would like to express my deepest sense of gratitude and indebtedness to my supervisor Professor D. Jed Harrison for allowing me to work in his group. Without his enthusiastic encouragement, supervision, scholastic guidance, invaluable suggestions and constant help, it would not be possible for me to finish this research. I am also very thankful to him for his patient support and time, during writing and correcting the thesis. I am also grateful to him for supporting me in different conferences and helping me to determining the next step of my life.

Besides my supervisor, I would like to express my gratitude to my supervisory committee members Prof. Charles Lucy and Prof. Glen Loppnow for their valuable suggestions and insightful questions during my research. I am also grateful to Prof. Mark McDermott and Prof. Alok Kumar for attending my candidacy exam and providing valuable suggestions. Special thanks to Dr. Jemere Abebaw for his encouragement, constant help and support throughout my PhD journey. I also want to acknowledge the help and support that I have received from Mr. Gareth Lambkin of Biological service lab, Nathan of EAS SEM lab, staffs from general office, machine shop, electronic shop, IT shop and Nanofab, without which my doctoral research would not have been completed smoothly.

I would like to thank Natural Sciences and Engineering Research Council (NSERC), and National Institute for Nanotechnology (NINT), Canada for funding the research, University of Alberta for funding Nanofab and Department of Chemistry for funding me. My sincere gratitude to all members of Harrison group for their help, encouragement, and thoughtful discussion during our group meetings which made my study in Alberta easier and interesting. I would like to thanks Dr. Wenmin Ye, Dr. Yongxin Zhao, Dr. Hamid Ramezani, Dr. Huiying Sheng, Dr. Chan Peng, Dr. Amr Mahmum Mohamed, Dr. Donghi Lin, Ali Malekpourkoupaei, Narges Shaabani, Yufeng Zhao, Ya Zhou, Jing Ji, Md. Minhazul Islma, Yuting Hou. I should specially mention Dr. Reshma Singh and Le Zhang, you guys are more than my group mates and are awesome.

Special thanks to my friends AKM Shahidullah, Dr. Mirza Galib, Dr. Rafiqul Islam Molla, Dr. Shafiul Azam, Dr. Delwar Sikder, Dr. Ehsanul Hoque, Dr. Abu Kausar, Dr. Hosney Mobarak, Dr. Ibrahim Al Rafia, Arif Rabbani, Shafiqul Islam, Swapan Ray, KM Shamsud Doha, Amirul Islam, Amran Howlader, Shahidul Islam and many more that I have met over the years, you guys made my life colorful and enjoyable.

No words can fully express my appreciation to my parents for their love and constant encouragement. Finally, my special thanks to my beloved wife, Bithi Scholastica Palma, my daughter, Shompriti Azim and son, Shureed Azim for their understanding, support trust and love which give me confidence in my research.

Table of Contents

Chapter 1: Introduction

1.1	Background and Motivation.....	1
1.1.1	Advancement of micro total analytical system.....	1
1.1.2	Recent trends in microchip protein separation.....	3
1.1.3	Scope and motivation.....	7
1.2	Fundamentals of electrophoresis.....	8
1.2.1	Electrophoresis.....	8
1.2.1.1	Electrophoretic mobility.....	8
1.2.1.2	Electroosmosis and origin of electroosmotic flow.....	10
1.2.2	Why capillary electrophoresis is important?.....	14
1.3	Size-based separation of proteins.....	16
1.4	Protein surfactants interaction.....	17
1.5	Radius of gyration, R_g and radius of Hydration, R_h	20
1.6	Separation matrices.....	22
1.6.1	Polymer matrix.....	22
1.6.2	Micro fabricated array.....	24
1.6.3	Colloidal self-assembly of nanoparticle	25
1.7	Sieving mechanism.....	27
1.7.1	Ogston regime.....	27
1.7.2	Reptation regime.....	30
1.8	Sieving through uniform pore structure.....	31
1.9	Outline of thesis.....	34

Chapter 2: Protein Separation Mechanism through Colloidal Self Assembled Nanoparticle Sieves in Microchips and Retardation Coefficient for on Chip Protein Sizing

2.1	Introduction.....	36
2.2	Materials and Methods.....	39
	2.2.1 Protein samples and chemicals.....	39
	2.2.2 Microchip fabrication and colloidal self-assembly.....	40
	2.2.3 Instrumentation	42
	2.2.4 Voltage orientation and separation.....	44
2.3	Results and discussion.....	48
	2.3.1 Packing study.....	48
	2.3.2 Optimization of separation voltage.....	52
	2.3.3 Separation performance of different particle beds.....	56
	2.3.4 Comparing separation models for CSA bed of nanoparticles.....	58
	2.3.4.1 The modified Ogston Morris Rodbard Chrambach (OMRC) equation for gel electrophoresis.....	58
	2.3.4.2 Retardation coefficient and protein sizing by Ferguson analysis.....	61
	2.3.4.3 Sieving through uniform pore structure: Giddings model.....	64
	2.3.4.4 Retardation coefficient and protein sizing using Giddings analysis.....	67
	2.3.5 Protein sizing using the retardation coefficient.....	69
2.4	Conclusions.....	72

Chapter 3: Fabrication of Highly Stabilized Colloidal Self-Assembled Nanoparticle Beds in Microchannels for High Performance Size-Based Protein Separations

3.1	Introduction.....	73
3.2	Theory of defect formation.....	75
3.3	Materials and methods.....	80
3.3.1	Protein samples and chemicals.....	80
3.3.2	Microchip fabrications and colloidal self-assembly.....	81
3.3.3	Instrumentation and separation.....	83
3.4	Results and discussions.....	84
3.4.1	Importance and effect of higher voltage separation.....	84
3.4.2	Heating of colloidal self-assembled bed.....	87
3.4.3	Defects in CSA beds.....	89
3.4.4	Global orientation order parameter	91
3.4.5	Crystal growth studies for narrow bore capillaries.....	93
3.4.6	Rational for increased stability.....	97
3.4.7	High performance protein separation.....	101
3.5	Conclusions.....	105

Chapter 4: Evaluation of SDS-Protein Separation Performance of Colloidal Self Assembled Nanoparticle Bed in Narrow Bore Capillaries

4.1	Introduction.....	106
4.2	Materials and methods.....	108
4.2.1	Protein samples and chemicals.....	108
4.2.2	Microchip fabrications and colloidal self-assembly.....	108
4.2.3	Instrumentation and separation.....	109
4.3	Results and discussion.....	110

4.3.1	Separation performance of 300 nm particle bed.....	110
4.3.2	Separation of SDS-protein complexes.....	115
4.3.3	Separation using smaller particle bed.....	117
4.3.4	Separation mechanism of 100 nm particle size CSA bed.....	123
4.3.5	Mass resolution for smaller particle bed.....	126
4.4	Conclusions.....	130

Chapter 5: Ortho Silicate Cross Linking (Sol-Gel) between the Particles of CSA Bed for Highly Stabilized Bed

5.1	Introduction.....	131
5.2	Sol Gel chemistry.....	133
5.3	Materials and methods.....	136
5.3.1	Protein samples and chemicals.....	136
5.3.2	Microchip fabrications and colloidal self-assembly.....	136
5.3.3	Gel formation inside the packed bed.....	137
5.3.4	Instrumentation and separation.....	138
5.4	Results and discussion.....	139
5.4.1	Conditioning CSA bed.....	139
5.4.2	Effect of catalyst on orthosilicate cross linking.....	141
5.4.3	Separation performance of 300 nm particle bed with base catalyzed gel.....	143
5.4.4	Stability and reproducibility	146
5.5	Conclusions.....	147

Chapter 6: Conclusions and Future work

6.1	Conclusions.....	149
6.2	Future work.....	153
	References	155

List of Tables

Table 1-1	Hydrodynamic radius and radius of gyration of proteins studied.....	21
Table 2-1	Separation performances of a 150 nm particle bed in microchip.....	53
Table 2-2	Free solution mobilities using capillary electrophoresis.....	63
Table 2-3	Retardation coefficient of α -lactalbumin and carbonic anhydrase.....	71
Table 2-4	Comparison of estimated molecular weight with supplier molecular weight	71
Table 3-1	Stability of different particle bed of 20 μ m thickness	87
Table 3-2	The global orientation parameter values of different thickness colloidal self-assembled bed.....	93
Table 3-3	The voltage stability of nanoparticles bed	100
Table 3-4	Resolution between the peaks at different separation voltages at 5 mm separation distances.....	103
Table 4-1	Peak Resolution at different separation distances, at 650 V/cm field strength.....	116
Table 4-2	Separation performance using 100 nm silica particles 10 μ m thick beds at different field strengths for 8 mm separation distance.....	117
Table 4-3	Resolution of separation using different particle bed at 200 V/cm separation voltage and 8 mm detection length.....	119
Table 4-4	Mass resolving capacity of different separation matrix in microchip....	129
Table 5-1	Resolution between different proteins and plates numbers at different separation voltage	145

List of Figures

Figure 1-1: a) High throughput Western blot microchip for simultaneously perform 48 blots in triplicate with 144 microchannels (reprinted with permission from reference 47. Copyright © by the National Academy of Sciences 109, 2012). b) Microfluidic native Western blotting device (reprinted with permission from reference 48. Copyright © 2011 American Chemical Society c) Micro chamber based Western blotting device (reprinted with permission from reference 49. Copyright © 2013 American Chemical Society).....	5
Figure 1-2: a) Photograph of nanowires embedded in microchannel; b) SEM image of nanowires embedded in microchannels; and c) SEM image of nanowire structures (reprinted from reference 50. Copyright © 2015, Nature Publishing Group).....	6
Figure 1-3: A schematic diagram of electrical double layer at a charge surface.....	12
Figure 1-4: Velocity profiles of flow in capillary from hydrodynamic flow and electroosmotic flow and their corresponding solute zone.....	13
Figure 1-5: Schematic representation of different SDS-protein complex models (reproduced with permission from reference 59. Copyright © 1990 Elsevier B.V.....	18
Figure 1-6: Two possible “necklace and bead structures” of protein-surfactant complexes: (a) the protein wraps around the micelles, and (b) the micelles nucleate on the protein hydrophobic sites (reproduced with permission from reference 60. Copyright © 1995 American Chemical Society).....	19
Figure 1-7: An SEM image of polyacrylamide gel (reprinted from reference 72 with permission. Copyright © 2006, Royal Society of Chemistry).....	23
Figure 1-8: A &B) Images of micro fabricated arrays of nanopillars (with permission from reference 20. Copyright © 2004 American Chemical Society) and C) Images of micro fabricated array using glancing angle deposition (with permission from reference 84. Copyright © 2011, Royal Society of Chemistry).....	24

Figure 1-9: (A) An SEM image of colloidal self-assembly of 2- μm polystyrene particles fabricated within a microchannel. The arrows indicate lattice defects. The scale bar is 10 μm (with permission from reference 14. Copyright © 2004 American Chemical Society) (B) schematic view of pores in a CSA bed.....25

Figure 1-10: A schematic of colloidal crystal formation inside the microchannel.....26

Figure 1-11: Three regimes of gel electrophoresis.....28

Figure 1-12: Schematic representation of the relationship between the logarithmic electrophoretic mobility and the molecular weight (with permission from reference 76. Copyright © 1996 WILEY-VCH Verlag GmbH & Co. KGaA, Weinheim)31

Figure 1-13: Reduced mobility behavior of a spherical analyte of radius R; through different types of pores. (With permission from reference 88. Copyright © 1968, American Chemical Society).....32

Figure 2-1: View of a microchip. 1, 2 3 & 4 are reservoirs. The distance between reservoirs 1 to 4 is about 15 mm. This channel acts as separation column. The distance between reservoir 2 to separation column and reservoir 3 to separation column is about 3 mm. These channels are used for injection. The offset of the two injection channels in the separation column is about 100 μm . The diameter of all reservoirs is 2 mm and the thickness of the PDMS is about 3 mm.....41

Figure 2-2: Mechanism of CSA formation: (A) First a uniform colloidal bead suspension was injected into one of reservoir. All the channels were flooded with solvent. Then the colloidal solution was injected into the two other reservoirs. The fourth reservoir was left empty. (B) The reservoirs containing the colloidal solution of beads were covered to prevent evaporation, and the evaporation of water started from the empty reservoir. (C) The chips were left in a Petri dish to complete the colloidal self-assembled bed formation in the micro channels.....42

Figure 2-3: Confocal epifluorescence apparatus for detection on a microchip43

Figure 2-4: Voltage orientation during injection of sample.....44

Figure 2-5: Voltage orientation during separation of sample.....	45
Figure 2-6: The equivalent circuit for the intersection of four channels.....	47
Figure 2-7: Colloidal self-assembly of nanoparticle bed formation with 150 nm particles. Reservoir 4 was left open for evaporation.	49
Figure 2-8: Colloidal self-assembly of nanoparticle bed formation with 50 nm particles. Reservoir 4 was left open for evaporation.....	49
Figure 2-9: Colloidal self-assembly of nanoparticle bed with 150 nm particles. Reservoir 3 was left open for evaporation. A) In most cases no crack was observed. B) Some cracks are observed in few cases, which did not propagated with time.....	50
Figure 2-10: Colloidal self-assembly of nanoparticle bed when reservoir 3 was left open for evaporation. A) Very little cracking observed for 50 nm particle packing which did not propagated with time B) No crack was observed for 150 nm particle packing even after 10 h of packing.....	51
Figure 2-11: Electropherograms of on chip SDS-protein separation using a 150 nm particle bed at different field strengths and 4 mm of separation distance ($L = 4$ mm) . The peaks of electropherograms are: 1) trypsin inhibitor, 20.1 kDa, 2) ovalbumin, 45 kDa and 3) BSA, 66 kDa.....	54
Figure 2-12: Image of 150 nm particle bed separation channels at (a) 30 V/cm (no crack was observed during separation), and (b) 65 V/cm (particles started to move from the walls of the chip, indicated by blue oval shaped). Both images were taken from the same chip during operation.....	55
Figure 2-13: Mobility vs. applied separation field strength plot of three different proteins; trypsin inhibitor, 20.1 kDa; ovalbumin, 45 kDa and BSA, 66 kDa. Error bars show the standard error (n=3).....	55
Figure 2-14: Electropherogram of four different proteins: 1) aprotinin, 6.5 kDa; 2) trypsin inhibitor, 20.1 kDa; 3) ovalbumin, 45 kDa; and 4) BSA, 66 kDa using different particle	

bed A) 690 nm B) 300 nm and C) 150 nm using 35 V/cm separation voltage for a 4 mm separation distance (L = 4 mm).....	57
Figure 2-15: The log mobility vs. molecular weight of protein plot using different size particle beds (690, 540, 300 and 150 nm). The error bars are the standard errors at the 95% confidence level (n=7).....	60
Figure 2-16: The double logarithmic plot of mobility vs. molecular weight of protein using different particle bed (690, 540, 300, and 150 nm). The error bars are the standard errors at the 95% confidence level (n=7).....	61
Figure 2-17: The plot of logarithmic mobility vs. pore size of the particles for different proteins. (aprotinin, 6.5 kDa; trypsin inhibitor, 20.1 kDa; ovalbumin, 45 kDa; and BSA, 66 kDa). The slope of each curve is the retardation coefficient of each protein. The retardation coefficients are aprotinin, 6.5 kDa, $K_r = 3.87 \times 10^{-4}$; trypsin inhibitor, 20.1 kDa, $K_r = 5.86 \times 10^{-4}$; ovalbumin, 45 kDa, $K_r = 1.06 \times 10^{-3}$; and BSA, 66 kDa, $K_r = 1.53 \times 10^{-3}$ (The error bars are the standard error at 95% confidence level, n=7)...	63
Figure 2-18: A calibration plot between the protein molecular weight and the retardation coefficient using random pore model.....	64
Figure 2-19: A plot of $\sqrt{\mu}$ vs. radius of hydration protein, R_H using different particle beds (The error bars are the standard error at 95% confidence level, n=7).....	66
Figure 2-20: A plot of square root of mobility, $\sqrt{\mu}$ vs. radius of gyration of protein, R_g (The error bars are the standard error at 95% confidence level, n=7).....	66
Figure 2-21: Square root of mobility vs. inverse of pore size of the particle beds plot. The slope of the line for each protein is calculated as aprotinin, 6.5 kDa, $= 8.12 \times 10^{-3}$; trypsin inhibitor $= 1.257 \times 10^{-2}$; ovalbumin $= 2.156 \times 10^{-2}$; and BSA $= 2.967 \times 10^{-2}$ (The error bars are the standard error at 95% confidence level, n=7).....	67
Figure 2-22: A calibration plot between protein molecular weight vs. retardation coefficient for CSA particle beds using the Giddings analysis.....	68

Figure 2-23: An electropherogram of 1) α -lactalbumin – 14.2 kDa; and 2) carbonic anhydrase – 29.2 kDa. Using a 150 nm particle bed at 35 V/cm field strength and detected at 4 mm separation distance	69
Figure 2-24: The superimposed electropherogram of α -lactalbumin: 14.2 kDa and carbonic anhydrase: 29.2 kDa (red color) in a previously achieved electropherogram of four protein mixture of : 1) aprotinin, 6.5 kDa, 2) trypsin inhibitor, 20.1 kDa, 3) ovalbumin, 45 kDa and 4) BSA, 66 kDa using 150 nm particle bed at 35 V/cm field strength and detected at 4 mm separation distance	70
Figure 3-1: Construction of Hexagonal Close Packed (HCP) and Face Centered Cubic (FCC) structures.....	79
Figure 3-2: Fabrication of CSA microchip: (A) final view of chip; and (B) mechanism of CSA formation.....	82
Figure 3-3: An electropherogram of the four protein mixture using a 300 nm particle bed at 35 V/cm separation voltage and detection at 5 mm.....	84
Figure 3-4: An electropherogram of the four protein mixture using a 300 nm particle bed at 160 V/cm separation voltage and detection at 4 mm.....	85
Figure 3-5: An electropherogram of four protein mixture using 300 nm particle 20 μ m thick bed at 450 V/cm separation and 5 mm detection.....	86
Figure 3-6: Condition of 300 nm particle packed chip after 3h heat treatment at 60 ^o C (photograph).....	89
Figure 3-7: SEM image of 300 nm silica particle self-assembly. The vacancies are shown in circles and the phase boundary is shown by the oval shape, while the arrows show the interstitial defects.....	90
Figure 3-8: SEM image of colloidal self-assembly of 300 nm silica particle surface A) 10 μ m thick bed; and B) 4 μ m thick bed.....	92

Figure 3-9: Microfluidic monodisperse colloidal crystal (mCC) growth over time for silica particles with different diameter for a 10 μm thick bed.....	94
Figure 3-10: Microfluidic monodisperse colloidal crystal (mCC) growth over time for 300 nm silica particles with different thickness microchannels	96
Figure 3-11: Explanation of particle migration to the void space created due to lattice defect in colloidal self-assembly.....	98
Figure 3-12: Explanation of greater stability in colloidal self-assembly due to wall effect. In the case of a thick bed (A) the wall has less influence on the bed than narrow bed (B).....	99
Figure 3-13: Electropherograms of four protein mixture using 300 nm particle 10 μm thick bed at 5 mm detection (A) at 950 V/cm and (B) 1250 V/cm separation voltage: 1) aprotinin, 6.5 kDa; 2) trypsin inhibitor, 20.1 kDa; 3) ovalbumin, 45 kDa; and 4) BSA, 66 kDa.....	102
Figure 3-14: An electropherogram of four protein mixture using 300 nm particle 4 μm thick bed at 1250 V/cm at 5 mm separation distance: 1) aprotinin, 6.5 kDa, 2) trypsin inhibitor, 20.1 kDa, 3) ovalbumin, 45 kDa; and 4) BSA, 66 kDa.....	103
Figure 3-15: Electropherograms of four protein mixture using 10 μm thick bed at 320 V/cm using a) 150 nm particle and b) 100 nm particle at 8 mm of separation distance.....	104
Figure 4-1: An illustration of the comparative pore size of larger and smaller particle assemblies.....	107
Figure 4-2: Superimposed electropherograms of 1 μM trypsin inhibitor (20.1 kDa) in varying electric fields in running buffer 4xTBE and 0.1% SDS, using 300 nm silica particles with 10 μm depth bed at 5 mm detection.....	110
Figure 4-3: (A) Migration rate of SDS-trypsin inhibitor complexes vs. applied electric field; and B) Plate height vs. migration rate plot.....	112

Figure 4-4: A highly linear relationship was achieved between peak variances vs. migration time plot.....	114
Figure 4-5: Electropherogram of SDS-denatured four-protein mixture at L= 10 mm separation distance and 650 V/cm field [1) aprotinin 6.5 kDa, 2) trypsin inhibitor, 20.1 kDa, 3) ovalbumin, 45 kDa; and 4) BSA, 66 kDa].....	115
Figure 4-6 : Electropherograms of 4 protein mixtures using 100 nm particle 10 μ m thick beds at different separation voltages at 8 mm separation distances, 1) aprotinin, 6.5 kDa, 2) trypsin inhibitor, 20.1 kDa, 3) ovalbumin, 45 kDa; and 4) BSA, 66 kDa.....	118
Figure 4-7: Electropherograms of a protein mixture using different particles bed of 10 μ m thickness at 160 V/cm separation voltage at 8 mm detection length A) 300 nm particle B) 150 nm particle C) 100 nm particle; 1) aprotinin, 6.5 kDa, 2) trypsin inhibitor, 20.1 kDa, 3) ovalbumin, 45 kDa; and 4) BSA, 66 kDa.....	121
Figure 4-8: Superimposed electropherograms of three consecutive separation runs at 160 V/cm using 100 nm particle 10 μ m thick bed.....	122
Figure 4-9: Plots of apparent mobility of SDS-protein complex vs protein molecular weight with least square fit using 100 nm particle at 160 V/cm. The error bars are the standard deviation (n=3) (A) a semi log plot; and (B) a log- log plot.....	124
Figure 4-10: A plot of $\sqrt{\mu}$ vs. radius of hydration protein, R_H using 100 nm particle beds The error bars (smaller than the marker) are the standard deviation (n=3).....	125
Figure 4-11: Electropherogram of two protein separation at 160 V/cm using 100 nm particle 10 μ m thick bed and 10 mm separation distance [1) lysozyme, 14.2 kDa; and 2) trypsin inhibitor, 20.1 kDa]	127
Figure 4-12: Electropherogram of two protein separation at 160 V/cm using 100 nm particle 10 μ m thick bed and 13 mm separation distance [1) lysozyme, 14.2 kDa; and 2) myoglobin, 17.1 kDa]	127

Figure 4-13: Electropherograms of separation at A) 320 V/cm; and B) 160 V/cm using 50 nm particles of 4 μ m thick bed and 5 mm separation distance.....	128
Figure 5-1: Two possible alternative where gel could be formed.....	132
Figure 5-2 : Photograph of chips (a) a good quality packed gel-chip in water after conditioning with alcohol, (b) a packed gel-chip completely dried condition; and (c) a chip without conditioning became dried from the middle	140
Figure 5-3: SEM image of A) base catalyzed gel formation inside the CSA bed of chip (highly magnified image is shown inset); and B) acid catalysed gel block all pores inside the CSA bed of nano particles.....	142
Figure 5-4: Electropherograms of four protein mixture using 300 nm particle bed stabilized with basic gel formation at 4 mm separation distance (A) at 1280 V/cm; and (B) 1600 V/cm separation voltage: 1) aprotinin, 6.5 kDa; 2) trypsin inhibitor, 20.1 kDa; 3) ovalbumin, 45 kDa; and 4: BSA, 66 kDa.....	144
Figure 5-5: A linear relationship between migration rate of SDS-aprotinin complexes vs. applied electric field	145
Figure 5-6: A nonlinear relationship between migration rates of SDS-aprotinin complexes vs. plate height.....	146
Figure 5-7: Superimposed electropherograms of three consecutive separation runs at 1280 V/cm using base catalyzed chip.....	147

List of Symbols

a	exponential power
A	multiple path length term, or eddy diffusion
b	a function of pore size of the matrix
B	longitudinal diffusion term
C	resistance to mass transfer term
c_i	concentrations of the ions in bulk solution, mol/cm ³
c	constant for an electrophoretic system
D	diffusion coefficient
D	diameter/pore size of particles
e	elementary charge
E	applied electric field
ΔE_{act}	activation energy of defect formation.
f	accessible volume fraction
F_{ef}	applied electric force
F_{fr}	frictional force
G_{hcp}	Gibbs free energy for hexagonal close packed crystal
G_{fcc}	Gibbs free energy for face centered cubic crystal
ΔG_{DF}	defect formation free energy for a single defect
H	plate height
ΔH_{DF}	enthalpy term of a defect
I	ionic strength

I_1, I_2, I_3, I_4	current through different channels
k_2	retention factor
k_B	Boltzmann's constant
K_r	retardation coefficient
L	length of column
M	molecular weight of the analyte
ΔM	difference in molecular weight of the proteins
N	number of theoretical plate
N	number of amino acid units in a protein
N_0	self- assembled moieties or features
N_A	Avogadro's number
N_p	total number of nearest neighbour particles
p	mean pore size
q	charge of the species
R	radius of a spherical analyte
r	radius of the gel fiber/ radius of the pore
R_g	radius of gyration
R_h	radius of hydration or hydrodynamic radius
R_1, R_2, R_3, R_4	resistance of different channels
R_s	resolution between those separated proteins.
R_r	resolving power
ΔS_{DF}	entropy difference between perfect and defective structure
t	time of growth

$\% T$	total acrylamide concentration in the gel
T	temperature in Kelvin
U	mobile phase velocity
V	electric field strength
V_j	potential at the double T intersection
V_1, V_2, V_3, V_4	potential of different channels
$w_{0.5}$	full width at half maximum of the peak
Y	growth of colloidal crystal
Z_i	valance of the ions

Greek Symbols

α	selectivity
β	angle between the two nearest neighbour of particles in a structure
γ	obstruction factor
γD	effective molecular diffusion
ϵ_0	permittivity of free space
ϵ	dielectric constant of the electrolyte solution
ϵ	porosity
ζ	zeta potential
η	viscosity of the medium
κ^{-1}	double layer thickness

μ_0	mobility in open solution
μ_{app}	apparent mobility
μ_{ep}	electrophoretic mobility
μ_{EOF}	electroosmotic mobility
v	velocity of the molecules
σ^2	variance
Ψ	global orientation order parameter

Abbreviations

μ -TAS	micro total analysis systems
bCC	binary colloidal crystals
BSA	bovine serum albumin
CGE	capillary gel electrophoresis
CSA	colloidal self-assembly
DMSO	dimethyl sulfoxide
DNA	deoxyribonucleic acid
DTT	dithiothreitol
EDTA	ethylene diamine tetra acetic acid
EOF	electroosmotic flow
FCC	face center cubic
FITC	fluorescein-isothiocyanate
^2H NMR	deuterium nuclear magnetic resonance
HCP	hexagonal closed pack
IHP	inner Helmholtz plane
LOC	lab-on-a-chip
mCC	mono disperse colloidal crystals
MCE	iniaturized capillary electrophoresis or microchip electrophoresis
OHP	outer Helmholtz plane
OMRC	Ogston Morris Rodbard Chrambach

PDMA	poly dimethyl methacrylate
PDMS	poly (dimethylsiloxane)
PEG	poly ethylene glycol
PMT	photo multiplier tube
POC	point of care
RSD	relative standard deviation
SDS	sodium dodecyl sulfate
SDS-CGE	SDS-capillary gel electrophoresis
SDS-PAGE	Sodium dodecyl sulfate-polyacrylamide gel electrophoresis
SEM	scanning electron microscopy
TBE	tris (hydroxymethyl) aminomethane (tris base) -boric acid–EDTA
TEOS	tetraethyl orthosilicate
vdW	Van der Waals
VLS	vapor-liquid-solid

Chapter 1

Introduction

1.1 Background and motivation

1.1.1 Advancement of micro total analytical system

The concept of micro total analysis systems (μ -TAS) or “Lab-on-a-Chip” (LOC) were introduced in 1990 by Manz et al.¹ to integrate all steps of chemical and biochemical analyses, such as sample introduction, sample preparation, sample enrichment, separation and detection on a micro-fabricated chip.^{2,3} The fundamental idea was based on microfluidics, which is the manipulation of small amounts of fluid (10^{-9} to 10^{-18} L) through channels with a diameter ranging from ten to hundreds of micrometres, with smaller channel lengths for shorter transport times. The application of microfluidic technologies offer several advantages over existing technologies: small amounts of sample and reagent are required, high resolution separation and high sensitivity detection is possible, with very short time for analysis, at a relatively low cost.^{4,5} The development of simple micro- and nanoscale fabrication techniques for the design of different functional components of microfluidic systems, along with the development of soft lithography in poly (dimethylsiloxane) (PDMS) for fabricating the prototype devices, are two important contributions for advancement in this area. Together with new fabrication methods, the microfluidics system exploited the fundamental differences of fluid phenomena in large

channels and in microchannels. These studies open windows into new phenomena in fluid physics.⁶ According to George M. Whitesides⁶ “Microfluidics is both a science and technology. It offers great - perhaps even revolutionary - new capabilities for future.” The capabilities and usefulness of microfluidics have already been demonstrated by a variety of theoretical models and academic proof of concept studies, in the separation and analysis of: proteins,⁷⁻¹⁸ DNA,^{7,10,13,14,19-22} drug development and discovery,²³⁻²⁵ analysis and sorting of cells,^{26,27} biomarker discovery,²⁸ development of point of care (POC) diagnostic devices for global health issues;²⁹⁻³³ and environmental monitoring.³⁴ The understanding of different aspects of microfluidics provides a strong foundation for this field, while the application of this technique in a wide range of areas provides the driving force for continued research.

The potential for producing practical devices is the main reason behind the excitement with microfluidics. Despite a lot of advantages, surprisingly few LOC-based diagnostic devices have been commercially introduced into the market.³⁵ Among them, point of care (POC) diagnosis devices have achieved a huge boost. The global market of POC devices is expected to increase from US \$12.91 billion in 2015 to US \$32 billion in 2022.³⁶ Microfluidics is an enabling technology for POC devices. Along with the basic advantages of microfluidics: low power consumption, accurate and precise control of multiple samples; and the ability to conduct high throughput screening of biological species with versatile formats of detection are a main reason behind the boost for POC diagnosis devices. The development of paper-based microfluidics with colorimetric detection has also made microfluidic-based POC diagnosis devices potentially affordable in developing countries.³⁷

Miniaturized capillary electrophoresis or microchip electrophoresis (MCE) is the most developed and characterized implementation of μ TAS devices.² In MCE, the advantages of the μ TAS concept are very evident. With the other benefits of μ TAS, the small volume greatly increases the role of molecular diffusion and improves heat transfer, so microchip electrophoresis devices permit very high voltage application without Joule heating. Due to shorter separation channels the analysis time decreases, and for parallelization, the throughput increases dramatically. Additionally, due to their portability, MCE devices have high potential for point of care diagnostics and even for planetary exploration.³

1.1.2 Recent trends in microchip protein separation

Analysis of proteins provides a path to diagnose diseases, to develop an understanding of the basic principles of how diseases start and propagate, to investigate cellular responses to drugs and to distinguish between normal cells and cancer cells.³⁸ The analysis of proteins has evolved as a very important area of research,³⁹ especially in biological fluids, clinical and pharmaceutical studies⁴⁰ and also in food and agricultural products⁴⁰The s

The separation of proteins is a very important part of their analysis. There are different methods available for separation, with size-based separation using electrophoresis techniques being very quick and easy for estimating the purity, size, quantity and protein integrity. Sodium dodecyl sulfate-polyacrylamide gel electrophoresis (SDS-PAGE) and SDS-capillary gel electrophoresis (SDS-CGE) have been used for size-

based protein separation for a long time. To achieve the advantages of a miniaturized system, and to integrate multiple analytical processes, SDS-PAGE can be adapted into a microchip platform. SDS-PAGE in micro-fabricated channels was first demonstrated by Yao et al.⁴¹ By transferring the separation into a microchip, they accelerated the separation by 20 times and showed improved separation efficiencies. The first integrated micro-fabricated chip for protein separation based on SDS-PAGE was reported by Bousse et al.⁴² They achieved excellent resolution of BioRad protein ladders. The on-chip SDS-PAGE of proteins was also reported by Han et al.¹⁸ and Herr et al.¹⁶ in 2004. They used photolithographically patterned micro-channels and cross-linked gel fabricated in situ. Herr et al.¹⁶ achieved good resolution of SDS protein complexes (14.2-66 kDa) with very high speed (<30 s) in a short column (4 mm). The separation efficiencies were as high as 4.41×10^5 plates/m and ~10 times better than the capillary system. According to their analysis, Ogston-like sieving was the mechanism of protein movement through the gel.

In 2007 Zeng and Harrison¹⁴ reported the colloidal self-assembly (CSA) of silica nanoparticles as three dimensional nanofluidic sieves for SDS-protein separation in a microchip. They used an evaporation induced method for colloidal self-assembly formation inside the microchannels. One of the best advantages of using nanoparticles was that the pore size could easily be engineered by using different size particles. Well-defined and uniform pore matrix fabrication were possible by using monodisperse particles. They reported high-resolution separation of SDS-protein (20.1-116 kDa) using 160 nm silica particles. As the separation was carried out at low field strength (30.9 V/cm), it took more than 16 minutes to complete the separation. The CSA of a native nanoparticle bed was unstable at higher voltage applications.

To perform high voltage separation, the Mary Wirth group⁴³ started to use polymerization techniques inside previously packed particle beds. The polymers inside the particle bed acted as a glue to hold the particles together and the CSA bed was stable up to 2000 V/cm. They used this approach for electro chromatography of native proteins,¹⁵ separation of SDS-protein complexes¹⁷ and separation of SDS-denatured pharmaceutically important antibodies.⁴⁴ Tao Liao et al⁴⁵ reported highly stable one step CSA bed packing in microchannels for amino acid and peptide separation. They used the concept of heating⁴⁶ while packing the particles in the microchannels by simply blowing away the vapor. They achieved CSA beds stable up to 2000 V/cm and 300 nm plate height for separation of FITC.

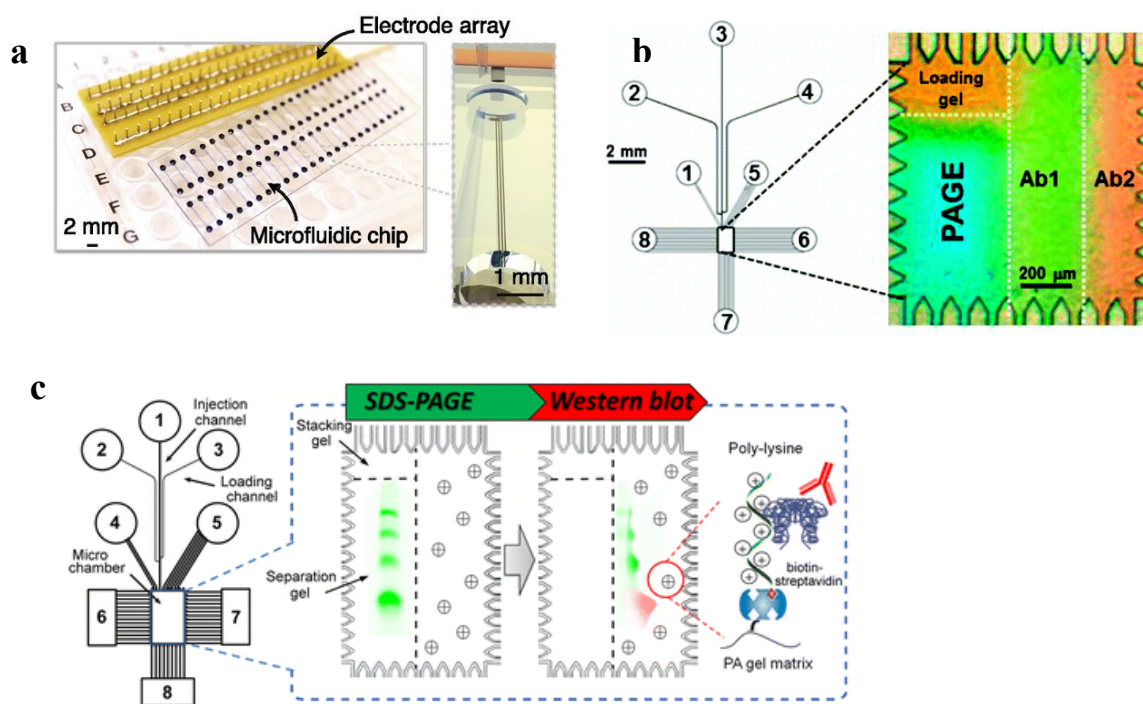


Figure 1-1: *a)* High throughput Western blot microchip for simultaneously perform 48 blots in triplicates with 144 microchannels (reprinted with permission from reference 47. Copyright © by the National Academy of Sciences 109, 2012). *b)* Microfluidic native western blotting device (reprinted with permission from reference 48. Copyright © 2011 American Chemical Society *c)* Micro chamber based Western blotting device (reprinted with permission from reference 49. Copyright © 2013 American Chemical Society).

One of the major improvements in protein separation is the miniaturization of the labour intensive Western blot by the Herr group.⁴⁷ They designed a microchip with 144 microchannels which can perform 48 Western blots simultaneously, in triplicate, within an hour. This technique reduced by 1000 fold both the sample and reagent consumption. Herr's group also demonstrated integrated Western blot in a micro-chamber.^{48,49}

Most recently the Baba⁵⁰ group reported ultrafast (within 5 s) SDS-Protein (20-340 kDa) separation using a three dimensional nanowire structure embedded in a microchannel. They separated proteins within 2 mm distance with 10^6 plates/m, but the resolution of separation was not that good. They used a Au catalyzed, vapor-liquid-solid (VLS) technique, for SnO₂ nanowire growth inside the channels. But the nanowire pore size distribution was large, and also the fabrication process was very complex.

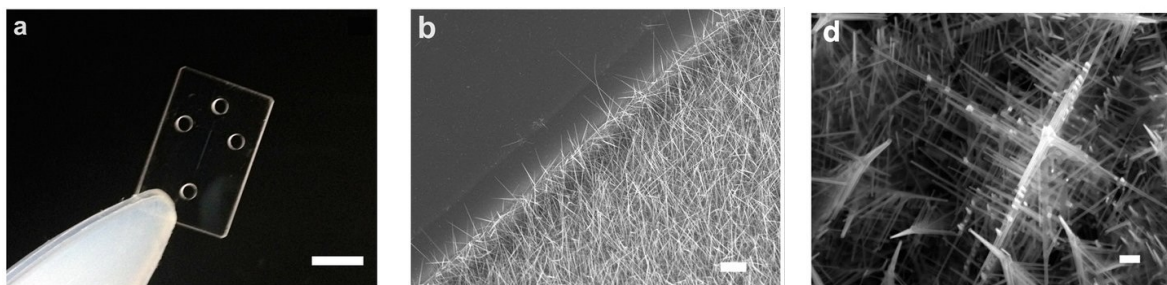


Figure 1-2: *a) Photograph of nanowires embedded in microchannel; b) SEM image of nanowires embedded in microchannels; and c) SEM image of nanowire structures (reprinted from reference 50. Copyright © 2015, Rights Managed by Nature Publishing Group).*

1.1.3 Scope and motivation

Though significant advancement in SDS-protein separation in micro-fabricated chips was achieved during last the decade, there is still room for improvement. Devices so far have been based upon gels with random pore sizes or structures with complex fabrication processes. To develop point of care (POC) diagnostic-based protein or medically important antibody separations, the chip should preferably be low cost, and easy to fabricate and use. A complex design and fabrication of the separation matrix increases the cost of the devices.

For high throughput protein electrophoresis, self-assembled colloidal crystals are termed an emerging material.⁴⁴ The fabrication process of a CSA bed inside microchannels is very easy and time effective. Highly ordered CSA bed formation is possible using mono disperse colloidal crystals (mCC) and binary colloidal crystals (bCC).⁵¹ The pore size of the CSA bed can easily be manipulated using different sizes of colloidal particles. One major drawback of CSA beds for separation is their instability at high voltage. To obtain the benefits of miniaturization, the CSA bed needs to be stable at high voltage. A few processes have already been reported to stabilize the CSA bed.^{15,45,52} But all of the processes add extra steps in the fabrication process and many involve the use of polymers. Moreover, it is very hard to get uniform pore CSA beds with the added formation of polymer coatings inside the pores. The polymers inside the pores also significantly increase chromatographic effects in separation, possibly complicating true electrophoresis. To achieve stability without adding extra steps and not adding characteristics that differ from true electrophoresis is still a goal. In this thesis I demonstrate the stabilization CSA beds of nano particles without adding extra steps in the fabrication process. I have also

evaluated the formation of silica gel inside the pores as a method of stabilization. The stabilization is evaluated by performing separation at high voltage. I have also evaluated the mechanism of protein separation in the pores of a CSA bed.

1.2 Fundamentals of electrophoresis

1.2.1 Electrophoresis

In the area of analytical science, electrophoresis is a very powerful and widely used separation technique for charged species. Electrophoresis is based on the differential mobility of charged species under an electric field. When charged species are placed in a conductive medium or electrolyte and an electric field applied, the charged species migrate. The rate and direction of their migration is dependent on the nature and density of the charge. Based on the relative migration rates, charged species can be separated. This is the basis of electrophoretic separation. There are two forces responsible for electrophoretic motion: i) electrophoretic mobility; and ii) electroosmotic mobility.

1.2.1.1 Electrophoretic mobility

When a charged species is placed into an electric field, the species experiences two kinds of force; i) an applied electric force (F_{ef}); and ii) a frictional force (F_{fr}).

The applied electric force (F_{ef}) depends on the applied electric field (E) and charge of the species (q). The F_{ef} is:

$$F_{ef} = q \times E \quad 1.1$$

If charge, q , is positive, the species moves toward the cathode or negative electrode and for a negative charge, the species migrates toward the anode or positive electrode.

During movement, the charged species is opposed by the frictional force (F_{fr}) from the solvent molecules. If the interaction of other species is negligible, then from Stoke's law the frictional force is:

$$F_{fr} = 6\pi\eta r v \quad 1.2$$

where η is the viscosity of the medium, r is the radius of the species and v is the velocity of the molecules.

At a constant field, an equilibrium is established between the two forces. So, at equilibrium, $F_{ef} = F_{fr}$ and velocity of the molecules become:

$$v = \frac{qE}{6\pi\eta r} \quad 1.3$$

The electrophoretic mobility (μ_{ep}) is the ratio of the migration velocity over the applied electric field. So,

$$\mu_{ep} = \frac{v}{E} = \frac{q}{6\pi\eta r} \quad 1.4$$

For a particular separation medium and temperature, the viscosity is constant. Thus the electrophoretic mobility is proportional to the charge to size ratio.

1.2.1.2 Electroosmosis and origin of electroosmotic flow

In the presence of a charged particle, the free ions of an electrolyte solution polarize in the region surrounding the charged particle. This is happened due to the electrostatic attraction of counter ions, forming an electrical double layer around the charged particles or surface (Figure 1.3). According to the Debye-Huckel equation, the thickness of the electrical double layer is characterized by the Debye length κ^{-1} and calculated by:

$$\kappa^{-1} = \left(\frac{\varepsilon_0 \varepsilon k_B T}{N_A e^2 I} \right)^{1/2} \quad 1.5$$

where ε_0 is the permittivity of free space, ε is the dielectric constant of the electrolyte solution k_B is the Boltzmann's constant, T is the temperature in Kelvin, N_A is the Avogadro's number, e is the elementary charge, and I is the ionic strength which can be calculated by:

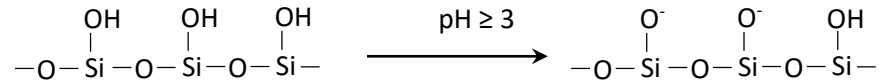
$$I = \frac{1}{2} \sum_{i=1}^n c_i Z_i^2 \quad 1.6$$

where c_i is the concentrations of the ions in bulk solution and Z_i is the valance of the ions.

The double layer can be quite complex in structure and made up of several layers. The first layer closest to the charged surface, contain immobile solvent molecules and sometimes specifically absorbed ions or molecules. This immobile inner layer is called the Helmholtz, compact or Stern layer. The locus of the center of specifically absorbed species is called the Inner Helmholtz plane (IHP), and ions in this layer are not surrounded by a full hydration shell. There is a solvated ion layer next to the IHP. The locus of the layer is called the Outer Helmholtz plane (OHP). Ions in the OHP, while solvated are also taken

to be immobile. Outside the OHP, is a charged region called the diffuse layer. In the diffuse layer, the potential drop is approximately exponential. Somewhere near the outer edge of the OHP, there is a boundary up to which all ions and solvent are immobile which is called the plane of shear. The exact thickness of the shear layer is not defined but is usually thought of as the inner boundary of the diffuse layer. The potential at this plane is called the zeta potential (ζ) and can be measured by electrophoretic potential measurement techniques. In calculations of double layer potentials, the potentials at the inner boundary of the diffuse layer is usually assumed to be the same as the zeta potential.

Double layer formation is observed when an electrolyte solution is placed inside a fused silica capillary. In this case, the surface silanol (-Si-OH) groups are ionized at or above pH 3 to the silonate group (-Si-O⁻). So an electrical double layer is formed on the surface of a negatively charged silonate surface.



When an external electric field is applied, the excess of cations in the diffuse layer are pulled towards the negatively charged cathode. Since the cations are solvated, they drag the bulk solution with them. This movement of bulk solution upon application of external electric field is called electroosmotic flow (EOF). This phenomenon is referred to as electroosmosis or electroendoosmosis in electrophoresis.

The EOF is directly proportional to the dielectric constant, ϵ , and the zeta potential ζ , of the surface, as well as the applied electric field strength, E, and inversely proportional

to the viscosity of the electrolyte or buffer. EOF is calculated by the Von Smoluchowski equation:

$$v_{EOF} = \left(\frac{\epsilon\zeta}{4\pi\eta} \right) \cdot E \quad 1.7$$

where, η is the viscosity of the buffer solution and E is the applied electric field.

The electroosmotic mobility is calculated by:

$$\mu_{EOF} = \frac{v_{EOF}}{E} \quad 1.7a$$

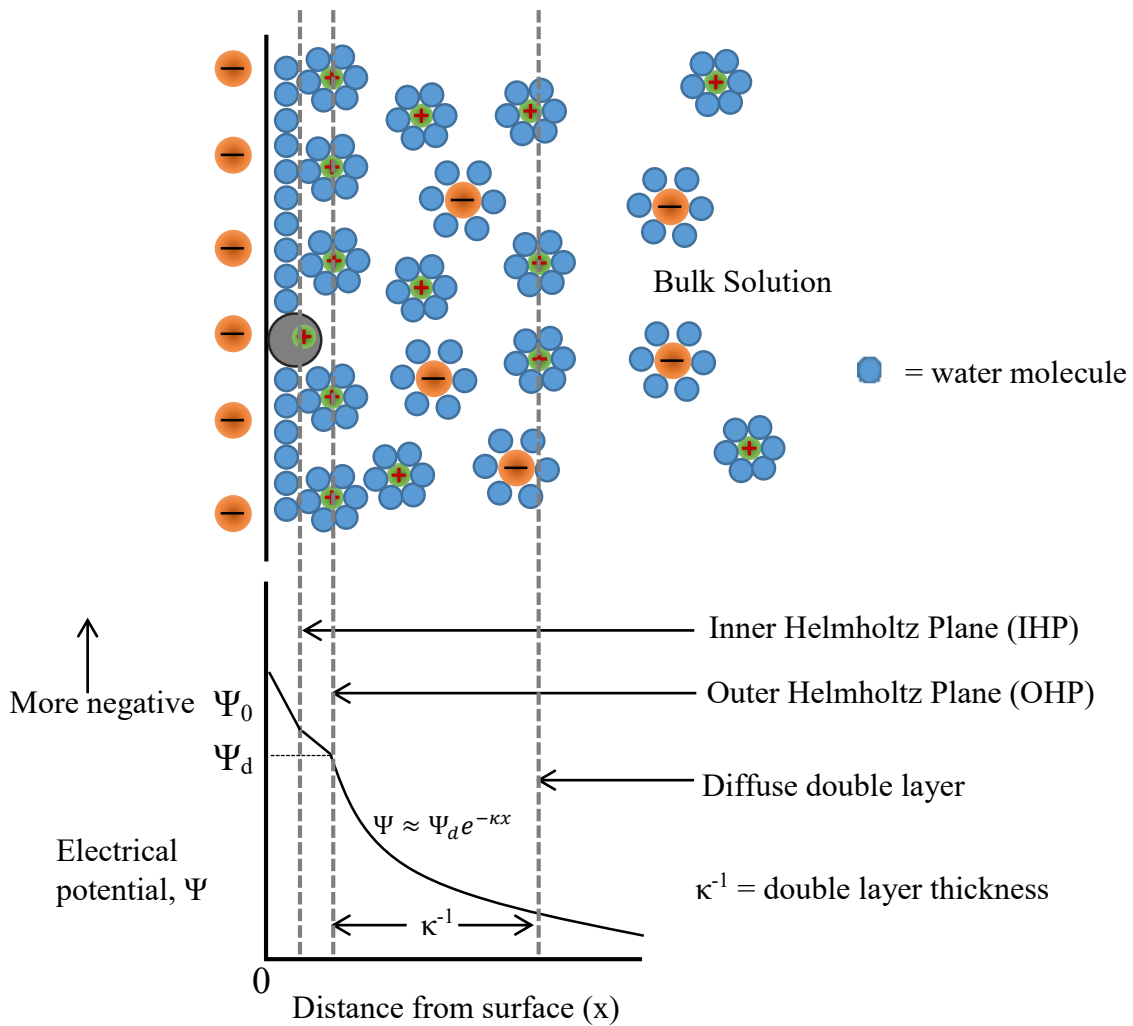


Figure 1-3: A schematic diagram of electrical double layer at a charged surface.

In hydrodynamic flow, the velocity is fastest at the center and slows to 0 at the walls, so the velocity profile of the fluid becomes parabolic or laminar. Due to the parabolic flow the solute zone becomes broad or disperse. With electroosmotic flow, the entire solution flows towards the cathode with an uniform plug like flow, which is a sharp contrast to hydrodynamic flow. One consequence is that there is less dispersion of the solute zone. The velocity profile of both flows and their corresponding solute zones⁵³ are shown in Figure 1.4.

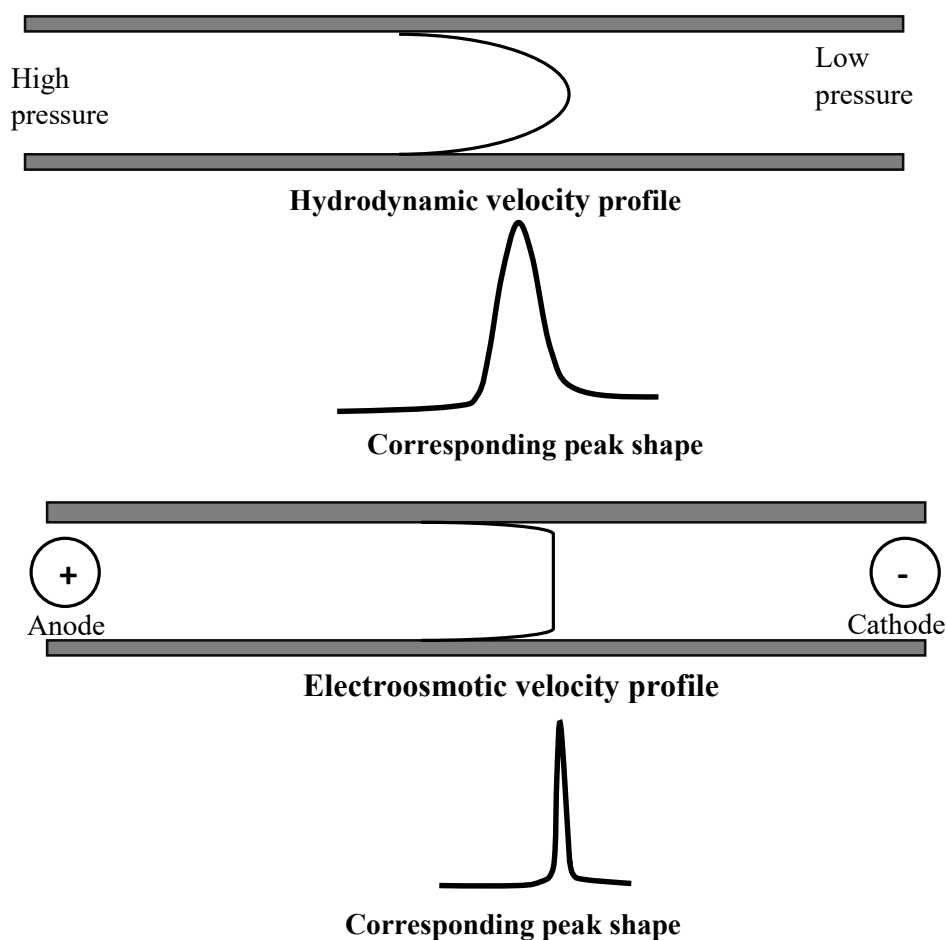


Figure 1-4: Velocity profiles of flow in capillary from hydrodynamic flow and electroosmotic flow and their corresponding solute zone

Increased flow induced dispersion reduces the separation efficiency for hydrodynamic flow compared to electroosmotic flow. Also, due to electroosmotic flow, all solutes have a net mobility vector component in one direction, which creates a difference between the overall observed electrophoretic mobilities among anions, cations and neutrals species. When μ_{EOF} is large enough all species have a net migration in the same direction.

1.2.2 Why capillary electrophoresis is important?

The efficiency of a column can be characterized by the number of theoretical plates (N) that can be packed in a given length along the separation axis. For a given length of column (L), the theoretical plate number depends on the plate height (H), and is defined as:

$$N = \frac{L}{H} \quad 1-8$$

If plate height (H) is reduced, higher plate number can be packed into a given length of column, which corresponds to higher efficiency separations.

According to the standard van Deemter equation, the plate height can be defined as:

$$H=A + \frac{B}{U} + CU \quad 1-9$$

where, A is a multiple path length term, or eddy diffusion, and depends on particle packing uniformity, B is the longitudinal diffusion term, C is the resistance to mass transfer term and U is the mobile phase velocity. The longitudinal diffusion term, B, is defined as $B=2\gamma D$, where D is the diffusion coefficient and γ is the obstruction factor defined as the ratio

of diffusion coefficients inside the medium to that in open solution. Clearly obstructed diffusion also depends on the uniformity and porosity of the medium.

In capillary electrophoresis, the mass transfer term, C, of the Van Deemter equation is zero because the separation is carried out in a single phase, i.e., there is no stationary phase.⁵⁴ The multiple path length term, A is also very close to zero for highly ordered well defined colloidal self-assembled (CSA) structures.⁴³ In electrophoretic separations path length variation is not convoluted with parabolic laminar flow profiles, which also reduces A significantly. The only factor that affects the plate height is in principle the longitudinal diffusion term, B.

For capillary electrophoresis with CSA the Van Deemter Equation can be idealized as:

$$H = B/U \quad 1-10$$

The mobile phase velocity is the product of the apparent mobility, μ_{app} and the applied voltage, E.

$$U = \mu_{app} \times E \quad 1-11$$

By applying a higher separation voltage, lower plate height should be achieved, i.e., better separation performance is possible, as has been readily proven by Lukacs and Jorgenson.⁵⁵

When voltage is applied, heat is generated, known as Joule heating, which is a consequence of fractional collisions between mobile ions and buffer molecules. The produced heat is proportional to the applied voltage. If the rate of heat dissipation is not equal to the rate of heat production, the temperature inside the capillary will rise, which develops a thermal gradient across the capillary. This gradient ultimately affects the

uniformity of mobility across the capillary and creates band broadening, decreasing the efficiency of separation. Due to the large ratio of surface area to volume, capillary walls can dissipate heat more efficiently than conventional slab gels do, allowing higher fields in a capillary.

1.3 Size-based separation of proteins

Proteins are large biomolecules consisting of one or more polypeptide chains. Polypeptides are macromolecules consisting of a sequence of amino acids. There are 20 amino acids in the universal genetic code⁵⁶ with different characteristics. The net charge of a protein depends on the types and number of amino acids present in the protein. The native shape of a protein depends on the number of molecular interactions; for example hydrogen bonding, ionic interaction between oppositely charged groups, hydrophobic interactions and disulfide cross linking between the amino acids presents in the backbone of a protein structure. For size-based separation, all of the interactions need to be destroyed and a uniform mass to charge ratio of the proteins needs to be established. To prepare proteins for size-based separation using an electrophoretic technique, proteins are denatured using surfactants (most commonly sodium dodecyl sulphate, SDS), reducing agent (mercaptoethanol /dithiothreitol (DTT)) and application of heat. SDS breaks up the native folded structure of the protein by non-covalently adsorbing on the protein and adding negative charge to the amino acid. SDS binds strongly with amino acids at a 1:2 ratio (1 SDS molecule per 2 amino acids), giving a more flexible, soluble structure that adopts a random coil conformation. Normally 1.4 g of SDS/1 g of protein is required for

denaturing and to maintain close to a constant mass to charge ratio.⁵⁷⁻⁵⁹ The amino acid cysteine contains a –SH group, which forms –S-S- linkages with other –SH groups. The –S-S- linkage is covalent in nature and cannot be disrupted with SDS. It requires a strong reducing agent like DTT or mercaptoethanol, to remove the disulphide linkage (-S-S-). To remove the hydrophobic interaction with other molecules like lipids and to allow SDS to bind in the hydrophobic region to complete denaturation, protein samples are heated to 85⁰ C for three to five minutes.

1.4 Protein surfactant interaction

For the development of protein separation, the interactions between proteins and surfactants are a key factor and still an active area of research. Several groups have studied the interaction of protein/surfactant complexes to learn their shape and size. Three models have been proposed to describe the structure of protein-SDS complexes⁶⁰ (Figure 1.5): (a) the rigid rod like particle model, which was proposed on the basis of viscometric measurements. According to this model the cross sectional radius of SDS-protein complexes is approximately 18 Å and the length of a rod is proportional to the protein molecular weight; and (b) the flexible helix model. According to this model, a flexible cylindrical micelle is formed from the interaction of hydrophilic segments of protein and SDS molecule. The sulphate –oxygen heads of SDS form a hydrogen bond with the amide nitrogen bonds of the peptide chain. and (c) the correlated necklace model which was proposed based on free boundary electrophoretic mobility. According to this model, the unfolded peptide chain is flexible in solution and micelle-like clusters of SDS are

distributed along the unfolded polypeptide chain. The extent of flexibility of the unfolded polypeptide chain and the forms of SDS aggregates in the SDS-protein complexes are the main differences among the various models.

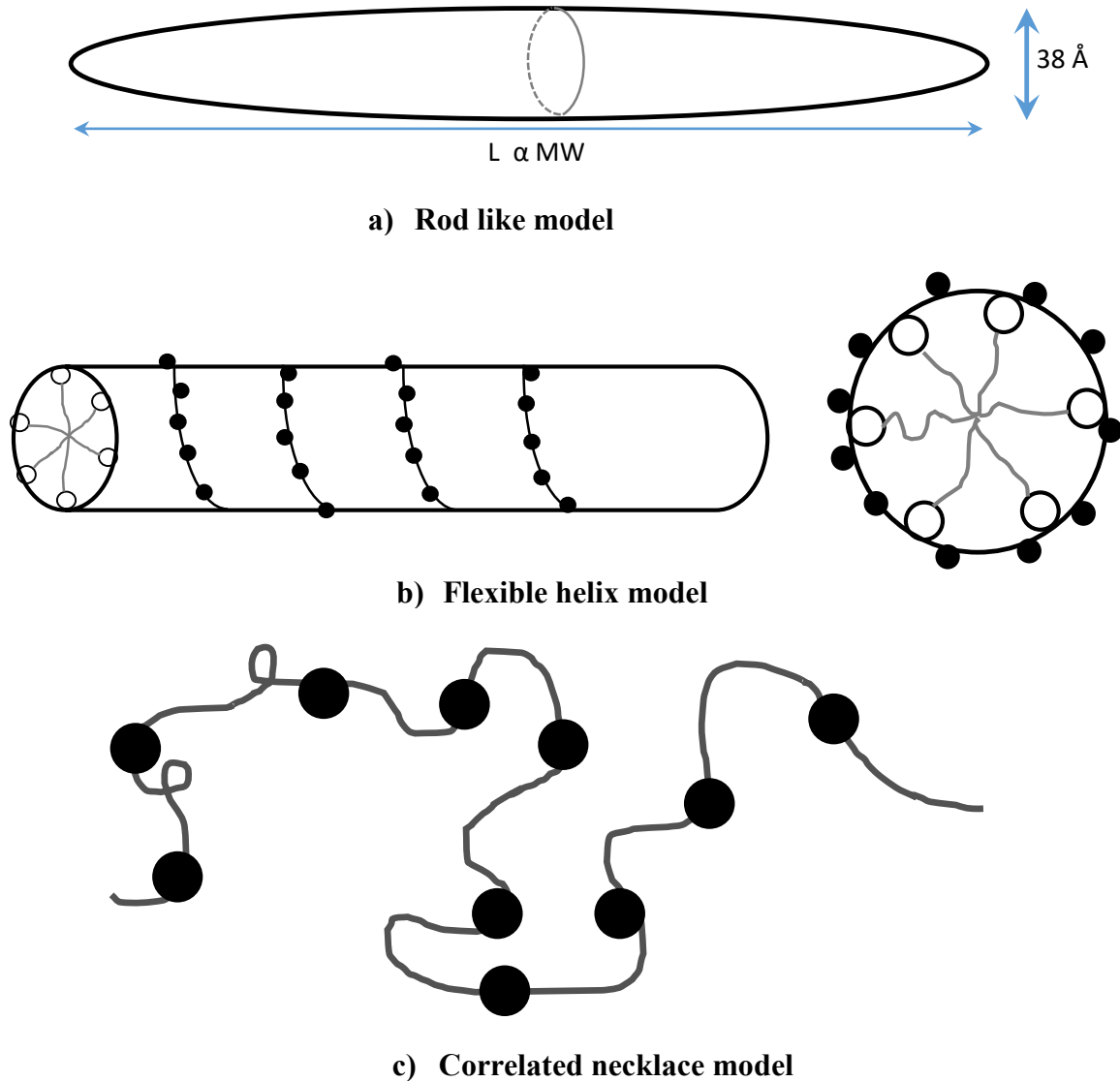


Figure 1-5: Schematic representation of different SDS-protein complex models (reproduced with permission from reference 59. Copyright © 1990 Elsevier B.V.).

Strong evidence for the necklace model has been reported in different studies. Turro et al⁶¹ proposed two possible necklace structures of SDS-protein complexes: (a) the proteins wraps around the micelles; and (b) the micelles nucleate on the hydrophobic sites of a protein. Based on fluorescence spectroscopy, ESR (electron spin resonance or electron paramagnetic resonance) and ²H NMR spectroscopy results, they confirmed that the first necklace model (Figure 1.6 a) with protein coiled around the exterior of micelles is most likely the predominant structure of the SDS-protein complex.

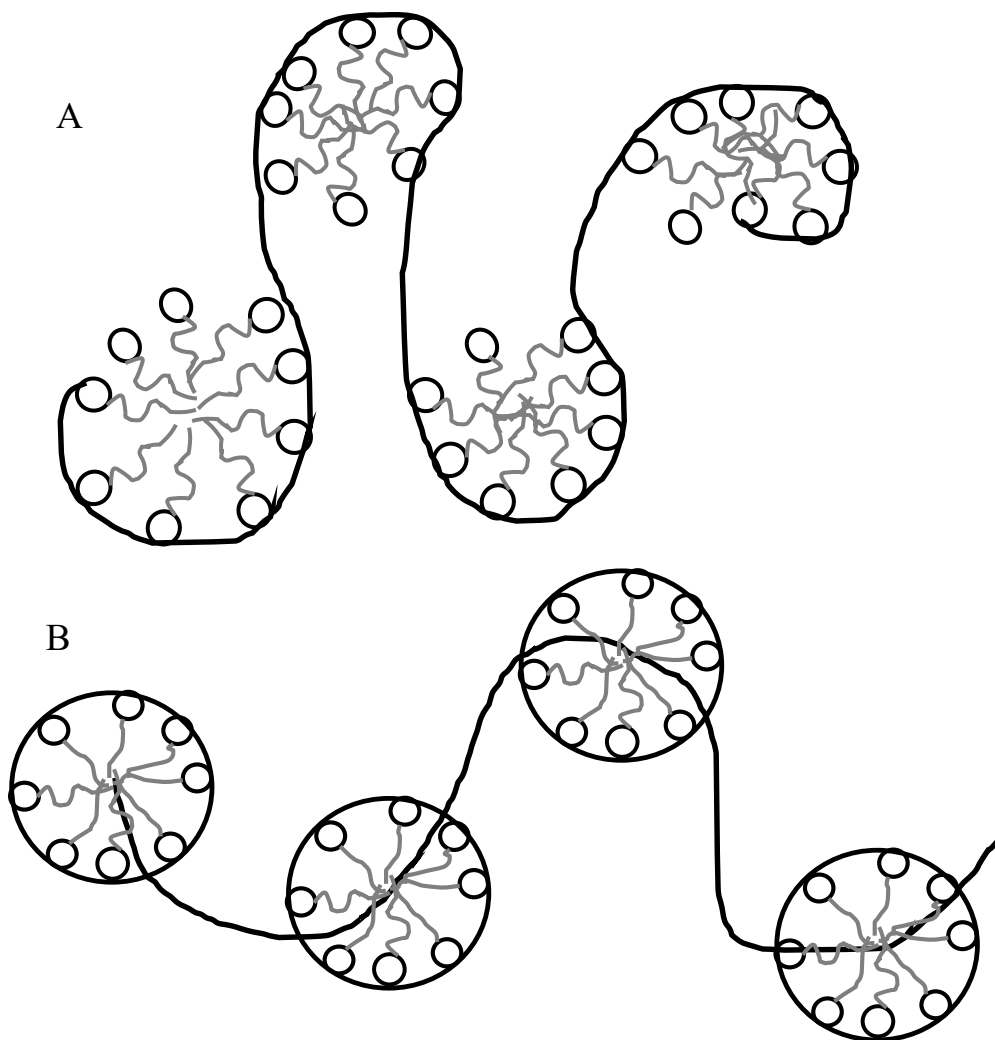


Figure 1-6: Two possible “necklace and bead structures” of protein-surfactant complexes: (a) the protein wraps around the micelles; and (b) the micelles nucleate on the protein hydrophobic sites (reproduced with permission from reference 60 Copyright © 1995 American Chemical Society)

1.5 Radius of gyration, R_g , and radius of hydration, R_h

For size-based separations, an estimate of the size of a protein is very important. The two most commonly used parameters to describe the molecular size of proteins are the radius of gyration (R_g) and the radius of hydration (R_h) or hydrodynamic radius. R_h is the Stokes radius of a polymer or a macromolecule-like a protein, which is defined as the radius of an equivalent hard sphere diffusing at the same rate of the molecule under observation. The radius of gyration, R_g is the mass-weighted average distance from the center of the molecule to each mass element in the molecule. For proteins and their complexes both R_h and R_g are of the same order of magnitude. The ratio of R_g/R_h is very important for protein characterization. For a spherical or globular protein the value of $R_g/R_h=0.775$.⁶² Wilkins et al⁶³ determined the hydrodynamic radius of native and denatured protein conformations by pulse field gradients NMR techniques. According to their experimental results the equations for hydrodynamic radius are:⁶³

$$R_h(\text{native}) = 4.75N^{0.29}\text{\AA} \quad 1.12$$

$$R_h(\text{denatured}) = 2.21N^{0.57}\text{\AA} \quad 1.13$$

where N is the number of amino acid residues in the protein.

Narang et al⁶⁴ computationally determined the radius of gyration of native protein using ab initio methods. Their proposed equation is:

$$R_g(\text{native}) = N^{3/5} \quad 1.14$$

In case of electrophoresis, the proteins both migrate and diffuse, both of which depend on the size and shape of the protein. Consequently, the hydrodynamic radius is more relevant for electrophoresis. As all proteins need to be denatured for size-based separations, the hydrodynamic radius based on equation 1.13 is the most appropriate to determine the protein radius.

In Table 1-1, the calculated R_h and R_g for native protein and R_h for denatured protein are shown, for the proteins studied in this work.

Table 1-1: Hydrodynamic radius and radius of gyration of proteins studied

Proteins	Number of amino acids	Molecular weight, kDa	R_h in native state, ⁶³ nm	R_g in native state, ⁶⁴ nm	R_h of denatured protein, ⁶³ nm
Aprotinin	58	6.5	1.542	1.143	2.236
Lysozyme	129	14.3	1.944	1.847	3.527
Trypsin inhibitor	181	20.1	2.145	2.262	4.278
Ovalbumin	385	45	2.670	3.558	6.578
Bovine serum albumin (BSA)	585	66	3.014	4.578	8.350

1.6 Separation matrices

As 1 SDS molecule binds with 2 amino acids of a protein, the SDS denaturing of the protein yields an essentially uniform charge-to-mass ratio for the SDS-protein complexes. So SDS-denatured protein complexes cannot be separated in free solution electrophoresis, as all proteins have the same electrophoretic mobility, regardless of their size. For separations, SDS-protein complexes require a matrix with pores to induce molecular sieving. Moving through the pores, the mobility of protein complexes will be different due to retardation or collision, also thought of as frictional retardation. In a particular matrix, the retardation depends on the size of the protein. Smaller protein complexes move through the pore at comparatively higher mobility than larger protein complexes. Due to the differences in mobility the proteins are separated. There are different types of matrices available for separation, with different pore sizes and different size distributions.

1.6.1 Polymer matrix

Among the separation matrices, polymer gels are well established and are a widely used technique.⁶⁵⁻⁷¹ Sodium dodecyl sulfate-polyacrylamide gel electrophoresis (SDS-PAGE) has been used for size-based separation of proteins for over four decades,^{39,67,72} and is the standard for protein separation and analysis. The gel pore size is not uniform. Instead there is a wide range of pores (an SEM image of gel is shown in Figure 1-7⁷³). The random pore distribution of gels produce random paths that give eddy diffusion like

pathways. The average pore size of a gel can easily be controlled by changing the concentration of acrylamide (%T) but the dispersion of pore size is very hard to control. Slab gel separations are slow, relatively labor intensive,⁴⁰ and complex to automate. SDS-capillary gel electrophoresis (CGE) opened up new possibilities. It can separate proteins with improved efficiency, giving great resolving power and accurate estimation of molecular weight,⁷⁴⁻⁷⁹ but run-to-run and column to column reproducibility,⁴⁰ void formation in capillaries as a results of gel shrinkage during polymerization,^{75,80} and clogging during separation are still problems. To improve the reproducibility and robustness, linear or slightly branched polymers like polyethylene oxide,^{59,81} dextrin, and polyethylene glycol (PEG),⁸² and non-crosslinked polyacrylamide gel⁸³ have been used in place of crossed-linked acrylamide gel for capillary gel electrophoresis. All the above matrices have already been adopted in microchips for separation provide nanometer sized pores, suitable for molecular sieving and filtering.⁸⁴ But the pore size dispersion of non-crosslinked gel is also random. So to achieve better separation in terms of resolution and speed, researcher have explored over the last decade if switching from disordered structures to ordered structures gives better separations.

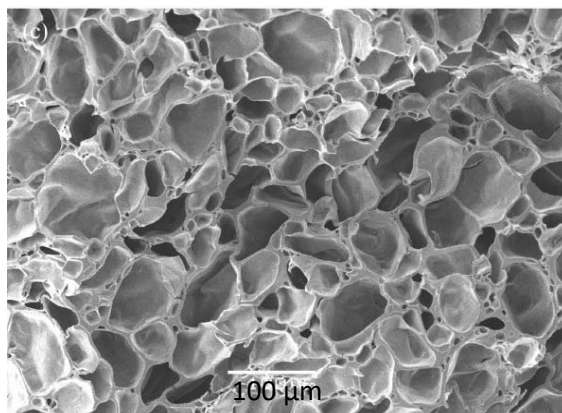


Figure 1-7: An SEM image of polyacrylamide gel (reprinted from reference 72 with permission. Copyright © 2006, Royal Society of Chemistry).

1.6.2 Micro fabricated arrays

Miniaturized micro/nano-fabricated systems provide improved efficiency and higher separation speed compared to conventional separation techniques.¹⁴ To achieve these advantages for size based bio-molecular separations, a microchip requires a separation matrix or media which has a significantly smaller plate height.³⁸ for that reason, researchers continue to explore alternative materials.

For a miniaturized microsystem, a micro-fabricated array structure can give an alternative separation matrix.^{20,85} A micro fabricated array may greatly enhance the performance of electrophoretic separation systems. It is possible to fabricate arrays of single pores, which are very good for DNA separation,¹⁹ but still smaller pore size fabrication that would be compatible with protein separation is much more difficult.

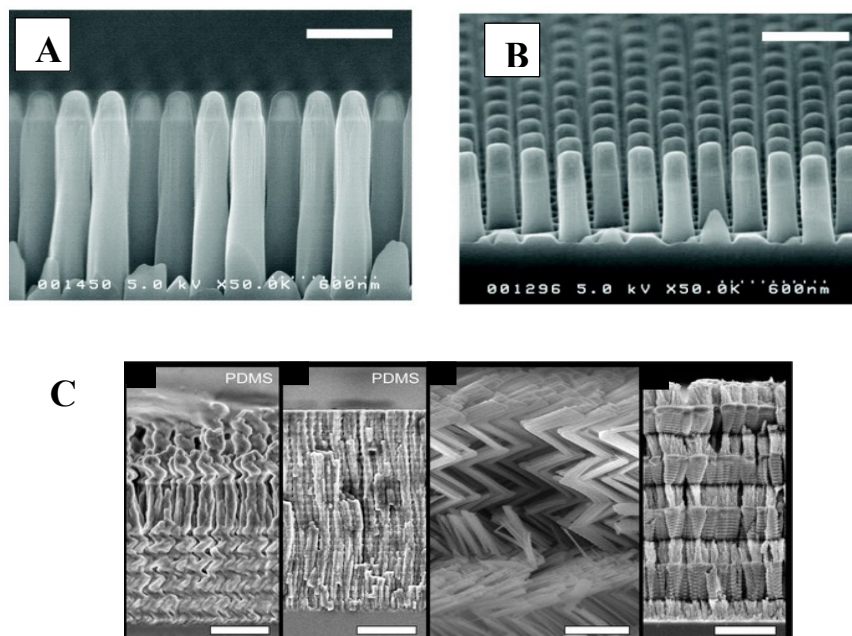


Figure 1-8: A &B) Images of micro fabricated arrays of nanopyllers (with permission from reference 20. Copyright © 2004 American Chemical Society); and C) Images of micro fabricated array using glancing angle deposition (with permission from reference 84. Copyright © 2011, Royal Society of Chemistry)

1.6.3 Colloidal self-assembly of nanoparticles

To explore a new separation matrix for miniaturized systems, Zeng et al.¹⁴ used colloidal self-assembly (CSA) of nanoparticles in microchips to form a nano-porous stationary phase. Spontaneous organization of mono-disperse micro- and nanometer-sized particles is known as a CSA. An SEM image of a CSA particle bed is shown in Figure 1-9A. There are several methods available for formation of colloidal self-assembly of particles,^{86,87} i.e., solvent evaporation, vertical deposition, horizontal deposition, sedimentation, electrostatic deposition, spin coating,⁸⁶ etc. Among all of the processes, evaporation induced formation is the simplest way to fabricate a CSA bed inside microfluidic channels. This CSA fabrication process is very easy and cost effective compared to microfabrication methods.

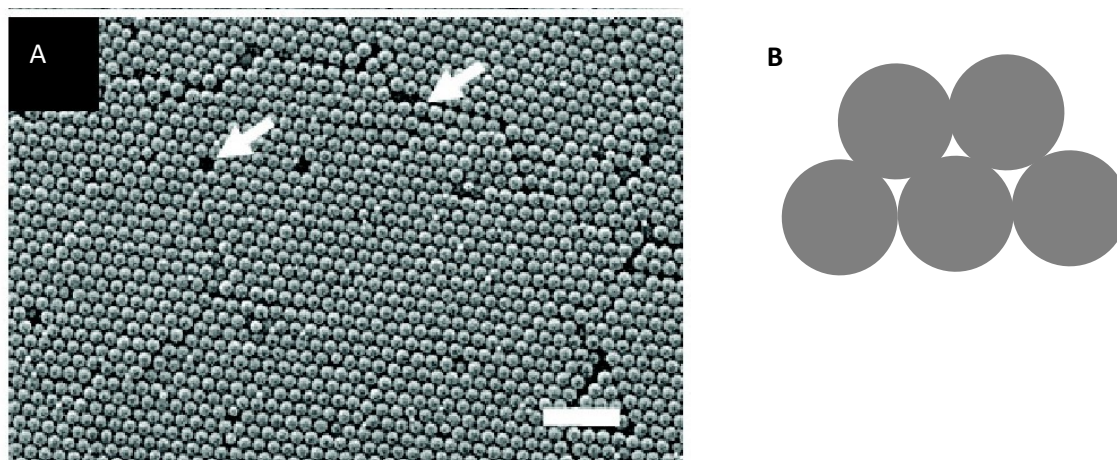


Figure 1-9: (A) An SEM image of colloidal self-assembly of 2- μm polystyrene particles fabricated within a microchannel. The arrows indicate lattice defects. The scale bar is 10 μm (with permission from reference 14. Copyright © 2004 American Chemical Society) (B) schematic view of pores in a CSA bed

In evaporation induced methods, one of the reservoirs in the microchannel network needs to be left empty for evaporation to occur. When a colloidal particle suspension is loaded into all but one of the reservoirs, and all channels are flooded with the colloidal suspension, water evaporates from the edge of the empty reservoir. The evaporation drives solvent and particle transport to the dry reservoir, and particles consolidate at the compaction front. The interface of a colloidal crystal and colloidal solution of nanoparticles is the compaction front. The crystalline regions advances smoothly with the advancement of the compaction front (Figure 1-10). The density of particles at the compaction front is much higher than the colloidal solution. At the compaction front, particles settle into the thermodynamically minimum energy location to initiate and then continue crystal growth.

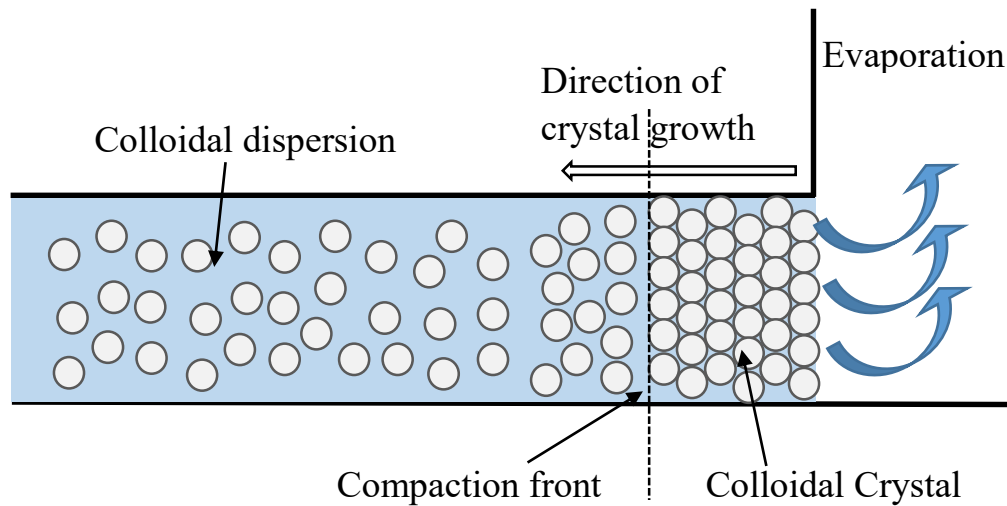


Figure 1-10: A schematic of colloidal crystal formation inside a microchannel.

The suitability of CSA with nanoparticles has already been extensively explored in the areas of sensors, photonics and new materials. The three dimensional pore structure in the interstitial space created by a CSA makes an alternative nanoporous sieve for separations. Due to the well-ordered and well-defined three dimensional sieve structure, the suitability of CSA for bio-molecular separation of DNA, proteins, peptides and even small molecules has been reported.

1.7 Sieving mechanism

Given the constant mass to charge ratio of analytes (such as DNA or SDS protein), sieving gels are needed for size-based separation. Depending on the size of analytes (DNA or SDS-protein complexes) and the pore size of the sieving matrix, there are three general regimes of mechanism, as shown in Figure 1.11. These are: 1) Ogston sieving, 2) Reptation without orientation, and 3) Reptation with orientation.

1.7.1 Ogston regime

Ogston theory assumes that the migrating species is a spherical object and the radius of gyration of an SDS-protein complex is smaller than the pore size of the gel. This method is also called electric field driven filtration. The transport mechanism through the gel was first derived by Ogston⁸⁸ and later was extended and refined for gel electrophoresis by Morries⁸⁹ and Rodbard & Chrambach.⁹⁰ According to Morries, the accessible volume fraction of any gel is the ratio of electrophoretic mobility, μ , and the mobility in open

solution, μ_0 . The modified Ogston Morris Rodbard Chrambach (OMRC) equation for gel electrophoresis in a matrix of random pore size is:

$$f = \frac{\mu}{\mu_0} = \exp(-c T (R + r)^2) \quad 1.15$$

where f is the accessible volume fraction, c is the constant for an electrophoretic system and T is the gel fiber concentration. The mean pore size, p , of the gel depends on T by the relation, $p = 1/\sqrt{T}$. R is the radius of a spherical analyte and r is the radius of the gel fiber.

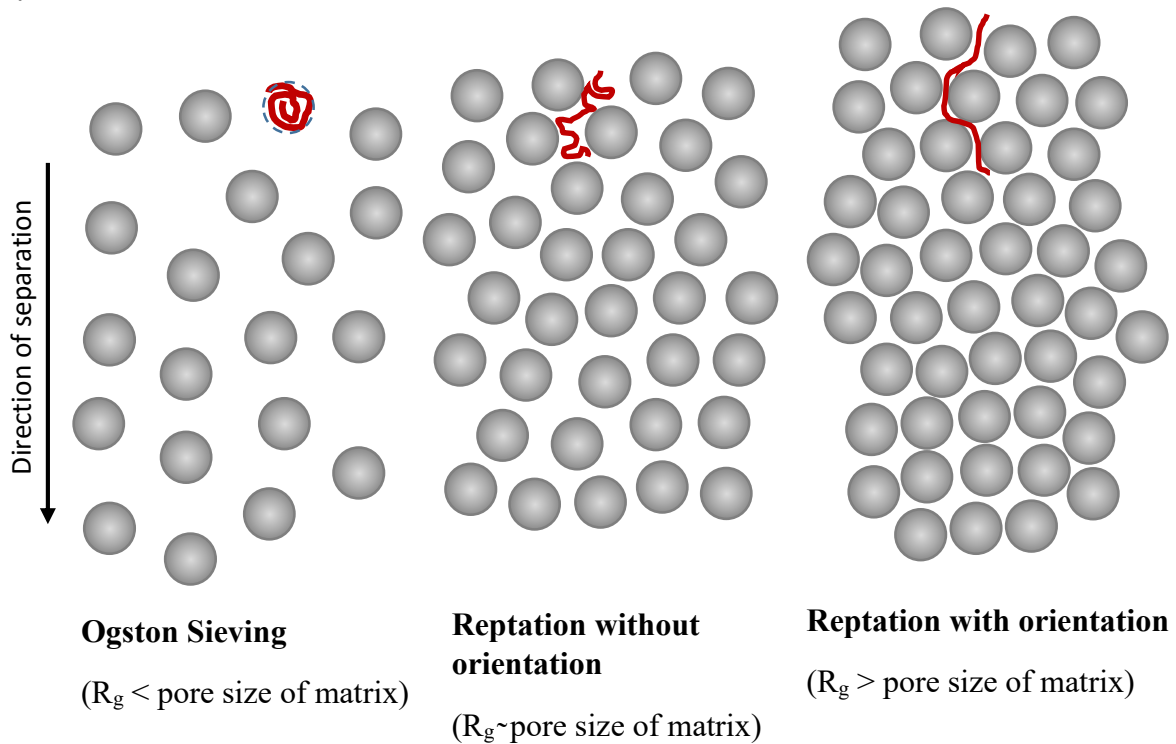


Figure 1-11: Three regimes of gel electrophoresis.

During electrophoresis, when any analyte moves through the gel, the mobility of analyte is reduced due to retardation. According to Rodbard & Chrambach,⁹⁰ the retardation coefficient, K_r , is related to the molecular radius by the equation:

$$\sqrt{K_r} = c(R + r) \quad 1.16$$

The retardation coefficient (K_r) solely depends on the size of the protein, (R) and relates the sieving properties of the separation matrix. The K_r value increases as the protein size or molecular weight increases.⁶⁹

Considering equation 1.16, equation 1.15 becomes,

$$\mu = \mu_0 \exp(-K_r T) \quad 1.17$$

$$\text{or, } \log \mu = \log \mu_0 - K_r T$$

The separation mechanism of size-based SDS-protein complex in a gel can be investigated by running a mixture of protein standards of different sizes through different gel concentrations. In the classical sense, effective molecular sieving exists only in the Ogston regime.⁸⁸ In this regime it is assumed that the migrating analytes behave like unperturbed spherical objects and the average pore size of the matrix is larger or in the same range as that of the hydrodynamic radius of the migrating analyte. The value of K_r increases as the protein size or molecular weight increases.⁶⁹ Based on empirical evidence K_r is known to be proportional to the molecular weight (M) of SDS-protein^{69,91} at a constant gel concentration, giving:

$$\log \mu \propto (-M) \quad 1.18$$

where M is the molecular weight of a protein.

From equation 1-18, a plot the logarithm of the mobility as a function of protein molecular weight should result in a linear curve with a negative slope, which is known as a Ferguson plot.

1.7.2 Reptation regime

Biopolymers with a flexible long chain like DNA or SDS-protein complexes, can migrate through gel networks with pore sizes similar to or significantly smaller than the analyte in a head first, snake like mechanism, which is called reptation. In the case of reptation, the logarithm of mobility is inversely proportional to the logarithm of the molecular weight of analyte.

$$\log \mu = -\log M \quad 1.19$$

At higher electric field, globular species change their conformation and stretch like a rod. In that case, the mobility of the migrating species is expressed as

$$\mu \sim \left(\frac{1}{M} + bE^2 \right) \quad 1.20$$

where b is a function of the pore size of the matrix, charge and length of the migrating species, and E is the applied electric field.

A common way to differentiate between the above mechanisms is a plot of log mobility of analyte versus the log of the analyte molecular weight⁷⁷ as shown in Figure 1.12.

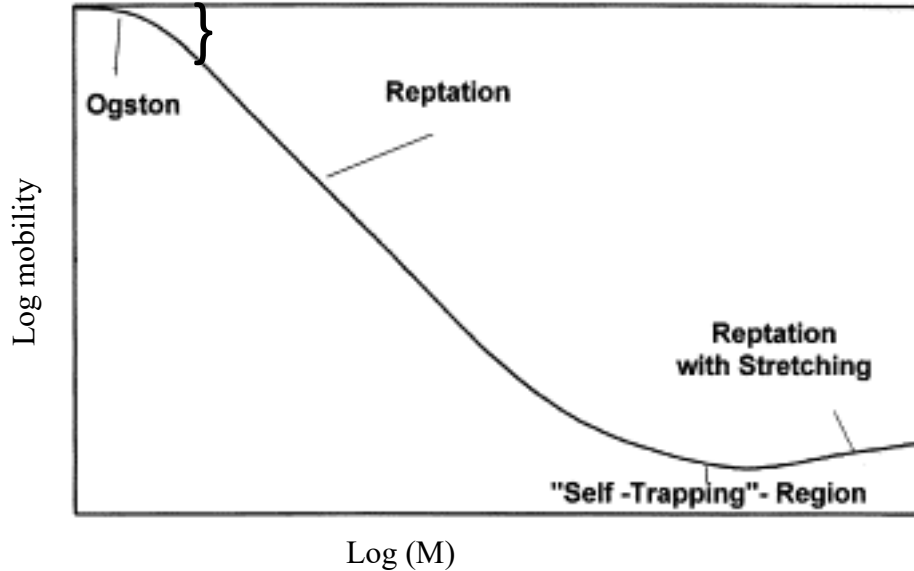


Figure 1-12: Schematic representation of the relationship between the logarithmic electrophoretic mobility and the molecular weight (with permission from reference 76. Copyright © 1996 WILEY-VCH Verlag GmbH & Co. KGaA, Weinheim)

1.8 Sieving through a uniform pore structure

Gels have highly random pores. So the equations derived for gels should not accurately describe the migration of species through a structure of uniform pores. Giddings⁹² first addressed this issue and proposed an equation for the accessible volume fraction:

$$f = \frac{\mu}{\mu_0} = \left(1 - \frac{R}{r}\right)^2 \quad 1.21$$

where R is the radius of analyte and r is the radius of the pore. Giddings showed that depending on the pore type, the migration behaviour can be considerably different. When the radius of analyte is very small compare to the pore radius, all migration behaviour will

be uniform. The accessible free volume or reduced mobility behaviour of a spherical analyte through different types of pore is shown in the Figure 1.13.

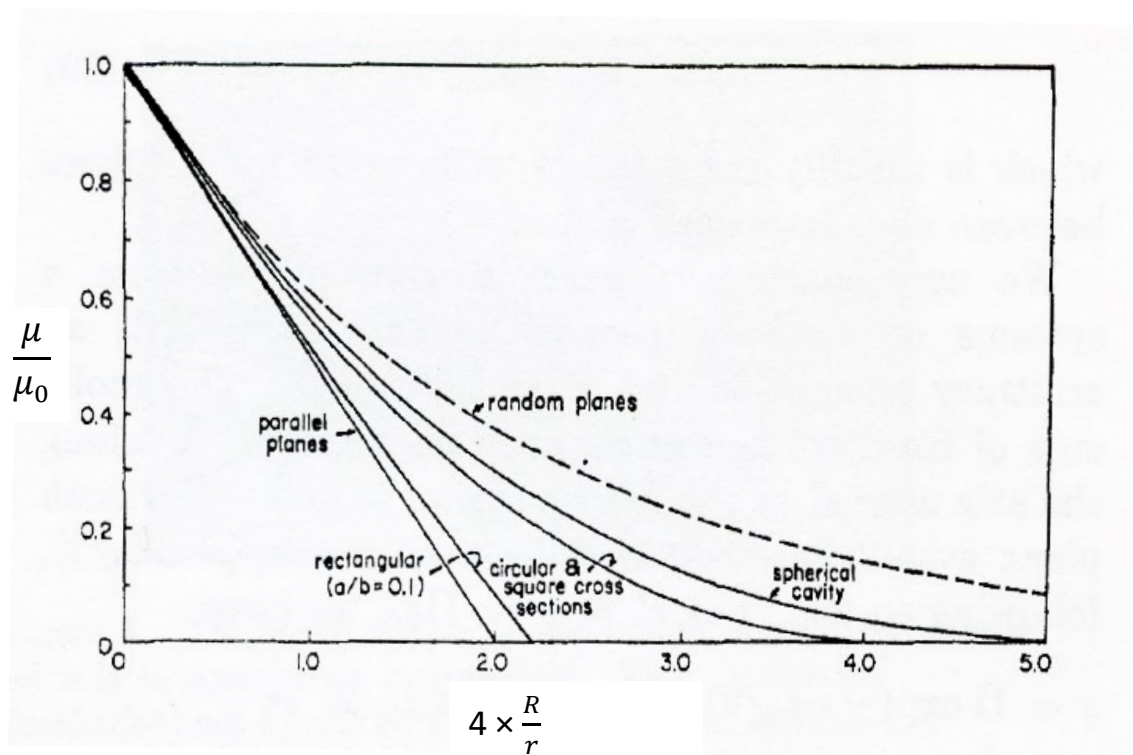


Figure 1-13: Reduced mobility behavior of a spherical analyte of radius R through different types of pores. (With permission from reference 91. Copyright © 1968, American Chemical Society).

One of the important observations from Figure 1.13 is that if the spherical analyte radius and cylindrical pore radius are the same, there should be no analyte movement through the pores.

Birdsall et al.¹⁷ refined the model for SDS-protein separation in a colloidal crystal by scaling the Giddings equation by the porosity ε . Their new model equation for uniform pores is:

$$\frac{\mu}{\mu_0} = \varepsilon \left(1 - \frac{R}{r}\right)^2 \quad 1.22$$

Recently S.B. King and coworker²² established the relationship of matrix order with separation mechanism using a colloidal self-assembly of nanoparticles. They prepared highly ordered uniform pore size CSA with 900 nm silica particles for DNA separation, and concluded that Ogston sieving does not depend on the geometry or symmetry of the matrix. But order has an effect on band broadening. S.B. King and coworkers²² findings of dependency of band broadening on the array order are in agreement with previously reported findings of Nazemifard et al.⁹³ The band broadening will be minimal for close-packed, monodisperse colloidal particle because monodisperse colloids produce uniform and well defined pores throughout the separation bed. These analysis are of particular value in understanding and interpreting the results with the CSA beds described in this thesis.

1.9 Outline of thesis

Colloidal self-assembly (CSA) of nanoparticles provides a new type of matrix for protein separations. In this thesis we combine CSA beds with microfluidic technology and exploit the usability of colloidal self-assembly of nanoparticle beds for size-based separation of SDS-protein complexes. The organization of this thesis is described below.

In Chapter 2, we discuss the formation of the colloidal self-assembly of nanoparticle beds inside the microchannel, especially for small particle packing. During small particle assembly, packing and cracking of the bed starts almost simultaneously, which is most unfortunate. So a modified packing process was implemented to prevent the cracking. In Chapter 2, we explore the sieving mechanism of SDS-proteins through highly ordered uniform pore size CSA beds. In exploration of the mechanism, the separation performances of different particle size CSA beds at optimum voltage is also discussed. Finally, the discussion of the retardation coefficient for different SDS-protein complexes and the utilization of the retardation coefficient concept for on chip protein sizing is presented.

During optimization of the separation voltage, it was observed that the CSA bed is not stable for high voltage ultrafast separation, and that the stability of a bed is highly dependent on particle size. A process to stabilize CSA beds for high voltage separation is presented in Chapter 3. We improve the stability of CSA beds by narrowing the capillary. The theory of defect formation is related to how narrowing the capillary gives less defects in the CSA formation. The study ultimately yielded highly stable beds for high voltage

separation. The high stability is demonstrated with some high voltage, ultrafast separations. The reasons for the high stability are discussed.

Chapter 4 mainly focuses on the separation performance of highly-stable narrow-bore capillary CSA beds. The separation performance was evaluated through determining the resolution, plate height/plate number and minimum protein mass resolving capacity of a CSA bed. The minimum protein mass resolving capacity using small sized particles is also described in this chapter.

By narrowing the capillary bore, highly stable CSA beds can be prepared. Unfortunately we cannot use these microchips for a long time. The process to prepare a microchip that is usable for up to a few days is described in Chapter 5. Using sol-gel chemistry, the silica gel is formed inside the packed particle bed, which acts as a glue to hold particles together for a long time. The chemistry of gel formation and optimization is described in this chapter. The usability of gel modified CSA beds for high performance SDS-protein separation is also described in this chapter.

Finally the findings of this thesis are summarized in Chapter 6, along with some future perspectives and proposed directions of research.

Chapter 2

Protein Separation Mechanism through Colloidal Self Assembled Nanoparticle Sieves in Microchips and Retardation Coefficient for on-Chip Protein Sizing*

2.1 Introduction

Size-based protein separation is a critical tool for analysis in proteomics, genomics and molecular biology.^{39,40,94} It is widely used in research⁴⁰ and in the pharmaceutical industry.¹⁷ So improvement in separation performance is very important. Separation performance improvement means improving resolution in a given analysis time. Improvement of resolution can only be achieved with material advances for separation matrices.¹⁵

Miniaturized micro/nano-fabricated systems provide improved efficiency and higher separation speed compared to conventional separation techniques. To achieve these advantages for size-based bio-molecular separations, a microchip requires a separation matrix or media which has significantly smaller plate height³⁸ than polymer gels. Smaller

* A version of this chapter has been published in Proceeding of 18th International Conference on Miniaturized Systems for Chemistry and Life Sciences as, “Colloidal self-assembled nanoparticles sieves with orthosilicate cross linking for protein separation in microchips and retardation coefficient for on chip protein sizing”, Mohammad Azim, Abebaw B. Jemere and D. Jed Harrison, MicroTAS 2014; San Antonio, USA; 2387-2389

Also, a version of this chapter has been submitted to Electrophoresis as “Evaluation of Protein Separation Mechanism and Pore Size Distribution in Colloidal Self-Assembled Nanoparticle Sieves for On-Chip Protein Sizing.” Mohammad Azim, Ali Malekpourkoupaei, Wenmin Ye, Abebaw B. Jemere and D. Jed Harrison. (Authors contributions are described in preface)

plate height may be achieved using a very uniform pore size matrix,^{22,93} so that development of an appropriate matrix for micro-systems is still an active research field.

For a miniaturized system, a micro-fabricated array structure can give an alternative separation matrix. A micro-fabricated array can greatly enhance the performance of an electrophoretic separation system. It is possible to fabricate single pore sized arrays, which are very good for DNA separations,¹⁹ but sufficiently small pore sizes fabrication compatible with protein separations is very difficult. To explore a new separation matrix for miniaturized system, Zeng et al.¹⁴ used colloidal self-assembly (CSA) of nanoparticles in microchips to form a nano-porous stationary phase. Spontaneous organization of mono-disperse micro- and nanometer-sized particles is known as CSA. The fabrication process of CSA is very simple and cost effective compared to nanofabrication methods. The suitability of CSA of nanoparticles has already been extensively explored in the areas of sensors,⁹⁵ photonics⁹⁶⁻⁹⁸ and new materials.⁹⁹ The three-dimensional pore structure in the interstitial space created by a CSA makes an alternative nano porous sieve for separations. Due to the well-ordered and well-defined three-dimensional sieve structure, the suitability of CSA for bio-molecular separations of DNA, proteins, peptides^{13-15,21,100-105} and even small molecules^{43,102,105} has been examined.

The sieving mechanism of SDS-protein complexes in gel is well studied but still under debate. Westerhuis et al.¹⁰⁶ evaluated the electrophoretic migration behaviour in polyacrylamide gels. They concluded that SDS-protein complexes in the 14-65 kDa range migrated by following a Ferguson plot below 15% gel concentration, and above 15% acrylamide gel concentration migration could be described by reptation theory. But

migration of small proteins through higher gel concentration or larger proteins through lower gel concentrations could not be described by either of these theories, i.e., the DNA-like Ogston sieving model is not appropriate. Cohen and Karger⁶⁵ separated proteins (14.2 -34.7 kDa) using high performance capillary SDS-PAGE. They used up to 10% gel concentration and confirmed a size-based separation mechanism. Guttman⁹¹ studied the separation mechanism of SDS-protein complexes (14.2 -97.4 kDa) in a polyethylene oxide mediated capillary. He concluded there is an Ogston sieving mechanism for protein separations through large pores, but suggested reptation with a stretching mechanism was active when the pore size of the gel was below the hydrodynamic radius of the SDS-proteins. Oliver et al¹⁰⁷ measured the electrophoretic mobilities and dispersion of SDS-protein complexes (10-200 kDa) in different molecular weight polydemethylacrylamide (PDMA) solutions on microfluidic chips. They found that plot of log mobility vs. PDMA concentration showed a linear correlation, but the Ogston model and the reptation model are not adequate to fit the retardation factors. On the other hand, Herr and Singh¹⁶ used photo-polymerized cross-linked polyacrylamide gel in a microchip for protein sizing (14.2-66 kDa), reporting that log mobilities of the SDS-protein complexes varied linearly with the gel concentration, and that the retardation coefficients depended on the molecular weight as expected from Ogston sieving. Recently Birdsall et al.¹⁷ proposed that the Giddings equation is more appropriate for SDS-protein separations using CSA particle beds.

The separation mechanism of SDS-protein complexes in a CSA bed has not been investigated, and the usefulness of CSA for fabricating very small pores that are ~ 15% of the particle size has not been fully exploited. The structures are presumed to have well-

ordered and well-defined pore sizes, in stark contrast to the random pore size distribution of polymer gels. Models of separation depend upon the pore size distribution,⁹² so that differences in detail can be expected between gels and CSA beds. Wirth and coworkers¹⁷ adapted the Giddings model⁹² for separation in an assembly of uniform pore sizes to describe separations in a polymer entrapped CSA bed. They measured all the relevant separation matrix parameters, and showed their results were accurately calculated by the model. In this Chapter we contrast the predictions of the classical Ogston sieving-based models for size-based separation of SDS-complexed proteins, with the Wirth/Giddings model for a uniform pore size bed. We also evaluate the mechanism of separation of SDS-protein complexes through a CSA bed of nanoparticles, and explore the effect of pore size on separation the quality. Finally, the retardation coefficient has been calculated for different SDS-protein complexes to calibrate the on-chip protein sizing to precisely determine the molecular weight of two model proteins.

2.2 Materials and methods

2.2.1 Protein samples and chemicals

Aprotinin (6.5 kDa), lysozyme (14.2 kDa), trypsin inhibitor (Soybean, 20.1 kDa), carbonic anhydrase (29.2 kDa), ovalbumin (chicken egg, 45 kDa) and bovine serum albumin (BSA, 66 kDa), were from Sigma-Aldrich and used as molecular weight standards. To prepare buffer, sodium dodecyl sulfate (SDS) (Sigma), 10x TBE (Tris (hydroxymethyl) aminomethane (tris base) 890 mM-boric acid 890 mM–EDTA 20 mM)

buffer solution (Sigma) and 2-mercapto-ethanol were used in different proportions. 4x TBE, 4 w/v % SDS and 8 v/v % 2-mercapto-ethanol were used as sample buffer and 4x TBE and 0.1 w/v % SDS were used as working or running buffer (pH 8.3). Fluorescein-isothiocyanate isomer-I (FITC, Sigma) was used to label proteins. All proteins were labeled using the Sigma-Aldrich standard protein labeling procedure with FITC. For labeling, 2–4 mg/mL protein solutions were prepared using freshly prepared 0.1 M bicarbonate buffer (pH 9). The FITC was dissolved in dimethyl sulfoxide (DMSO) to prepare ~1 mg/mL solution. In each mL of protein solution 50 μ L of FITC solution was added in 5 μ L aliquots and gently stirred. The FITC-protein solution was incubated overnight at 4⁰C in the dark. Aliquots of FITC labeled protein solutions were mixed with sample buffer and incubated in a dry incubator at ~85⁰C for about 5 min to denature the proteins. After cooling to room temperature, denatured protein samples were filtered and diluted with working buffer and refrigerated. Before separation, protein solutions were mixed together and the final concentrations were adjusted to 10⁻⁵ to 10⁻⁴ mM for each protein, using working buffer. Deionized water (18.2 M Ω) from an ultrapure water system (Millipore, Milford, MA) was used to prepare all reagents and samples.

2.2.2 Microchip fabrication and colloidal self-assembly

Microchips were assembled using polydimethylsiloxane (PDMS) with a glass slide support, as described previously.¹⁴ A view of a microchip is shown in Figure 2-1. Briefly, 15 mm long separation and 3 mm long injection channels (~100 μ m wide and ~20 μ m deep with a ~100 μ m offset in the double T design) were patterned in a silicon wafer using a

photolithography process. PDMS base (Sylgard 184, Dow Corning) mixed with crosslinking agent in 10:1 proportion was poured on the wafer and cured overnight at 60⁰ C. The PDMS replicas were removed from the wafer and cut into pieces and reservoir holes were punched to access the channels. The clean and dry PDMS (cleaned with 100% ethanol and MilliQ water, and dried with nitrogen) pieces were attached to clean glass slides to complete fabrication. The glass slides were cleaned using piranha solution containing 3:1 ratio of H₂SO₄ and H₂O₂.

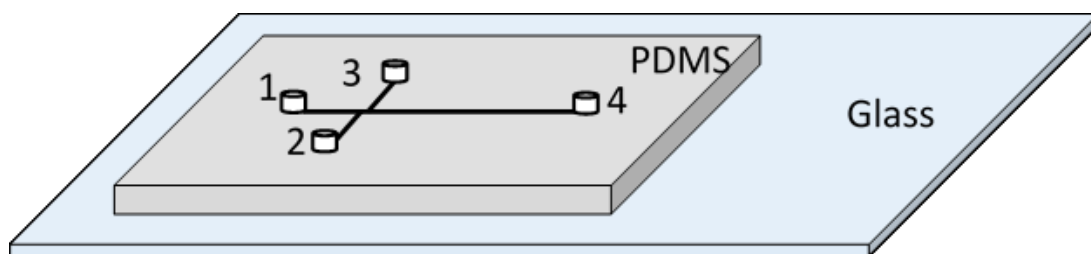


Figure 2-1: View of a microchip 1, 2 3 & 4 are reservoirs. The distance between reservoirs 1 to 4 reservoirs is about 15 mm. This channel acts as separation column. The distance between 2 to separation column and 3 to separation column is about 3 mm. These channels are used for injection. The offset of the two injection channels in the separation column is about 100 μ m. The diameter of all reservoirs is 2 mm and the thickness of the PDMS is about 3 mm.

The process of colloidal crystal formation inside the microchannels is shown in Figure 2-2. An evaporation-induced colloidal self-assembly mechanism was used for nanoparticle bed formation. 5.4 % to 10 % aqueous suspensions of mono dispersed silica particles (50-690 nm) (Bang Laboratories, Poly Sciences inc) (depending on availability) without any modification or treatment were used for fabrication of colloidal self-assembled (CSA) structures in the microchips. According to the manufacturer's statement the size range of each particle was: 50 \pm 10, 150 \pm 30, 300 \pm 40, 540 \pm 60, and 690 \pm 70 nm. The colloidal solution was injected in three of the reservoirs and one reservoir was left empty (air) for evaporation.

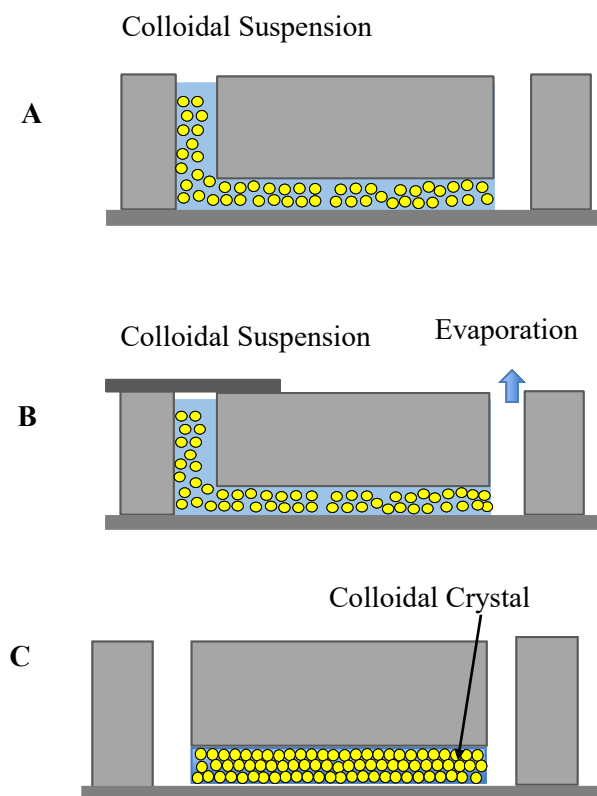


Figure 2-2: Mechanism of CSA formation: **(A)** First a uniform colloidal bead suspension was injected into one of reservoir. All other channels were flooded with solvent. Then the colloidal solution was injected into the two other reservoirs. The fourth reservoir was left empty. **(B)** The reservoirs containing the colloidal solution of beads were covered to prevent evaporation, and the evaporation of water started from the empty reservoir. **(C)** The chips were left in a Petri dish to complete the colloidal self-assembled bed formation in the micro channels.

2.2.3 Instrumentation

A confocal epifluorescence microscope¹⁰⁸ (Figure 2-3) was used to monitor the separation. The chip was mounted on an XYZ stage for translation in the horizontal (XY) and vertical (Z) directions. The Z direction is the optical axis. The FITC labeled SDS-protein complexes were excited with a 488 nm argon ion laser. The fluorescent response

was collected with a Rollyn 10:1x, 0.30 NA lens, a 505 dichroic mirror, an 800 μm pinhole, a 530 ± 30 nm bandpass filter, and a photomultiplier tube (PMT). A Labview program was used to store the PMT responses and to control the power supply, which was used to apply the required electrode voltage. All data was analyzed using Origin software.

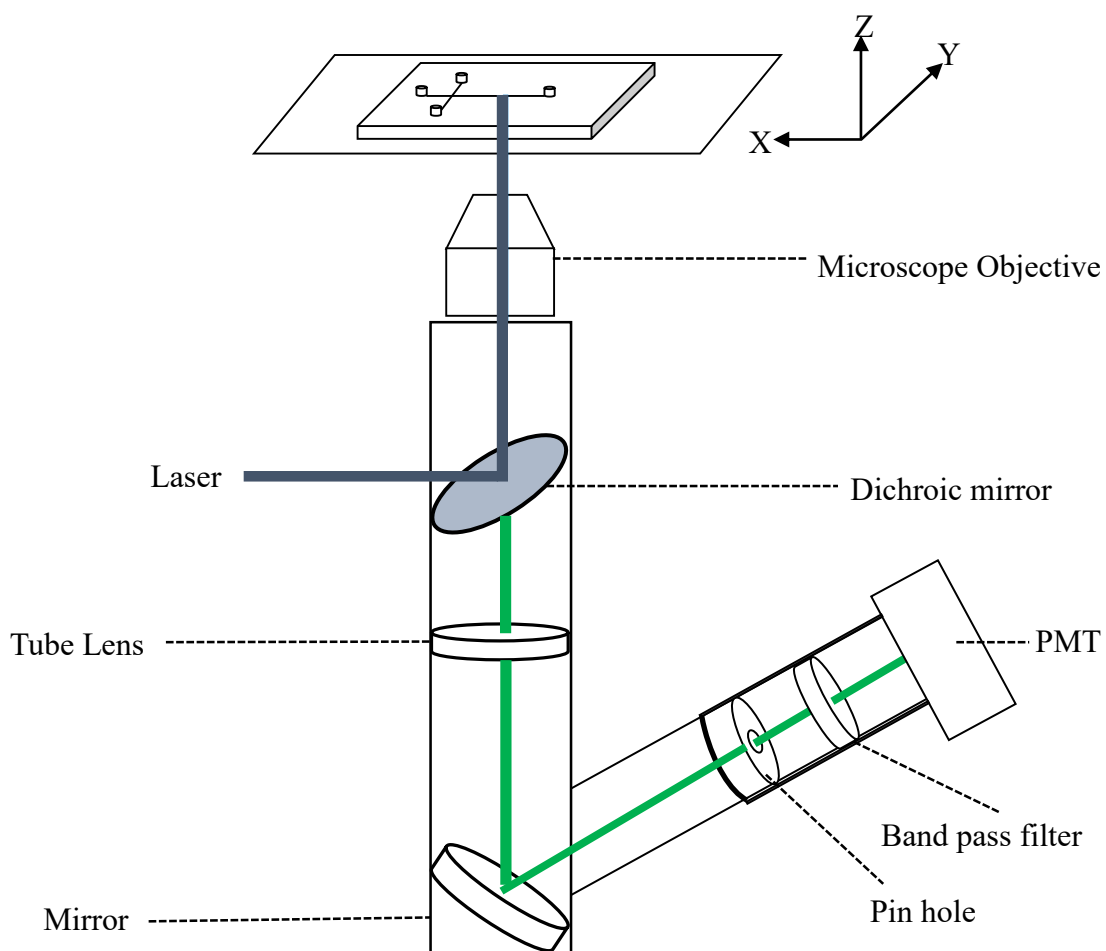


Figure 2-3: Confocal epifluorescence apparatus for detection on a microchip

2.2.4 Voltage orientation and separation

Before separations the aqueous/colloidal suspension in the reservoir was substituted with working buffer and left for ~20-25 min to equilibrate the device. The working buffer was then run at ~30 V/cm for 20-30 min to obtain stable current through the channels.

During injection, the SDS-protein mixture was injected from reservoir 2. A 30-40 V potential was applied in the electrode of reservoir 3 with all other reservoirs grounded, to form a shaped injection plug, which reduced the band broadening during separation.

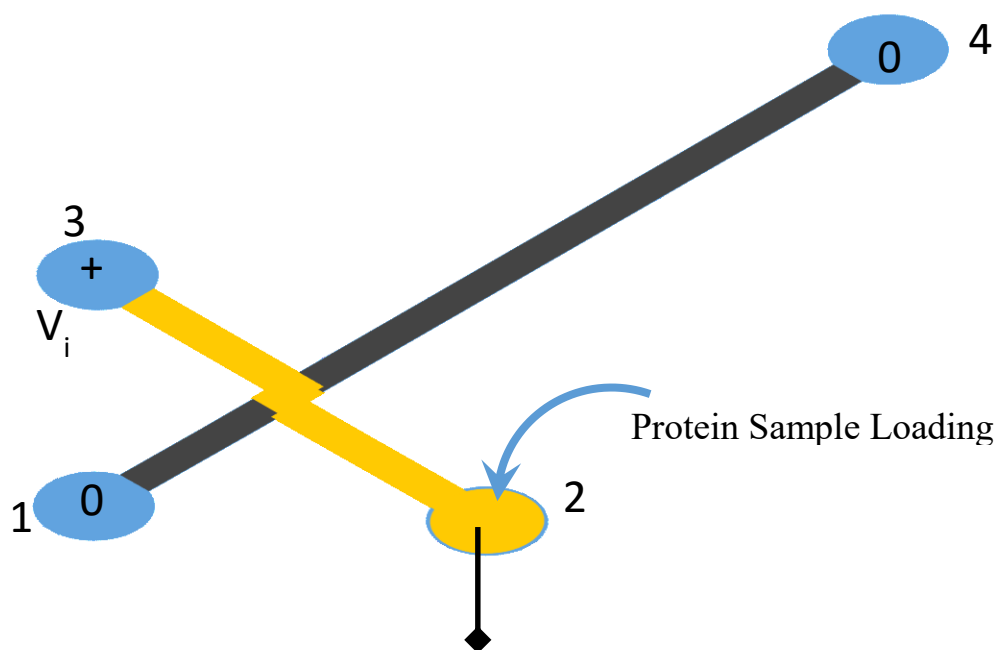


Figure 2-4: Voltage orientation during injection of sample.

During separation equal positive and negative potentials were applied to separation channel reservoirs 1 and 4, with reservoirs 2 and 3 held at zero volts by being grounded. The negative potential applied in reservoir 1 served as a push back potential to prevent sample leakage from the grounded sample loading arms. The negatively charged SDS-protein complexes migrated towards the anode and the laser spot was located at a fixed distance (4 mm) from the double T position to excite the FITC molecules attached with SDS-protein complexes.

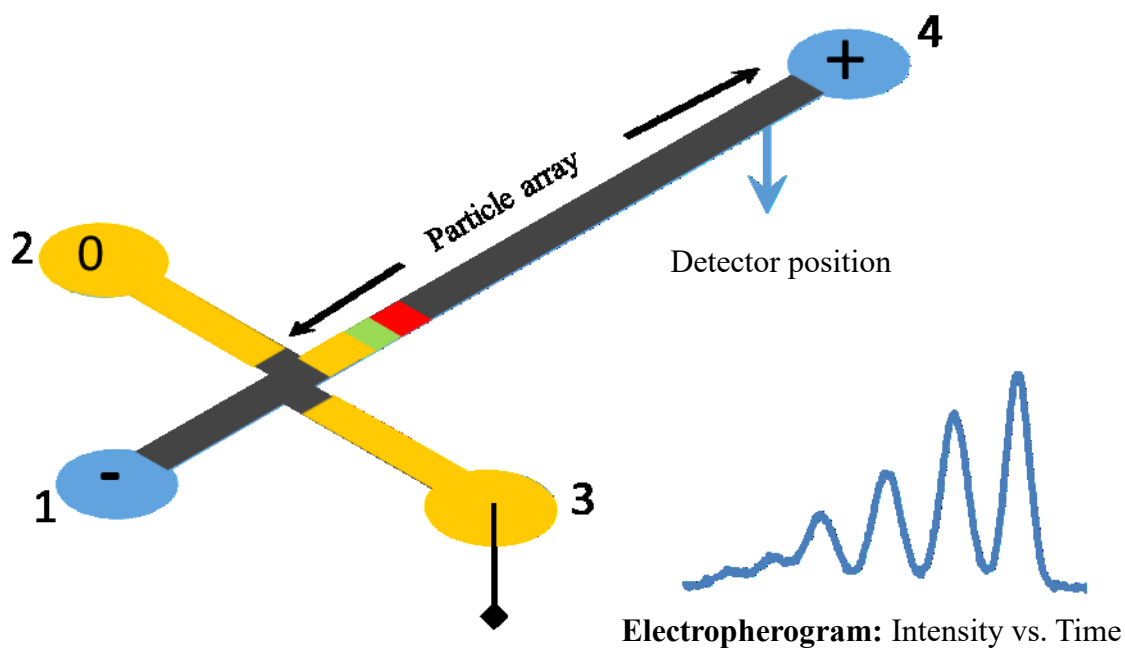


Figure 2-5: Voltage orientation during separation of sample.

To calculate the true separation voltage, the potential at the double T intersection (V_J) needs to be known. The intersection potential was calculated from the equivalent circuit of the chip (Figure 2-6) using Kirchoff's equation. With three voltage sources and a ground connected to the channels, according to Kirchoff's rules, the current and potential are expressed as:

$$I_3 = I_1 + I_2 + I_4 \quad 2.1$$

$$\frac{(V_4 - V_J)}{R_4} + \frac{(V_1 - V_J)}{R_1} + \frac{(V_2 - V_J)}{R_2} = \frac{V_J}{R_3} \quad 2.2$$

By solving equations 2.1 and 2.2 for V_J gives:

$$V_J = \frac{V_4 R_1 R_2 R_3 + V_1 R_2 R_3 R_4 + V_2 R_1 R_3 R_4}{R_2 R_3 R_4 + R_1 R_3 R_4 + R_1 R_2 R_4 + R_1 R_2 R_3} \quad 2.3$$

As the cross sectional area of each channel, as well as the electrolyte resistivity, is same, the resistance of each channel should be proportional to the length (l) of the channel. So equation 2.3 becomes:

$$V_J = \frac{V_4 l_1 l_2 l_3 + V_1 l_2 l_3 l_4 + V_2 l_1 l_3 l_4}{l_2 l_3 l_4 + l_1 l_3 l_4 + l_1 l_2 l_4 + l_1 l_2 l_3} \quad 2.4$$

The potential at the intersection was calculated using equation 2.4.

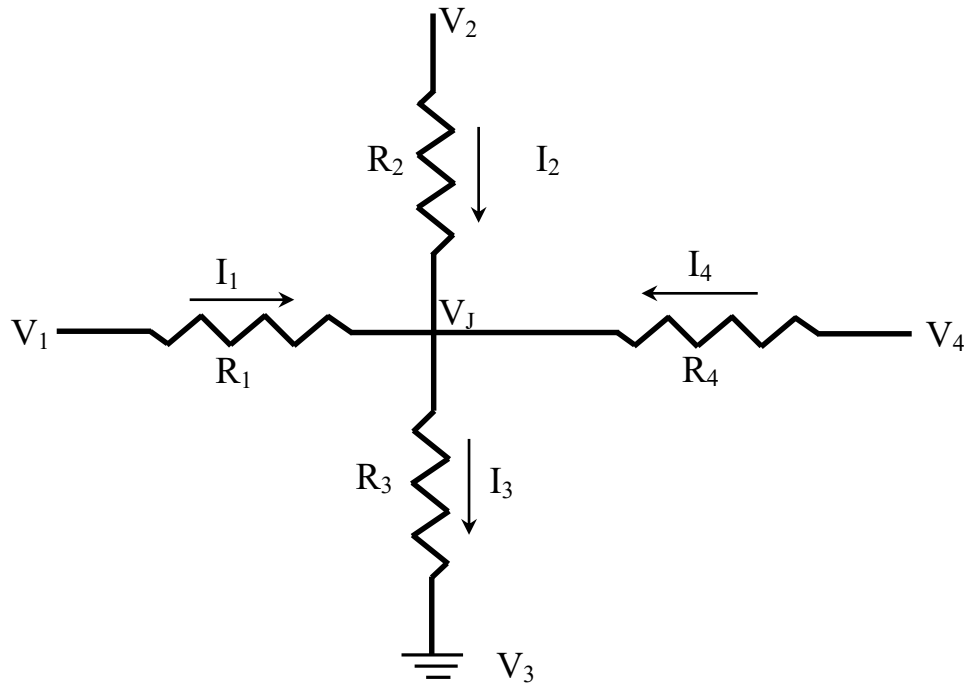


Figure 2-6: The equivalent circuit for the intersection of four channels.

2.3 Results and discussion

2.3.1 Packing study

In their study, Zeng et al.¹⁴ injected colloidal solution in reservoirs 1, 2 and 3, with reservoir 4 left empty for evaporation. This process worked well for 300 nm and bigger nanoparticles, but for smaller nanoparticles, ≤ 150 nm, if reservoir 4 was left empty, packing and cracking started almost simultaneously (Figure 2-7). The situation was worse for even smaller particles, e.g. 50 nm (Figure 2-8). In all cases, the cracks propagate with time and make the separation channels unusable for separation, as the cracks allow for fluid channeling.

Diffusion and capillary forces drive the fluid flow to the drying edge. The evaporation at the drying edge and the fluid flow through the compact region determine the overall fluid transport. At the beginning, the compacting region presents negligible resistance to flow. Thus evaporation is limited by diffusion in the gas phase, and the rate is constant. The evaporation of water creates strong particle wetting, which prevents air invasion into the colloidal assembly. As the compacted region grows, the resistance to flow also increases, which eventually limits the evaporation rate.^{109,110} Due to reduced water transport, air can invade the colloidal assembly and start causing stress-induced cracking while the bed is drying. Smaller particles also show greater cracking stress evident by Figure 2.8.

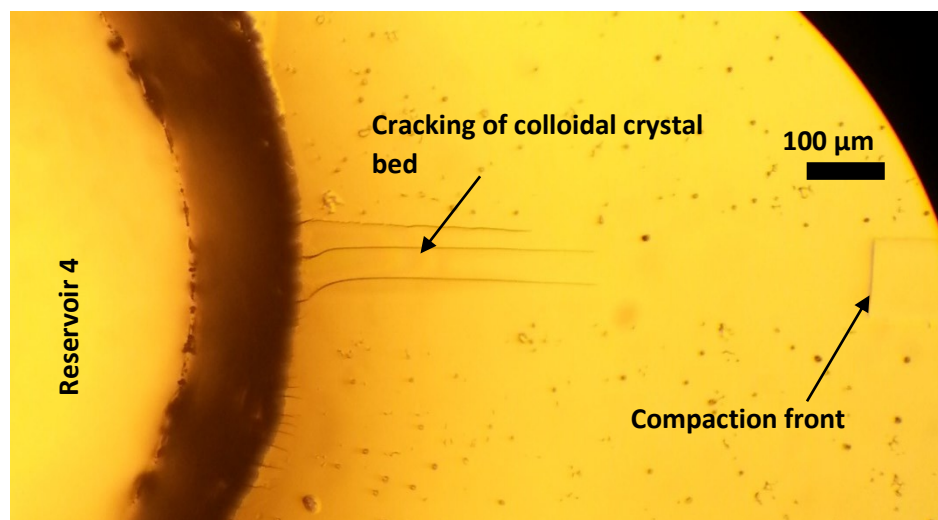


Figure 2-7: Colloidal self-assembly of nanoparticle bed formation with 150 nm particles. Reservoir 4 was left open for evaporation.

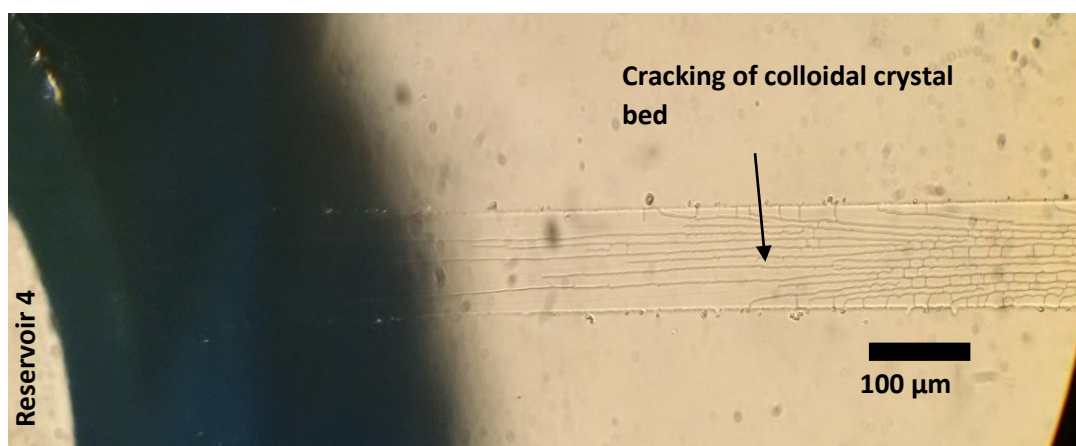


Figure 2-8: Colloidal self-assembly of nanoparticle bed formation with 50 nm particles. Reservoir 4 was left open for evaporation.

A more satisfactory bed packing is observed if reservoir 3 (Figure 2-9) is left empty, instead of reservoir 4. In most of the cases no crack is observed at the drying edge for assembly of 150 nm particles (Figure 2-9A). In a few cases for 150 nm particles and

most cases for 50 nm particles, some cracks were observed at the beginning of packing in channel 3 (Figure 2-9B and Figure 2-10A) but the crack does not propagate with time (Figure 2-10). As reservoir 3 is the buffer waste for the injection, the small cracks do not create any problem for separation. This result is probably due to lower resistance to flow of water due to the short distance of reservoir 3 from reservoirs 1 and 2 compared to reservoir 4.

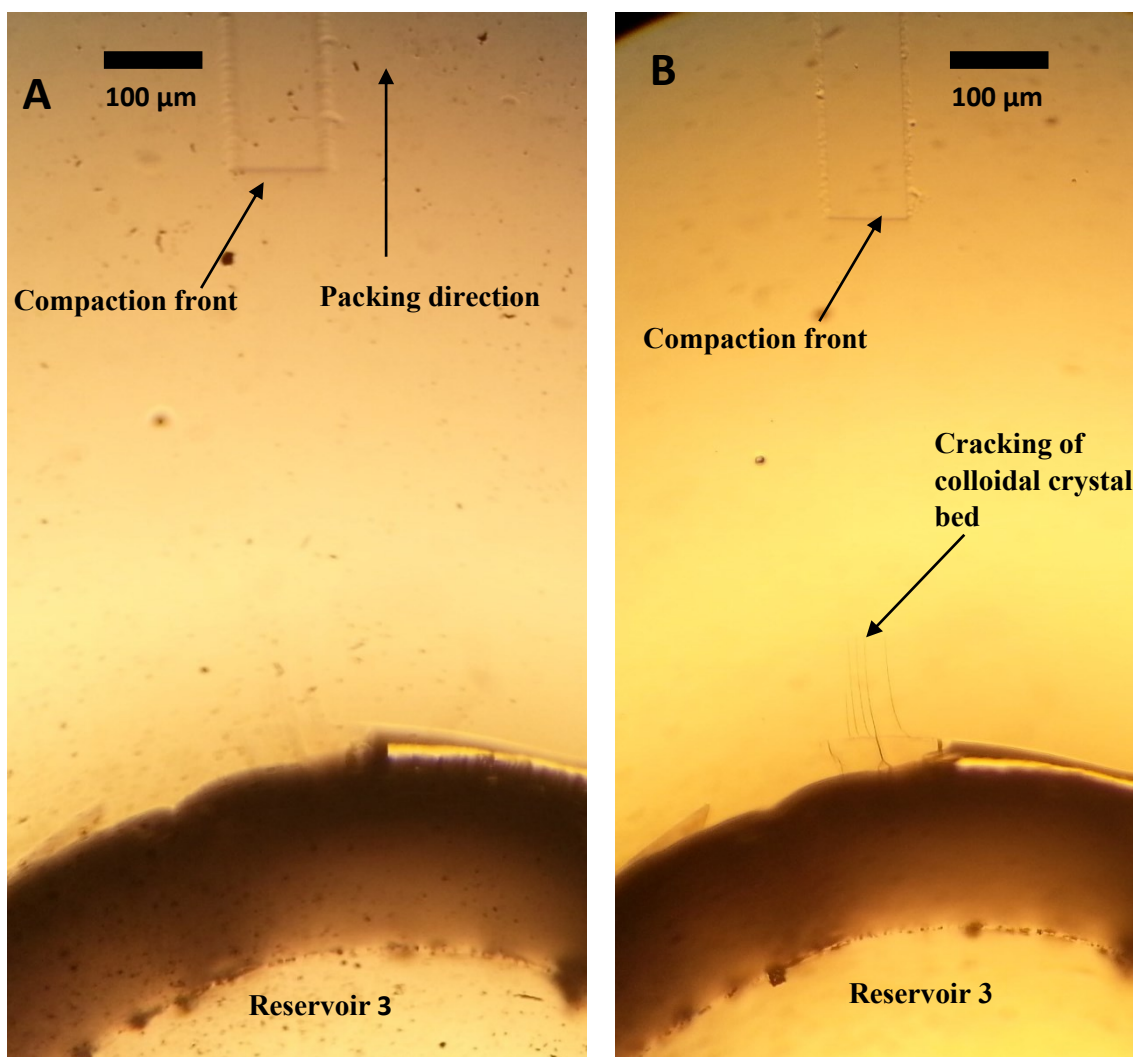


Figure 2-9: Colloidal self-assembly of nanoparticle bed with 150 nm particles. Reservoir 3 was left open for evaporation. **A)** In most cases no crack was observed. **B)** Some cracks were observed in few cases, which did not propagated with time.

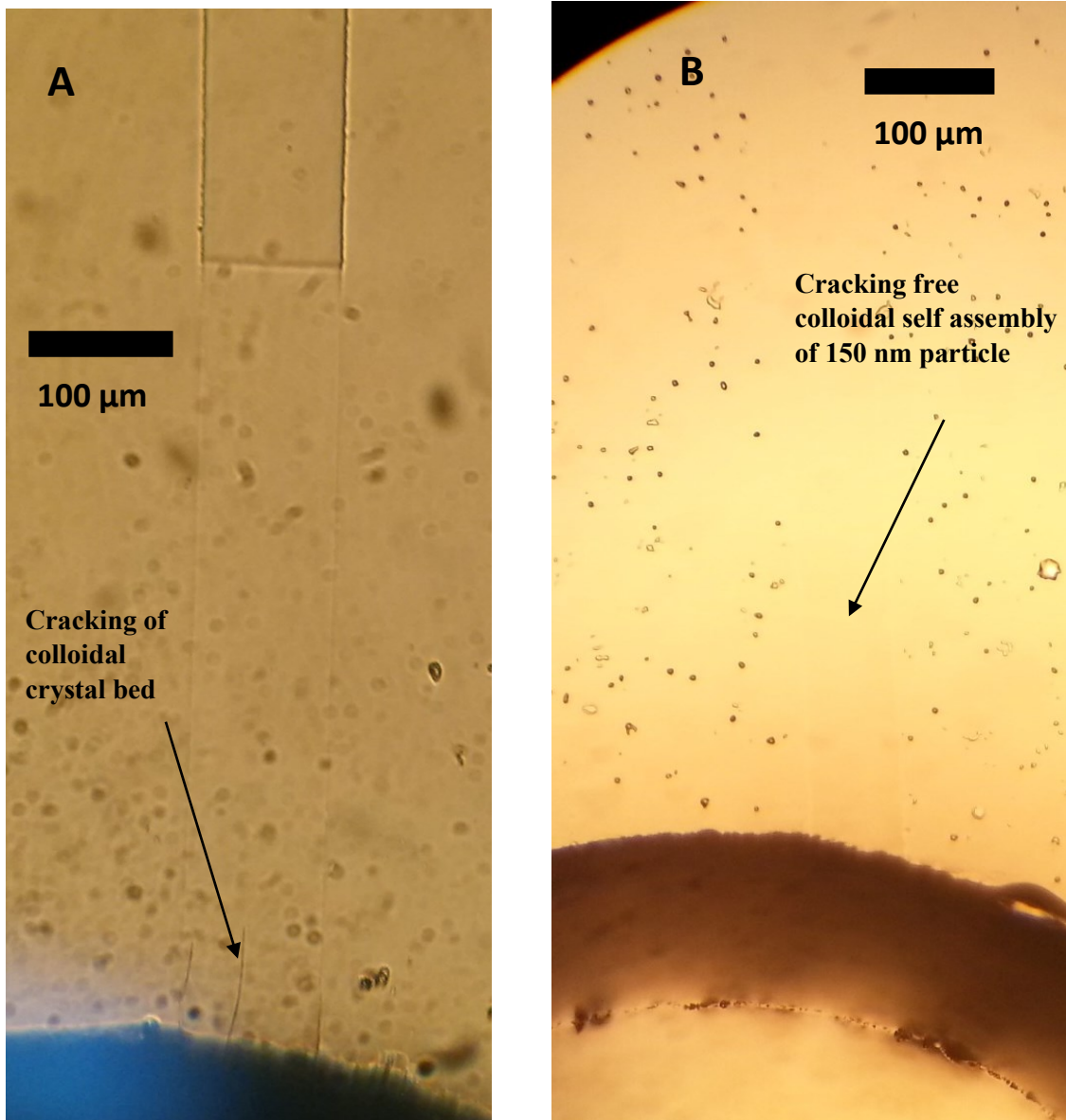


Figure 2-10: Colloidal self-assembly of nanoparticle bed when reservoir 3 was left open for evaporation. **A)** Very little cracking observed for 50 nm particle packing which were not propagated with time. **B)** No crack was observed for 150 nm particle packing even after 10 h of packing.

2.3.2 Optimization of separation voltages

To determine the optimum field strength for separation, a series of separations were performed using 150, 300, 540 and 690 nm CSA particle beds at different applied field strengths. It was observed that the stability of the CSA bed was highly dependent on the particle size. As particle size decreased, the stability of the bed also decreased. The 300 and 150 nm particle beds were stable at ≤ 320 V/cm and ≤ 60 V/cm, respectively. Any applied field strength above these values resulted in no effective separation. Within 2-3 run attempts the whole bed was completely washed away from the channel, with only one peak observed for a mixture of proteins. The electropherograms in 150 nm particle beds at a variety of applied field strengths are shown in Figure 2-11. It is clear that smaller protein migrates first, and the migration time is decreased with increasing field strength, as expected. Better separation was achieved with good resolution up to 55 V/cm, while above 55 V/cm the resolution decreased, which is a sign of bed cracking. Above 90 V/cm, no significant separation was possible. The photograph (Figure 2-12) of a separation bed exposed to different separation voltages confirmed this interpretation. At lower separation voltages, the separation channel was in very good shape, but as the voltage increased the evidence of cracks was visualized with a normal camera.

The separation performance of a 150 nm particle bed is shown in Table 2-1. From Table 2-1, it is very clear that effective separation is possible using a 150 nm particle bed. The minimum plate height decreases with increasing applied field strength as expected, from 3.2 μm at 25 V/cm to 2.1 μm at 45 V/cm. This plate height and plate number is comparable to other results for colloidal self-assembled nanoparticle beds in microchip,¹⁴ and for cross-linked polyacrylamide gel¹⁶ in microchip.

Table 2-1: Separation performances of a 150 nm particle bed in microchip

Field strength V/cm	Peak to peak resolution		Efficiency	
	Trypsin inhibitor- Ovalbumin	Ovalbumin- BSA	Minimum plate height, μm	Plate number, $\text{N/m} \times 10^5$
25	1.4	1.7	3.2	1.9-3.0
30	1.3	1.5	2.8	2.0-3.5
35	1.3	1.5	2.4	3.0-4.0
45	1.5	1.5	2.1	2.7-4.3

Figure 2-13 shows the effect of applied separation field strength on the electrophoretic mobility of proteins. There was no significant difference in the apparent mobility of each protein observed, i.e., the apparent mobility is almost constant with applied voltage, as expected. Considering these results, 35 V/cm was taken as the optimum voltage for ensuring reproducible results in further investigations.

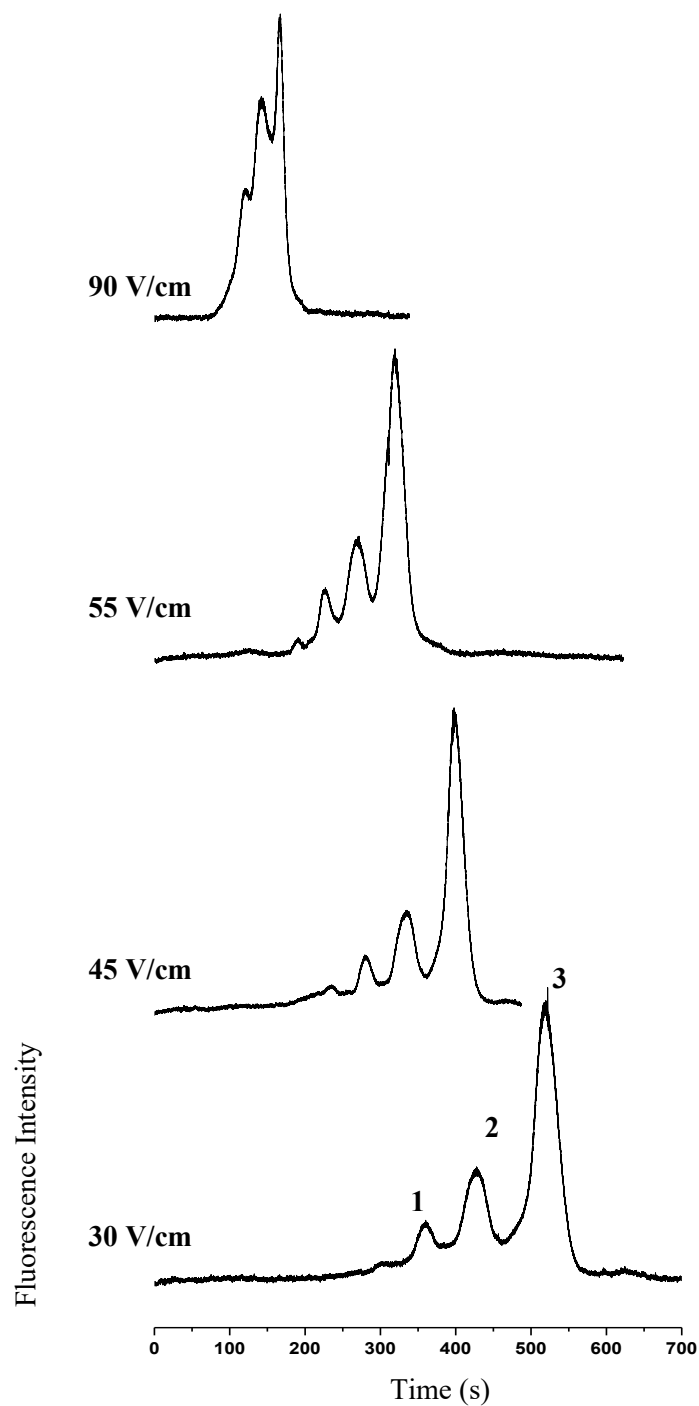


Figure 2-11: Electropherograms of on chip SDS-protein separation using a 150 nm particle bed at different field strengths and 4 mm of separation distance ($L = 4$ mm) . The peaks of electropherograms are: 1) trypsin inhibitor, 20.1 kDa, 2) ovalbumin, 45 kDa, and 3) BSA, 66 kDa.



Figure 2-12: Image of 150 nm particle bed separation channels at **(a)** 30 V/cm (no crack was observed during separation), and **(b)** 65 V/cm (particles started to move from the walls of the chip, indicated by blue oval shaped). Both images were taken from the same chip during operation

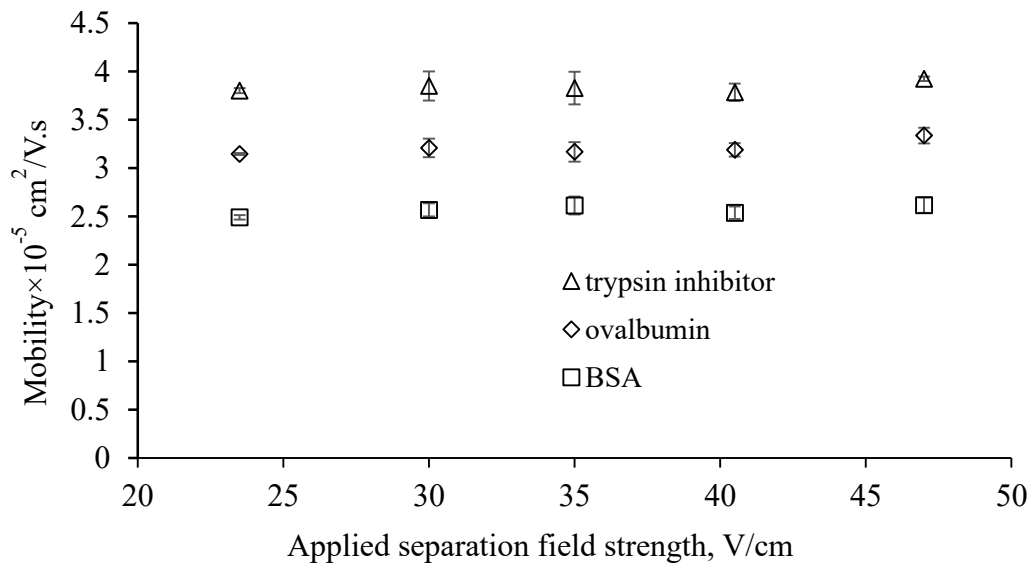


Figure 2-13: Mobility vs applied separation field strength plot of three different proteins; trypsin inhibitor, 20.1 kDa; ovalbumin, 45 kDa, and BSA, 66 kDa. Error bars show the standard error ($n=3$).

2.3.3 Separation performance of different particle beds

Figure 2-14 shows electropherograms obtained at 35 V/cm with nominal pore sizes of 103, 45 and 22 nm in particle beds formed from 690, 300 and 150 nm particles are for a mixture of 4 proteins, as the nominal pore size is the 15% of the particle size. The best performance (Figure 2-14c) was obtained with 150 nm particles, which yield the smallest pore size of ~22 nm. In this bed, the minimum plate height decreases with increasing applied field strength as expected, from 3.2 μm at 25 V/cm to 2.1 μm at 45 V/cm. This results are comparable to previous work with unstabilized colloidal self-assembled nanoparticle beds in microchip,¹⁴ and for crossed linked polyacrylamide gel¹⁶ in microchips. With the largest pore size studied, the mixtures of four proteins were not completely resolved from each other (Figure 2-14a), presumably due to insufficient frictional drag as the proteins passed through the 103 nm pores. As the pore size decreased, resolution of each of the proteins improved (Figure 2-14 b and c). The mobility of the smallest protein, aprotinin, was almost the same for all of the pore sizes, indicating aprotinin could move freely through the bed with essentially no retardation effect. For all large proteins, there was increasing retardation of protein migration with decreasing pore sizes.

The sieving process for SDS-protein complexes in gel is well studied⁷⁷ and there is a strong dependence of molecular weight. The size and shape of SDS-protein complexes has been extensively considered with a rod-like structure decorated by a “pearl necklace” of SDS micelles being the dominant model⁶¹. The size and length of SDS-protein complexes depends on their structure. The frictional interaction of SDS-protein along the length is proposed to control retardation in the pore lattice. This model allows to conclude

that due to insufficient retardation by friction with the pore walls, the largest pore sizes do not resolve the proteins. When proteins experience enough retardation from a lattice they can be resolved by migration rate differences, explaining the improved resolution seen with smaller pores.

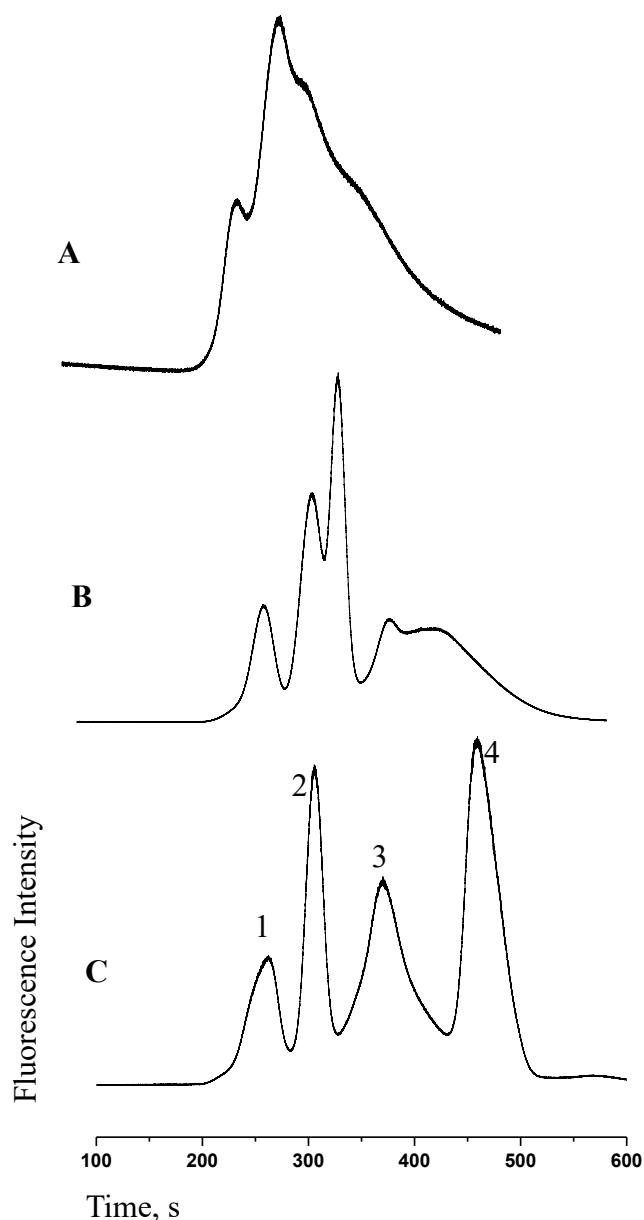


Figure 2-14: Electropherogram of four different proteins: 1) aprotinin, 6.5 kDa; 2) trypsin inhibitor, 20.1 kDa; 3) ovalbumin, 45 kDa; and 4) BSA, 66 kDa using different particle beds: A) 690 nm; B) 300 nm; and C) 150 nm using 35 V/cm separation voltage for a 4 mm separation distance ($L = 4$ mm).

2.3.4 Comparing separation models for a CSA bed of nanoparticles

The separation mechanism of SDS-protein complexes was evaluated with two differing models, one which considers a random pore distribution about a mean value, and the other which assumes a uniform pore size. Testing both models may provide an alternative method to characterize the actual pore structure. Model 1, the modified Ogston Morris Rodbard Chrambach (OMRC) ^{17,90,91} equation, is applied to gel electrophoresis. Model 2, sieving through a uniform pore structure is Wirth's adaptation ¹⁷ of the Giddings model. ⁹² Here we examine the quality of fit of both models, and present a simple approach to using the Wirth/Giddings approach for molecular weight calibration curves.

2.3.4.1 The modified Ogston Morris Rodbard Chrambach (OMRC) equation for gel electrophoresis

In the classical sense, effective molecular sieving exists only in the Ogston regime. ⁸⁸ In this regime it is assumed that the migrating analytes behave like unperturbed spherical objects, and the average pore size of the matrix is larger or in the same range as that of the hydrodynamic radius of the migrating analyte. The modified Ogston Morris Rodbard Chrambach (OMRC) equation ⁹⁰ for mobility in gel electrophoresis in a medium with a random pore size distribution is:

$$\mu = \mu_0 \exp(-K_r T) \quad 2.5 \text{ a}$$

or
$$\log(\mu) = \log(\mu_0) - K_r T \quad 2.5 \text{ b}$$

where μ (cm^2/Vs) is the mobility of SDS-protein complex in a medium, μ_0 is the mobility of in free solution, K_r is the retardation coefficient of the SDS-protein complex and T is the total acrylamide concentration in the gel. Equation 2.5b is known as the Ferguson equation.¹¹¹ The retardation coefficient depends on the size of the protein and the sieving properties of the separation matrix, arising from frictional forces between the protein and walls of the pores. The value of K_r increases as the protein size or molecular weight increases.⁶⁹ Based on empirical evidence, K_r is known to be proportional to the molecular weight (M) of SDS-protein^{69,91} at a constant gel concentration, giving:

$$\log \mu \propto (-M) \quad 2.6$$

where M is the molecular weight of protein. Equation 2.6 provides a convenient way to experimentally prepare a molecular weight calibration curve with protein standards.

A mixture of protein standards was run through different size particle CSA beds, giving the plot of $\log \mu$ vs. molecular weight shown in Figure 2-15, for each particle size. The plot of equation 2.6 for each particle bed shows good linearity ($R^2 = 0.980$ to 0.997). The linear plots indicate an Ogston-like sieving mechanism applies for SDS-protein complexes between 6.5 and 66 kDa in the particle bed.

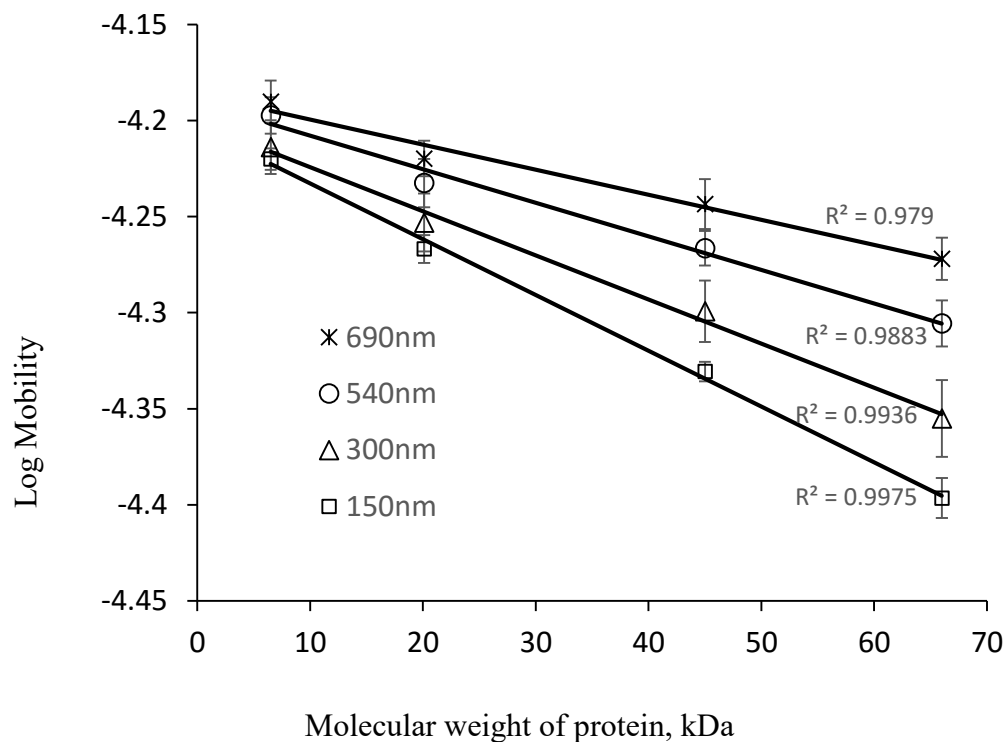


Figure 2-15: The log mobility vs molecular weight of protein plot using different size particle beds (690, 540, 300 and 150 nm). The error bars are the standard errors at the 95% confidence level ($n=7$)

Another known test for the Ogston regime is to evaluate if a plot of $\log \mu$ of SDS-protein vs. $\log M$ shows a non-linear trend.^{77,91} The non-linear curve shapes observed for such plots (Figure 2-16), for every particle diameter, are consistent with the Ogston sieving regime (Figure 1-12).

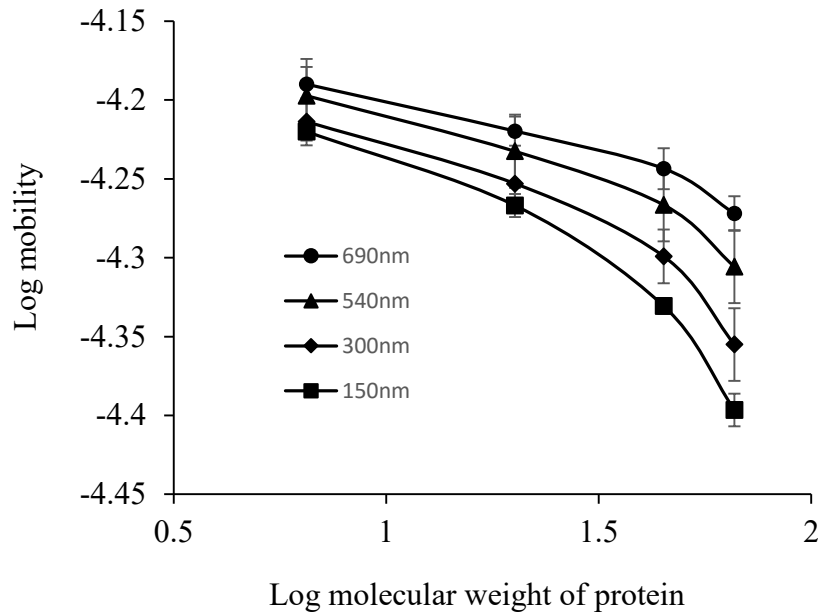


Figure 2-16: The double logarithmic plot of mobility vs. molecular weight of protein using different particle beds (690, 540, 300, and 150 nm). The error bars are the standard errors at the 95% confidence level ($n=7$).

2.3.4.2 Retardation coefficient and protein sizing by Ferguson

Analysis

A plot of the Ferguson equation (2.5b) for a gel gives the retardation coefficient from the slope.¹⁶ In a gel, increasing %T decreases the pore size,⁹⁰ which is the relevant parameter to describe the frictional retardation. Whereas in the CSA bed increasing the particle diameter, D , also increases the interstitial pore size. By analogy to equation 2.5b, the equivalent Ferguson equation for a CSA bed has the form of:

$$\log \mu = \log \mu_0 + K_r' D \quad 2.7$$

where D is the diameter of the particles (or the interstitial pores), and the sign is changed from equation 2.5b, since the dependence on the size parameter is inverted with the gel.

To determine the retardation coefficient in CSA beds, standards were separated using 690, 540, 300 and 150 nm particle beds under the same conditions. The plot of $\log \mu$ versus the nominal pore size (15% of the particle size) of the bed yields the equivalent of a Ferguson plot, Figure 2-17. The least squares fit for each protein standard showed high linearity ($R^2 = 0.990$ to 0.999), and the curves illustrate that larger proteins are retarded more effectively as the pore size decreases. A plot of retardation coefficient, K'_r (slope of the lines from Figure 2-17), vs. protein molecular weight is shown in Figure 2-18. This illustrates that the retardation coefficient is highly correlated with protein molecular weight ($R^2 = 0.995$). The results show that use of the classical gel-based separation equations can provide a means to analyze the mobility versus molecular weight data and to calibrate the molecular sieving process.

The free solution mobility, in the case of gel electrophoresis, is readily calculated from the 0% gel concentration. But it is very hard to get the free solution mobility from the nanoparticle bed Ferguson plot (Figure 2-17). To get an idea about the free solution mobility, the same proteins were individually studied by capillary zone electrophoresis instrument with a 75 μm ID bare silica column, using same buffer composition giving the values shown in Table 2-2, after correcting for electroosmotic flow. The results indicate that the free solution mobility of SDS-protein complex is independent of molecular weight of protein. This result is expected as the mass to charge ratio of each SDS-protein complex is the same to first approximation.

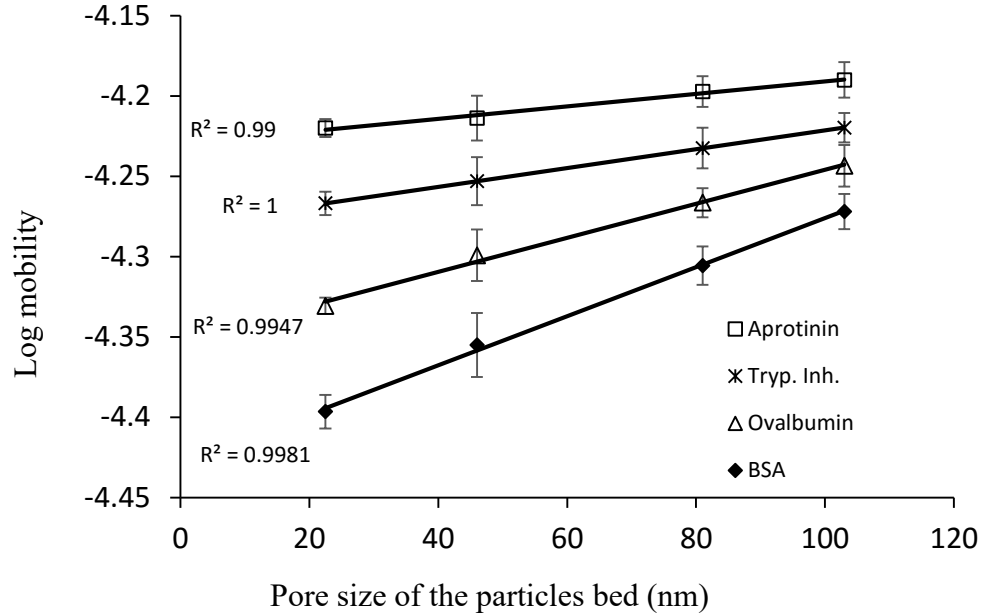


Figure 2-17: The plot of logarithmic mobility vs pore size of the particles for different proteins. (aprotinin, 6.5 kDa; trypsin inhibitor, 20.1 kDa; ovalbumin, 45 kDa; and BSA, 66 kDa). The slope of each curve is the retardation coefficient of each protein. The retardation coefficients are: aprotinin, 6.5 kDa, $K_r = 3.87 \times 10^{-4}$; trypsin inhibitor, 20.1 kDa, $K_r = 5.86 \times 10^{-4}$; ovalbumin, 45 kDa, $K_r = 1.06 \times 10^{-3}$; and BSA, 66 kDa, $K_r = 1.53 \times 10^{-3}$ (The error bars are the standard error at 95% confidence level, $n=7$)

Table 2-2: Free solution mobilities using capillary electrophoresis

Protein	Free solution mobility (cm^2/Vs)
Aprotinin, 6.5 kDa	3.86×10^{-4}
Trypsin Inhibitor, 20.1 kDa	3.85×10^{-4}
Ovalbumin, 45 kDa	3.78×10^{-4}
BSA, 66 kDa	3.70×10^{-4}

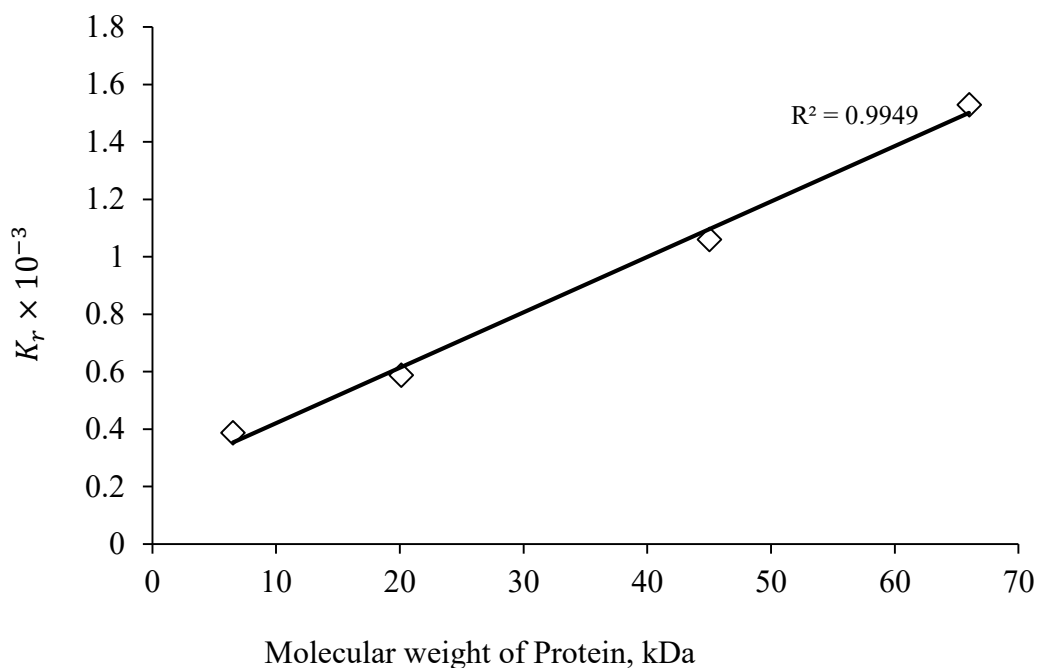


Figure 2-18: A calibration plot between the protein molecular weight and the retardation coefficient using random pore model (slope from the plot 2-17, each point of this plot is generated from 28 points)

2.3.4.3 Sieving through a uniform pore structure: Giddings model

These CSA beds are thought to be comprised largely of a uniform pore size, though various defects are expected to expand the range of pore sizes on the high side, so that the classical gel model discussed above is not strictly accurate. Giddings description of accessible fractional volume within uniform cylindrical pores⁹² of colloidal crystal was scaled by a porosity factor, ϵ , by Birdsall et al.¹⁷ to describe the reduced free volume in a bed packed with solid particles. The revised model for SDS-protein separation derived in a uniform pore size matrix becomes:

$$\frac{\mu}{\mu_0} = \varepsilon \left(1 - \frac{R}{r}\right)^2 \quad 2.8$$

where μ is the mobility of analyte, μ_0 is the free solution mobility, R is the radius of analyte, and r is the radius of the pore. Wirth and coworkers¹⁷ demonstrated equation 2.8 fit the data obtained with a polymer entrapped CSA bed after determining all of the parameters of the column and analytes, such as ε , r and μ_0 . However, this approach is not convenient for everyday experimental performance, for which a simple calibration curve approach equivalent to equation 2.5b is desirable.

Rearranging equation 2.8 provides a form that can be readily plotted and used to evaluate mobility versus molecular weight data with molecular weight standards:

$$\sqrt{\mu} = C - C/r \times R \quad 2.9$$

where $C = \sqrt{\mu_0 \varepsilon}$, the free solution mobility of SDS-protein complex, μ_0 , is constant and for ideal face centered cubic crystal porosity, $\varepsilon = 0.26$. So C is also constant. The spherical radius of analyte is calculated as the radius of hydration of a denatured protein using:⁶³

$$R = 2.21 N^{0.57} \text{Å} \quad 2.10$$

where N is the number of amino acid units in a protein. A plot of $\sqrt{\mu}$ vs. the radius of protein, R , in different particle sizes of beds is shown in Figure 2-19. The plot for each particle bed shows better linearity ($R^2 = 0.992$ to 0.997) than the equivalent fit to the OMRC equation ($R^2 = 0.98$ to 0.997). We note the fit is of the same quality when using the expression for the radius of gyration of native proteins⁶⁴, R_g , (Figure 2-20), as done by Birdsall et al. to approximate the size of SDS denatured protein complexes.

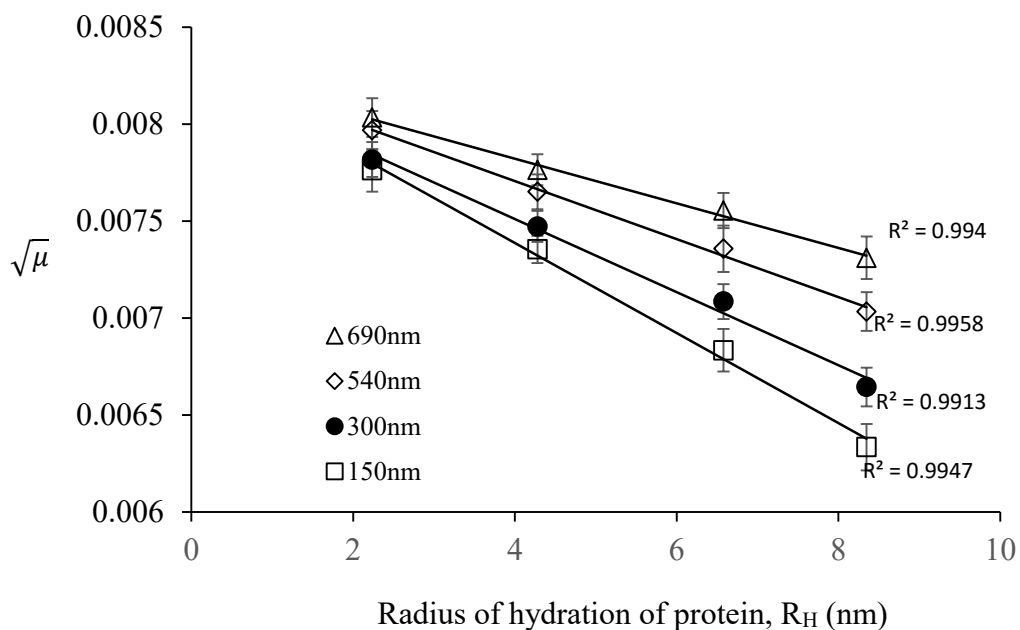


Figure 2-19: A plot of square root of mobility, $\sqrt{\mu}$ vs. radius of hydration protein, R_H , using different particle beds. (The error bars are the standard error at 95% confidence level, $n=7$)

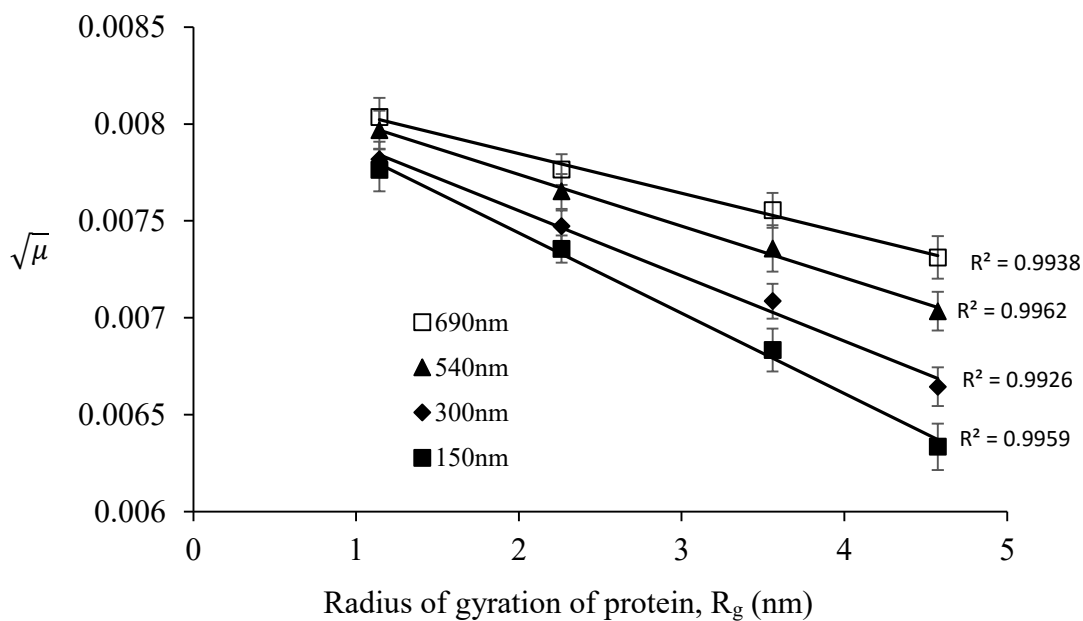


Figure 2-20: A plot of square root of mobility, $\sqrt{\mu}$ vs. radius of gyration of protein, R_g , using different particle beds. (The error bars are the standard error at 95% confidence level, $n=7$)

2.3.4.4 Retardation coefficient and protein sizing using Giddings analysis

From equation 2.9, a plot of $\sqrt{\mu}$ vs $\frac{1}{r}$ for a given protein hydrodynamic radius, R_H , should be linear, and is the equivalent of a Ferguson plot, with the slope of each line (Figure 2-21) giving a retardation coefficient, $K_r'' = CR$. The least squares fit for each protein standard showed very high linearity ($R^2 = 0.990$ to 0.991). As the protein size increases the steepness of the line also increases, just as in a Ferguson plot. It is common to make the approximation that molecular weight can be substituted in the mobility expressions in equation 2.5 to give equation 2.6 for a gel, and this is supported empirically.

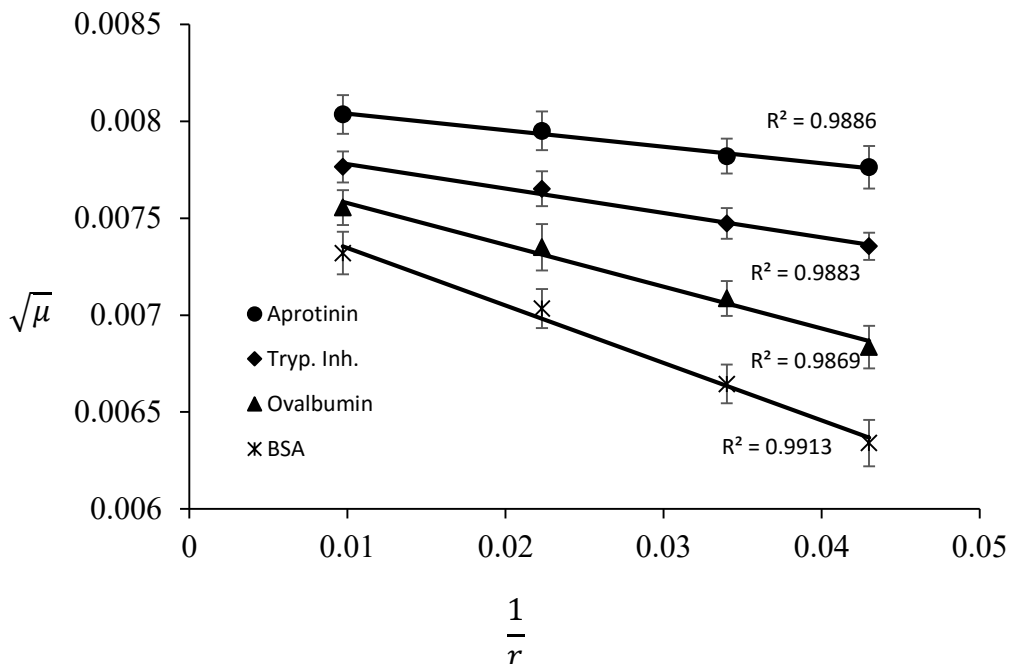


Figure 2-21: Square root of mobility vs. inverse of pore size of the particle beds plot. The slope of the line for each protein is calculated as: aprotinin = 8.120×10^{-3} ; trypsin inhibitor = 1.257×10^{-2} ; ovalbumin = 2.156×10^{-2} ; and BSA = 2.967×10^{-2} (The error bars are the standard error at 95% confidence level, $n=7$)

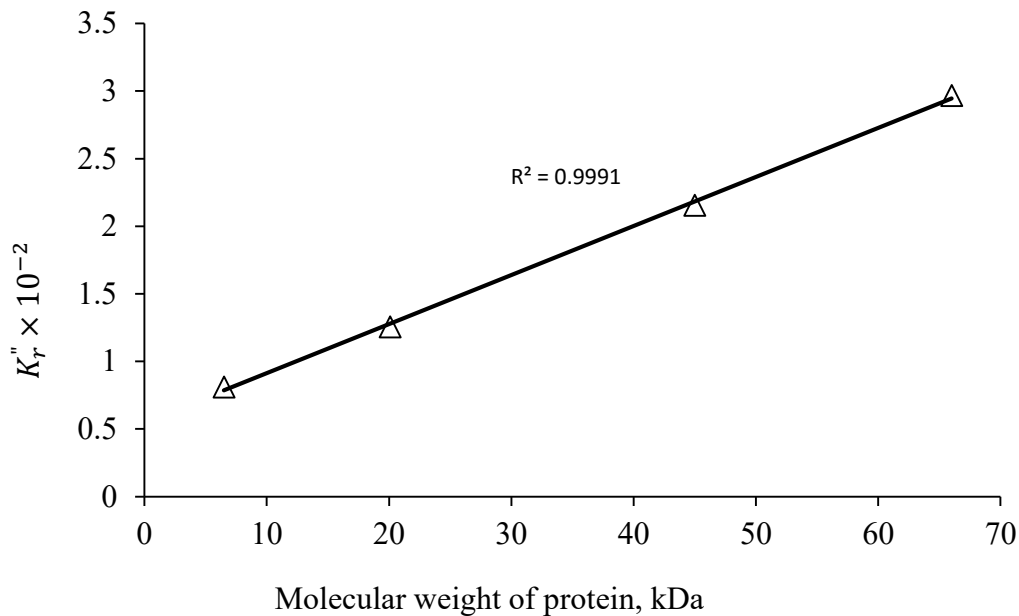


Figure 2-22: A calibration plot between protein molecular weight vs retardation coefficient for CSA particle beds using the Giddings analysis of uniform pore (slope from the plot 2-21, each point of this plot is generated from 28 points)

The calibration curve for the retardation coefficient, K_r'' , from the Wirth/Giddings formulation (equation 2.9) vs. molecular weight is shown in Figure 2-22. The fit to this equation for a uniform pore size shows higher linearity ($R^2 = 0.9991$) than the calibration plots using the modified Ferguson equation (equation 2.7).

These findings indicate that CSA beds are better described as a uniform pore size bed than as a random pore size bed. Given the difficulty of actually measuring the pore size in the very low volume beds formed by CSA for separations, this observation can also be taken as confirmation that the beds do tend toward a uniform pore size.

2.3.5 Protein sizing using the retardation coefficient

The same four proteins explored above were used as a set of molecular weight standards, to then determine the molecular weight of two other “test” proteins; 1) α -lactalbumin (14.2 kDa) and 2) carbonic anhydrase (29.2 kDa). The molecular weights of these two proteins are in-between the molecular weight of proteins used for the calibration curve of the retardation coefficients. Both proteins were denatured with SDS and the SDS-protein complexes were run individually, and also in a mixture. An electropherogram of the mixture using 150 nm particle beds at optimized field strength is shown in Figure 2-23.

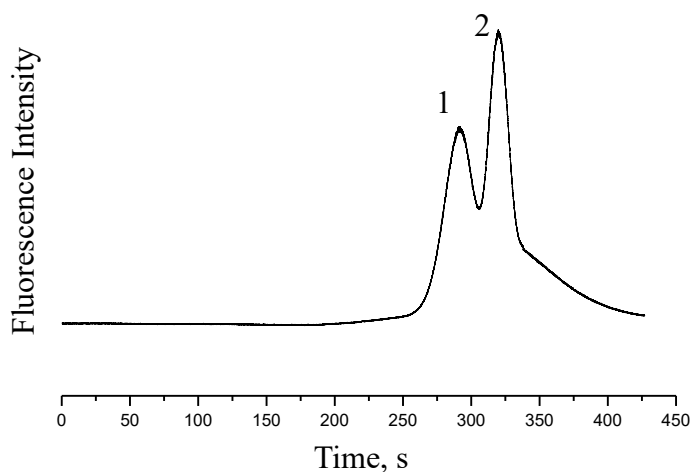


Figure 2-23: An electropherogram of: 1) α -lactalbumin – 14.2 kDa and 2) carbonic anhydrase – 29.2 kDa using a 150 nm particle bed at 35 V/cm field strength and detected at 4 mm separation distance

The electropherogram of the pair in a 150 nm particle bed at 35 V/cm is superimposed on the electropherogram of the standards (Figure 2-24). It is clear that the position of the α -lactalbumin and carbonic anhydrase peaks straddle the 20.1 kDa peak of

trypsin inhibitor, as they should. The plot demonstrates that protein sizing is possible using colloidal self-assembled nanoparticle beds in microchannels.

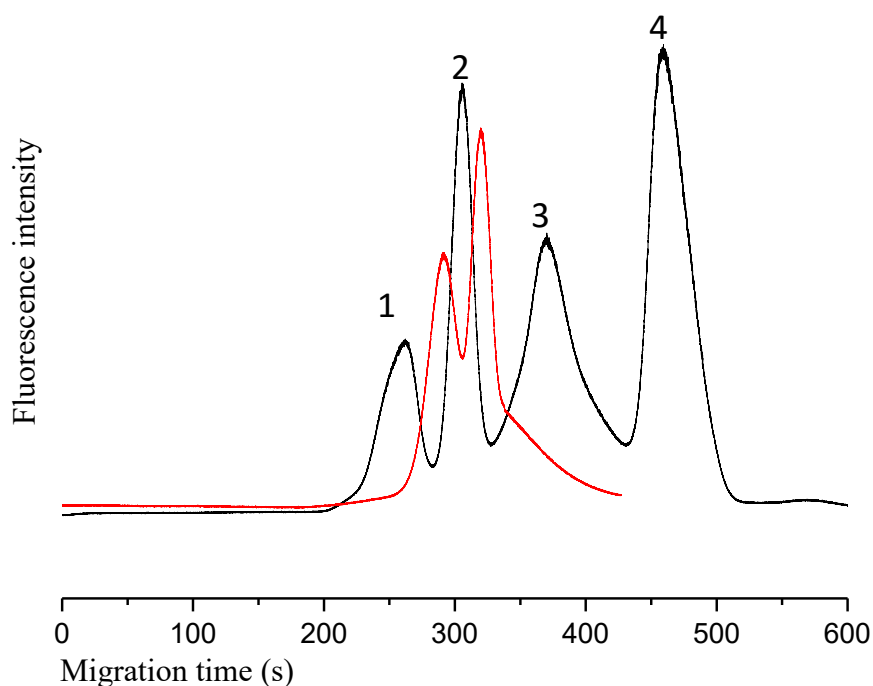


Figure 2-24: The superimposed electropherogram of α -lactalbumin: 14.2 kDa and carbonic anhydrase: 29.2 kDa (red color) in a previously achieved electropherogram of four protein mixture of: 1) aprotinin, 6.5 kDa, 2) trypsin inhibitor, 20.1 kDa, 3) ovalbumin, 45 kDa; and 4) BSA, 66 kDa using a 150 nm particle bed at 35 V/cm field strength and detected at 4 mm separation distance

The molecular weights of α -lactalbumin (14.2 kDa) and carbonic anhydrase (29.2 kDa) were estimated using a least squares fit of $\log \mu$ vs molecular weight for the individual particle beds (Figures 2-17 and 2-21). However, just as in gel electrophoresis,^{16,59,91} it is more accurate to determine the retardation coefficients using various pore sizes. Using the calculated retardation coefficient from both pore size models (Table 2-3), the molecular

weight of the test proteins were estimated from the respective calibration curves (Figures 2-18 and 2-22) for each model by the least squares method.

Table 2-3: Retardation coefficient of α -lactalbumin and carbonic anhydrase

Protein	Retardation coefficient	
	Using Ferguson Equation $10^{14}nm/(V.s)$	Using Giddings equation $\frac{10^7nm^2}{\sqrt{V.s}}$
α -lactalbumin	4.63×10^{-4}	1.10×10^{-2}
carbonic anhydrase	7.15×10^{-4}	1.62×10^{-2}

The estimated molecular weights from both models are presented in the Table 2-4 and compared with the supplier reported molecular weight. From Table 2-4, it is clear that retardation coefficient, K_r'' , from the modified Giddings equation (2.9) gives more precise molecular weight estimation for both proteins when using the CSA particle beds.

Table 2-4: Comparison of estimated molecular weight with supplier molecular weight

Protein	Molecular weight, kDa	Estimated molecular weight, kDa	
		Using Ferguson Equation	Using Giddings equation
α -Lactalbumin	14.2	13.2 ± 0.8	14.6 ± 0.6
Carbonic Anhydrase	29.2	25.8 ± 0.7	29.0 ± 0.8

2.4 Conclusions

This work compares the analysis of SDS-protein complex separations in a colloidal self-assembled particle bed by classical, modified Ogston sieving for protein separation in a porous media, and with the Wirth/Giddings modified expression for separation in a single pore size medium. The results show improved fits and better predictive interpolations of the molecular weight of unknowns using the Wirth/Giddings model for a uniform pore structure. The better predictive power of the single pore size model indicates that it is meaningful to characterize these structures as having a predominantly single pore size. Additionally, we have shown that simple manipulation of the Wirth/Giddings equation gives a convenient method to generate calibration curves for a function of mobility versus molecular weight of protein standards, as is commonly done in gel electrophoresis.

Chapter 3

Fabrication of Highly Stabilized Colloidal Self-Assembled Nanoparticle Beds in Microchannels for High Performance Size-Based Protein Separations*

3.1 Introduction

During the last two decades, the advancement of protein separation techniques has received less attention compared to protein analysis and characterization.¹¹² Protein separation is very important as an analytical tool; leading to better understanding of diseases at a molecular level, the discovery of protein biomarkers for diseases and protein-based drug development.¹⁵ Size-based protein separations are routinely used in research⁴⁰ and the pharmaceutical industry,¹⁷ so further improvement in size-base protein separation performance remains important. Separation performance improvement means improving the resolution in a given analysis time. The resolution of separated compounds is a combination of three terms: column efficiency, selectivity and retention, as summarized in Equation 3-1:^{15,113}

$$R_S = \frac{\sqrt{N}}{4} \times \left(\frac{\alpha-1}{\alpha}\right) \times \left(\frac{k_2}{1+k_2}\right) = \frac{\sqrt{L/H}}{4} \times \frac{\Delta t}{\langle t \rangle} \quad 3.1$$

* A version of this chapter has been published in the Proceeding of 19th International Conference on Miniaturized Systems for Chemistry and Life Sciences as, "Highly Stabilized Colloidal Self Assembled Nanoparticle bed in Microchannels for High Performance Size Based Protein Separation" Mohammad Azim, Abebaw B. Jemere and D. Jed Harrison, MicroTAS 2015; Gyeongju, South Korea ; 1978-1980

where R_s is the resolution, N is the plate number, which is the ratio of separation length, L , and plate height, H . The selectivity, α , and retention factors, k_2 , can be expressed as the ratio of migration time difference and average migration time, i.e. $\Delta t/\langle t \rangle$. Among all the parameters, plate height is very important for increasing resolution. The smaller the value of H , the sharper the peak, so that better resolution is achieved. Improving H requires material advances for the separation matrices.¹⁵

Colloidal self-assembly (CSA) of nanoparticle beds in a microchip column for biomolecule separation has the potential to provide ultra-high separation efficiencies, as a result of the nano-scale pore sizes and efficient packing. One of the major advantages of a miniaturized system is higher separation speed. Higher speed and better separation performance should be easily achieved if the separation field strength is high. However, native CSA nanoparticle bed performance is currently limited, by the instability of the packed bed at higher voltages (≥ 320 V/cm).

Several approaches have been reported to stabilize a colloidal self-assembly of particles. Among them, heat treatment is one of the widely reported processes; for example, heat treatment after packing,^{46,52,114,115} and heating and blowing away the vapor during packing⁴⁵. Efficient protein separation requires smaller pores, which can be fabricated using nanoparticles. But cracking of the dried nanoparticle colloidal films frequently occurs.^{109,110,116-121} Moreover, heating can create more defects in a crystalline assembly, affecting subsequent separations. Writh's group has reported the use of a polymer layer formed by horizontal polymerization to immobilized silica particles in capillaries to separate proteins^{15,43} and dyes.¹⁰⁵ These approaches are useful, but introduce

additional steps in fabrication and increase the time it takes to make a functional chip for separation.

The crystalline quality of CSA beds and their defect density depends on the thickness of the bed and the crystal growth rate.¹²² With increasing thickness and higher growth rate, a poorer crystal quality is observed. Here we report a new approach to stabilization by improving the crystal lattice. By narrowing the capillary bore in which the CSA bed grows, we greatly stabilize the bed, due to the reduced number of defects, and perhaps also the greater influence of the capillary wall on the bed. The usability of very narrow bore CSA beds for high voltage separations of SDS-protein complexes by sieving-based separations is demonstrated.

3.2 Theory of defect formation

The types and reasons for defect formation in a CSA bed need to be understood in order to improve crystal quality. Koh et al.¹²³ and Teh et al.¹²² studied the type and nature of defects and growth imperfections in self-assembled colloidal crystals, and the origin of these defects. According to their studies, macro-defects such as cracks and micro-defects such as vacancies, stacking faults or phase boundaries are the major types of defects, and very common in three dimensional colloidal self-assembly of nanoparticles. Teh et al.¹²² confirmed that the overall crystalline quality, i.e., the number of defects or imperfections, increases with increasing thickness of the colloidal film. The et al.¹²² prepared different thicknesses of self-assembled colloidal films at a constant temperature and concluded that

as the thickness increases the flux of nanoparticles increases due to the more rapid evaporation. Because nanoparticles get insufficient time to shift to the thermodynamically favoured condition, the result is a relatively poorer quality crystalline array, with different types of defects.

O'Mahnoy et al¹²⁴ studied the thermodynamics of defect formation in self-assembly systems. A reasonable concentration of distinct irregularities or defects is present in every self-assembly. The defect formation free energy, ΔG_{DF} , for a single defect is given by:

$$\Delta G_{DF} = \Delta H_{DF} - T\Delta S_{DF} \quad 3.2$$

The enthalpy term of a defect, ΔH_{DF} , is the energy associated with disrupting ideal self-assembly, and relates the enthalpy difference between the two structural arrangements ($\Delta H_{DF} = \Delta H_{defect} - \Delta H_{perfect}$). As the ideal/perfect system is a thermodynamically minimum energy system, the value of ΔH_{DF} is positive (+). So, a relatively low concentration of defects might be expected if ΔH_{DF} is high, while a reasonable defect population would be seen if there is a low ΔH_{DF} value. The entropy difference between perfect and defective structures is then, $\Delta S_{DF} = S_{defect} - S_{perfect}$.

If, ΔG_{DF} is negative there will be a finite number of defects in the self-assembly.

The concentration of defects can be calculated by

$$\frac{N}{N_0} = \exp\left(\frac{-\Delta E_{act}}{RT}\right) \quad 3.3$$

where N is the number of defects present in a structure of N_0 self-assembled moieties or features, R is the gas constant, T is the temperature in Kelvin and ΔE_{act} is the activation energy of defect formation.

From equation 3.3, it is clear that at a particular temperature, the ratio of defect lattice population to correct lattice site population is constant. For a structure of the same particle size and same length, the number of self-assembled moieties, N_0 , increases with the bed thickness. At a constant temperature the number of defects also increases with thickness, which was experimentally demonstrated by Teh et al.¹²²

Vacancies are indigenous in colloidal crystals. It is entropically favourable for a system to have some vacancies, so every self-assembly process results in some vacancies. The colloidal particles in solution have random Brownian motion. When the particles are freshly assembled in a packed structure, before they fully condensed, the layers of water around the particles allows them to oscillate about their lattice position. Vacancies can form during this period of oscillation, with cooperative displacement along the packed colloid.¹²³

Interstitial defects or dislocations are directly linked with the uniformity of the silica particle size used for colloidal crystal formation.¹²³ To minimize the crystal imperfection and maintain long range order better than 2% polydispersity is required.^{113,125}

Self-assembled colloidal spheres can be stacked into different shapes,¹²⁶ with crystalline arrangements, face centered cubic (FCC) and hexagonal close packed (HCP) being common. Both have very similar equations of state,¹²⁷ but FCC packing is slightly more thermodynamically stable than HCP. The structural differences between FCC and

HCP are illustrated in Figure 3-1. Both are constructed in three layers with no difference in the first two layers. In the first layer, the spheres are arranged in a hexagonal pattern. Then a second layer with the same structure is added, but is slightly shifted from first layer, filling the gaps of the first layer. For an HCP structure the third layer is formed directly over the same positions as the first layer, but for FCC, the third layer forms over gaps in the second layer, without aligning with the first layer. The Gibbs free energy difference between these two phases is very small¹²⁷⁻¹²⁹ ($G_{hcp} - G_{fcc} = 0.005RT$). So a colloidal self-assembled crystal is generally a polycrystalline mixture of FCC and HCP crystals, which results in a large number of plane stacking defects.¹²³ For slowly grown crystals, FCC is favoured over the HCP.^{130,131}

The evaporation temperature and crystal growth rate are two important parameters governing crystal quality. There is always an optimum temperature for better crystal structure. But the higher the evaporation rate, i.e., the higher the crystal growth rate, the more defects form. The kinetics associated with crystallization thus further increase the defect density. Yet the above analysis shows that defects can always be expected. Slower crystal growth and a decreased number of particles are the two easily controlled factors that can be used to reduce defects.

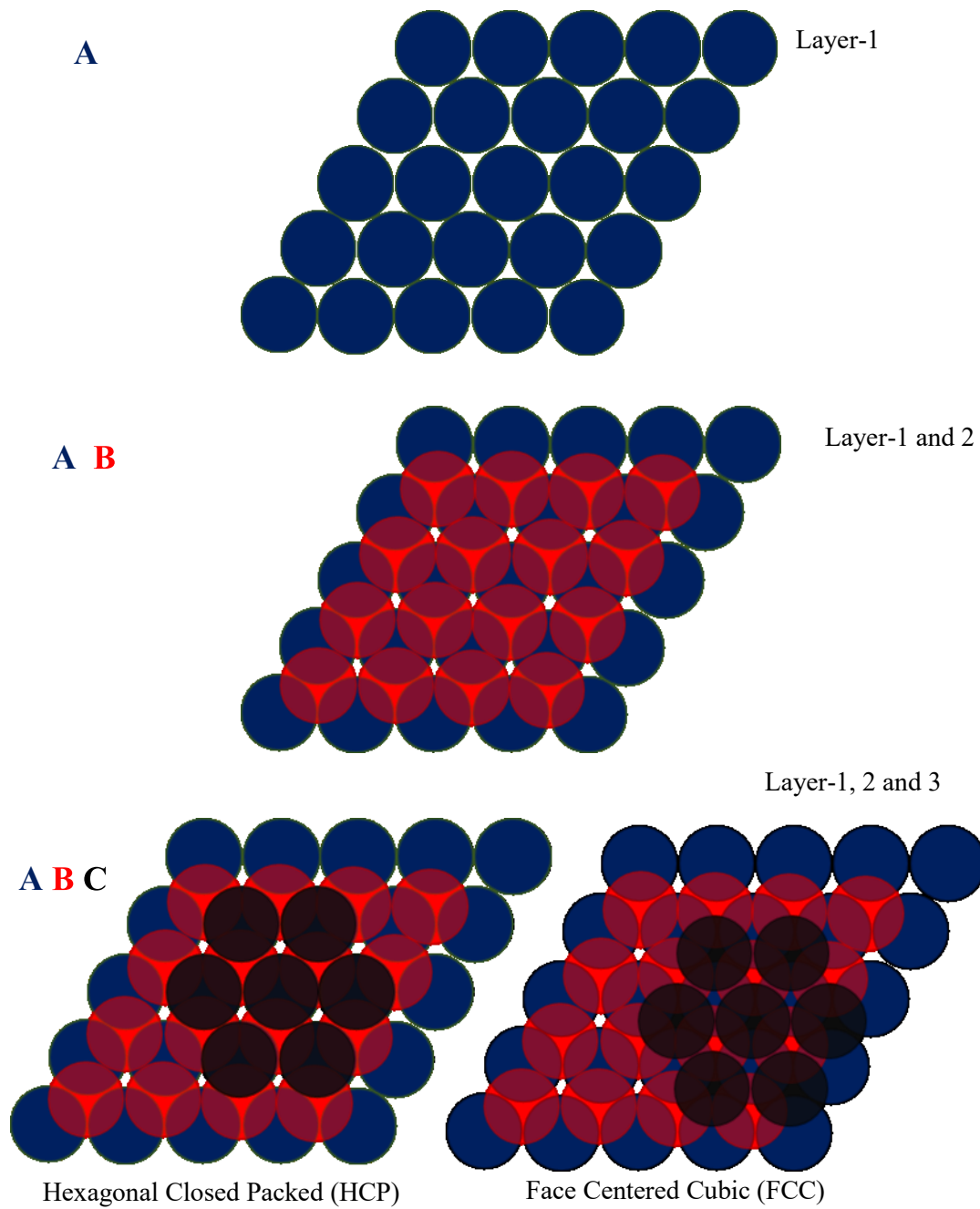


Figure 3-1: Construction of Hexagonal Close Packed (HCP) and Face Centered Cubic (FCC) structures.

3.3 Materials and methods

3.3.1 Protein samples and chemicals

As molecular weight standards, aprotinin (6.5 kDa), trypsin inhibitor (soybean, 20.1 kDa) ovalbumin (chicken egg, 45 kDa) and bovine serum albumin (BSA, 66 kDa), were from Sigma-Aldrich. All proteins were labeled with fluorescein-isothiocyanate isomer-I (FITC, Sigma) using the Sigma-Aldrich standard protein labeling procedure. For labeling, 2–4 mg/mL protein solutions were prepared in fresh 0.1 M bicarbonate buffer at pH 9. FITC was dissolved in dimethyl sulfoxide (DMSO) to prepare ~1 mg/mL solution. Fifty μ L FITC solution was added in 5 μ L aliquots in each mL of protein solution. The protein solution was gently stirred during addition of FITC solution. After labeling, the FITC-protein solutions were incubated overnight at 4⁰C in the dark. The labeled FITC-protein solutions were filtered using a 3 kDa molecular weight cut off filter at 13000 rpm for 30 min, then diluted with bicarbonate buffer and filtered again at the same rpm for another 30 min, to completely remove any unreacted FITC. To prepare buffer sodium dodecyl sulfate (SDS) (Sigma), 10x TBE (Tris (hydroxymethyl) aminomethane (tris base) 890 mM-boric acid 890 mM –EDTA 20 mM) buffer solution (Sigma) and 2-mercapto - ethanol were used in different proportions. 4x TBE, 4 w/v % SDS and 8 v/v % 2-mercapto-ethanol were used as sample buffer and 4x TBE and 0.1 w/v % SDS were used as working or running buffer. Aliquots of FITC labeled protein solutions were mixed with sample in the same proportion and incubated in a dry incubator at ~85⁰ C for about 5 min to denature the proteins. After cooling to room temperature, denatured protein samples were diluted with working buffer and refrigerated. Before separation, protein solutions were mixed

together and the final concentrations were adjusted to 10^{-5} to 10^{-4} mM for each protein with working buffer. 18.2 M Ω deionized water from an Ultrapure water system (Millipore, Milford, MA) was used to prepare all reagents and samples.

3.3.2 Microchip fabrication and colloidal self-assembly

Microchips were assembled using polydimethylsiloxane (PDMS) with a glass slide support as described previously.¹⁴ Briefly 15 mm long separation and 4 mm long injection channels (~ 100 μm wide and ~ 20 μm deep with a ~ 100 μm offset in the double T design) were patterned in a silicon wafer using photolithography. PDMS base (Sylgard 184, Dow Corning) mixed with crosslinking agent in 10:1 proportion was poured on the wafer and cured overnight at 60⁰ C. The PDMS replicas were removed from the wafer and cut into pieces and reservoir holes were punched to access the channels. The PDMS pieces were cleaned with 100% ethanol and MilliQ water, and dried with nitrogen. The clean and dry PDMS was attached with previously clean glass slides to get the microchips. The glass slides were cleaned in piranha solution (3:1 volume ratio of H₂SO₄ and 30% H₂O₂ (Caution: the piranha solution is highly corrosive, so proper safety gear must be worn. When first prepared the mixture becomes very warm and care must be taken it does not over heat while mixing. The mixture also evolves gas, so should not be stored tightly sealed). A view of the microchip and a simplified cartoon of CSA formation is shown in Figure 3-2.

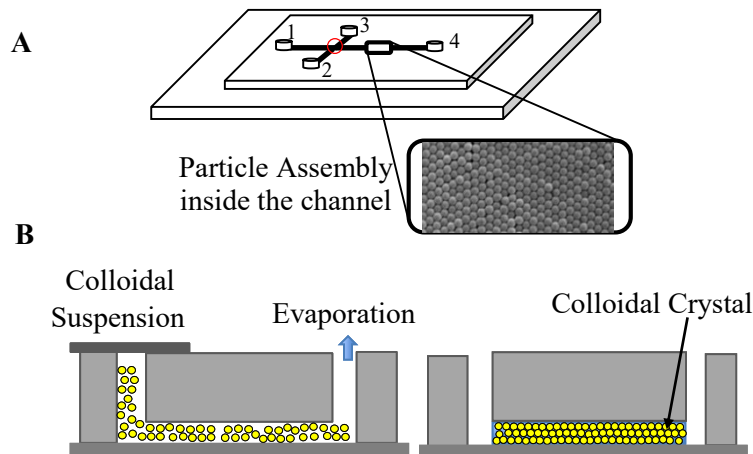


Figure 3-2: *Fabrication of CSA microchip: (A) final view of chip, and (B) mechanism of CSA formation.*

An evaporation-induced colloidal self-assembly mechanism was used for nanoparticle bed formation. 5.4 % to 10 % aqueous suspensions of monodisperse silica particles (Bang Laboratories, Poly Sciences Inc, manufacturer defined sizes were 150 ± 30 , 300 ± 40 , 540 ± 60 , and 690 ± 70 nm) were used (depending on availability), without any further modification or treatment for fabrication of the colloidal self-assembled (CSA) structure in the microchips, following the protocol described by Zeng et al.¹⁴ Zeng et al injected a colloidal suspension of nanoparticles in reservoirs 1, 2 and 3 with reservoir 4 left empty for evaporation (Figure 3-2A). This process worked well for 300 nm and even larger particles, but for smaller particles of 150, 100 nm or smaller diameter, if reservoir 4 was left empty, packing and cracking started almost simultaneously. The cracks propagated with time, making the separation channel unusable for separation. When either reservoir 2 or 3 were left empty instead of 4, with colloidal suspension in the other reservoirs, the separation channel was packed without any cracking. Before separation, the silica particles/water suspensions were replaced in all the reservoirs with working buffer and the devices were left for about 40 min to equilibrate.

3.3.3 Instrumentation and separation

A confocal epifluorescence microscope¹⁰⁸ was used to monitor the separation. The FITC labeled SDS-protein complex was excited with a 488 nm argon ion laser. The fluorescent response was collected with a Rollyn 10:1x, 0.30 NA lens, a 505 dichroic mirror, an 800 μm pinhole, a 530 ± 30 nm bandpass filter, and a photomultiplier tube (PMT). A Lab view program was used to store the PMT signal and to control the power supply, which was used to apply the required electrode voltage. All PMT signals were analyzed using Origin software.

The working buffer was run through the separation channel for about 20-30 min at 100 V before the separation started to give stable current through the channels. During injection, SDS-protein mixture was loaded from reservoir 2. A 60-80 V potential was applied in the sample waste reservoir 3, with all other reservoirs grounded. This formed a shaped injection plug which reduced the band broadening during the separation. During separation, equal positive and negative potentials were applied between the separation reservoirs (1 and 4) with the other two reservoirs grounded. The negative potential applied in reservoir 1 served as a push back potential to prevent sample leakage from the sample loading arms. The potential at the double T position (red circle position in Figure 3-2 A) was estimated by application of Kirchhofs rules.¹³² The negatively charged SDS-protein complexes migrated towards the anode and the laser spot was located at a fixed distance (5, 10 and 13 mm) from the double T position to excite the FITC labelled SDS-protein complexes.

3.4 Results and discussion

3.4.1: Importance and effect of higher voltage separations

An electropherogram of aprotinin (6.5 kDa), trypsin inhibitor (20.1 kDa), ovalbumin (45.0 kDa) and BSA (66.0 kDa) mixture using a 300 nm particle bed at 35 V/cm and 4 mm detection point is shown in Figure 3-3. BSA took about 7 min to migrate the 4 mm and the resolution between trypsin inhibitor and ovalbumin was very low. The calculated plate number for aprotinin is 1.4×10^5 plate/m, which is low. Among many other advantages, fast and high resolution separations are the main capabilities on offer from microfluidic technologies.¹³³ Yet these advantages were not achieved at this low field strength.

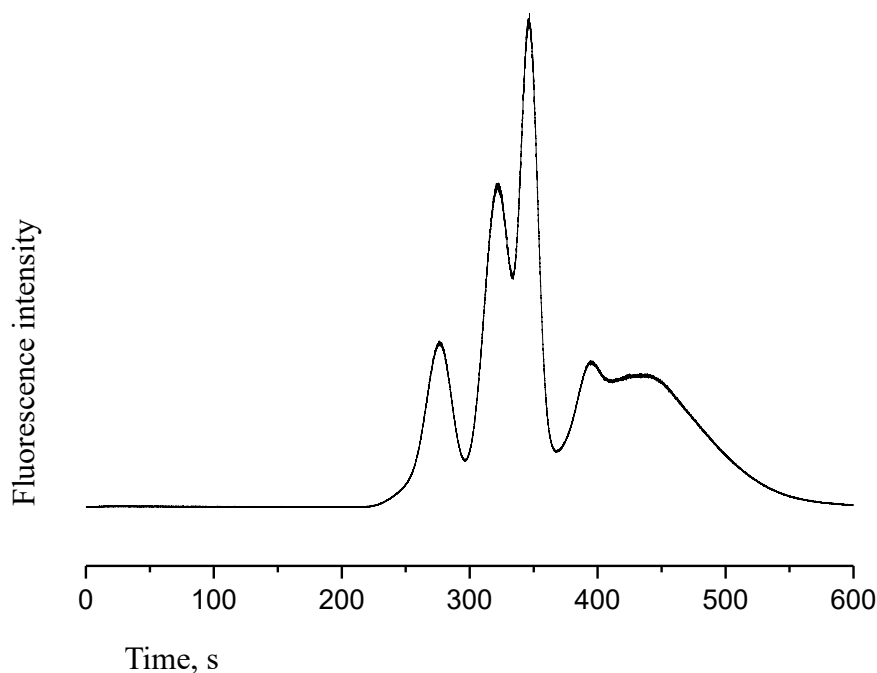


Figure 3-3: An electropherogram of the four protein mixture using 300 nm particle bed at 35 V/cm separation voltage, and detection at 4 mm

When the separation was performed at 160 V/cm (Figure 3-4) comparatively better separation was achieved, in terms of both separation resolution and time. Significant improvement in plate number was seen for aprotinin, which is increased from 1.4×10^5 plate/m (at 35 V/cm) to 4.5×10^5 plate/m. BSA took just over a minute to migrate through the 5 mm distance, but still there is scope for better separation.

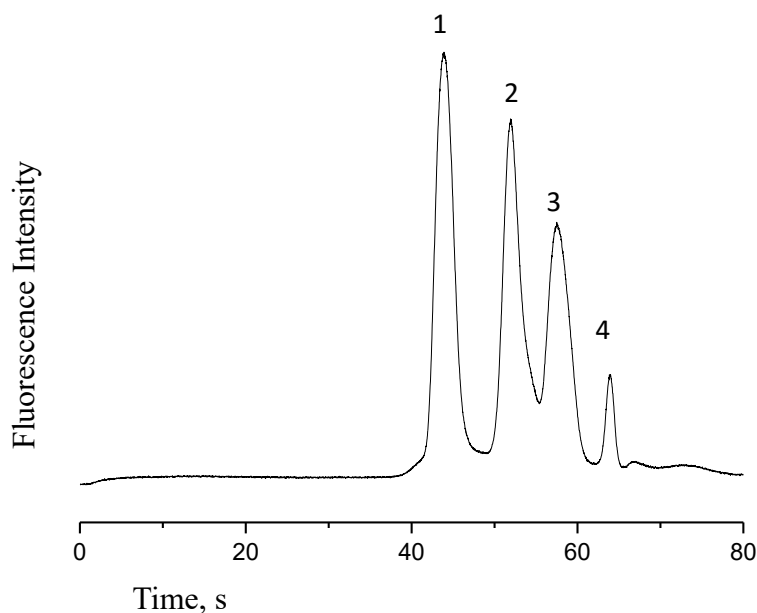


Figure 3-4: An electropherogram of the four protein mixture using a 300 nm particle bed at 160 V/cm separation voltage and detection at 5 mm (1: aprotinin, 6.5 kDa, 2: trypsin inhibitor, 20.1 kDa, 3: Ovalbumin, 45 kDa, and 4: BSA, 66 kDa).

Obviously, to achieve better separation performance in terms of resolution, plate height and time, and to exploit the maximum benefit of a miniaturized system, a high electric field separation is very important. Unfortunately, the colloidal self-assembled nanoparticle bed is not stable at higher voltages. An electropherogram using a 300 nm

particle bed at 450 V/cm is shown in Figure 3-5. It is clear that no effective separation was achieved. The four protein mixture produced only one peak, even though separation was achieved at 160 V/cm separation voltage (Figure 3-4). At higher separation voltage, the bed was not stable enough to give effective separation. The visual evidence makes it clear the particles in the bed are mobilized, as the bed vanished towards the anode.

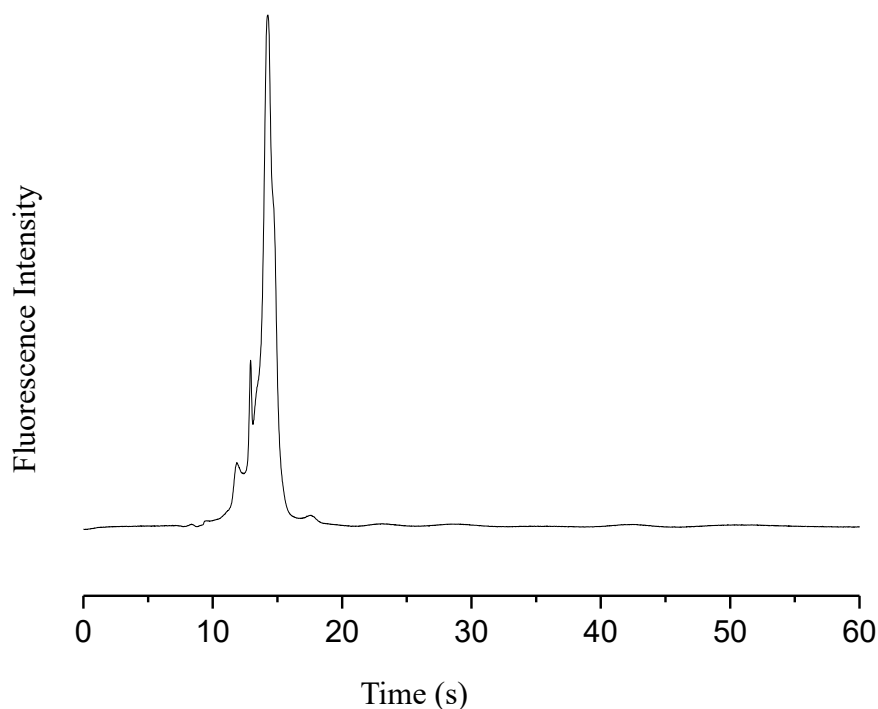


Figure 3-5: An electropherogram of four protein mixture using 300 nm particle 20 μ m thick bed at 450 V/cm separation and 5 mm detection.

The stability of a bed was found to be highly dependent on the particle size. The 300 nm particle, 20 μ m thick bed, was stable up to 320 V/cm, whereas it was very hard to work with a 100 nm particle, 20 μ m thick bed. Whatever voltage was applied, the smaller

particle (100 nm and below) beds cracked, and no effective separation was achieved. Table 3-1 summarizes the stability of the different particle beds studied.

Table 3-1: Stability of different particle bed of 20 μm thickness

Size of silica nanoparticles	Stability of 20 μm thick packed bed
300 nm	≤ 320 V/cm
150 nm	≤ 60 V/cm
100 nm	Very hard to work with

To exploit the maximum benefit from the smaller particle assembly and to make the chip suitable for higher voltage applications, stabilization of particle beds is needed.

There are many methods reported in the literature to stabilize the colloidal self-assembled nanoparticle bed, for example: heating,^{46,52,114} use of polymer formation to act as a glue^{15,17,43} to hold the particles together, etc. All of the methods add some extra steps to fabrication. Moreover, some of them are not suitable for smaller particle bed stabilization.

3.4.2 Heating of colloidal self-assembled beds

Heat treatment is one of the widely reported processes used to stabilize CSA beds for high voltage/pressure applications. Adam et al.⁴⁶ proposed a mechanism of stabilization of a colloidal assembled bed of particles by hydrothermal treatment involving inter-particle bonding. They postulated that upon heating, a saturated solution of polysilic

acid is formed by dissolution of the silica in water at the outer surface of particles. During cooling, the polysilic acids re-deposit as silica and fuse the particles together chemically. The same process was applied by Ceriotti et al.⁵² in microchip. They packed microchannels with 3 μm size silica particles, and then the chip was heated at 115⁰ C overnight (10 h). The interstitial spaces of the packed bed in the microchannels were filled with water when the heating started. Due to the prolonged heating, a saturated solution of polysilic acids was formed, and upon cooling it redeposited as silica, fusing the particles together. Ceriotti et al. rewetted the dried chip with buffer for separation. The same principle was applied by Liao et al.⁴⁵ in a bit different way in microchannels with 500 nm particle packing. They blew hot air over the evaporation reservoirs to achieve almost the same effect of Ceriotti et al.

The stabilization of particles in a bed by heating works for large sized particles, but does not work well for particles of 300 nm diameter or smaller. A photograph taken after only 3 h heat treatment of a 300 nm silica particle bed at 60⁰C is shown in Figure 3-6. The temperature was about half and the time less than one third of the Ceriotti method.⁵² Within 3 h of heating, the bed was completely dried and many cracks were formed. It became very difficult to rewet the bed with buffer and the chip was unusable for separations. Cracking of the dried colloidal films frequently takes place, particularly in those made from nanoparticle suspensions, as already reported.^{109,110,116-121} Consequently, heating appears to be of limited value for stabilizing the smaller particle beds.

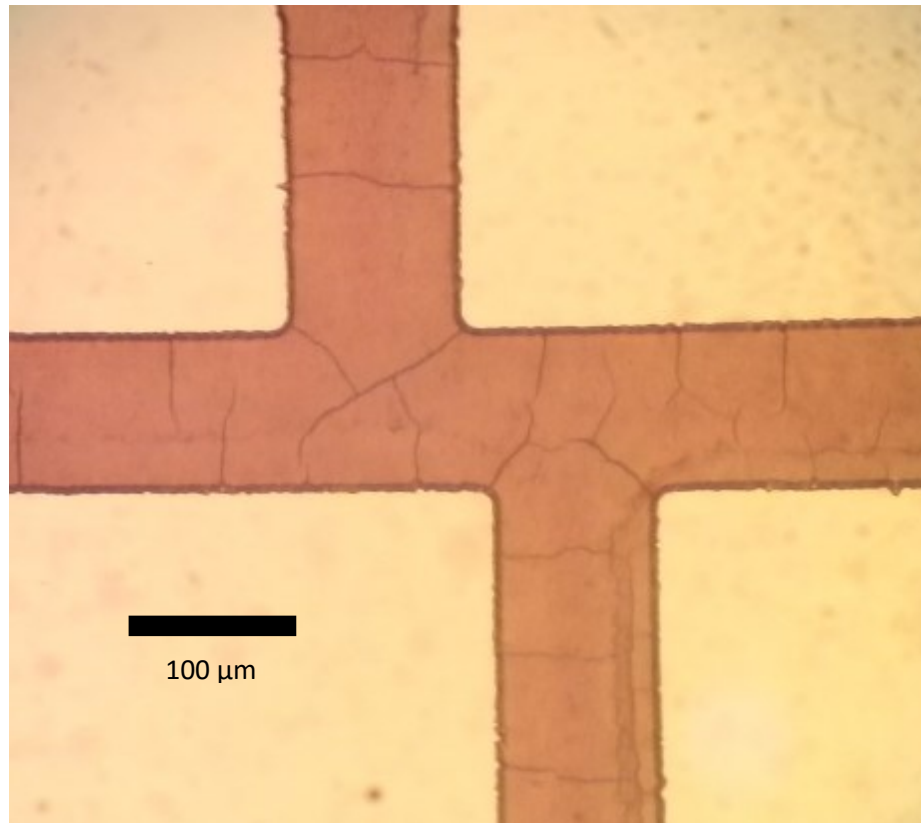


Figure 3-6: Condition of 300 nm particle packed chip after 3hrs heat treatment at 60^o C (photograph).

3.4.3 Defects in CSA beds

An SEM image of a 300 nm silica particle bed is shown in Figure 3-7. The SEM is taken after drying the CSA bed in microchannels. In this structure, vacancies, phase boundaries and interstitial defects are all present. Macro-scale cracks are formed after drying. Cracks are unwanted in this structure, because the channels formed due to cracks provide a pathway that does not assist separation. By keeping the microchip columns in a wetted condition, cracks are usually avoided.

Defects are part of a colloidal crystal lattice; it is very hard to prepare a perfect CSA crystal. Figure 3-7 shows a number of different defects. The vacancies shown in the SEM image might form either due to defect formation or to removal of particles from the CSA bed during removal of the PDMS, but other defects are not likely to be artifacts.

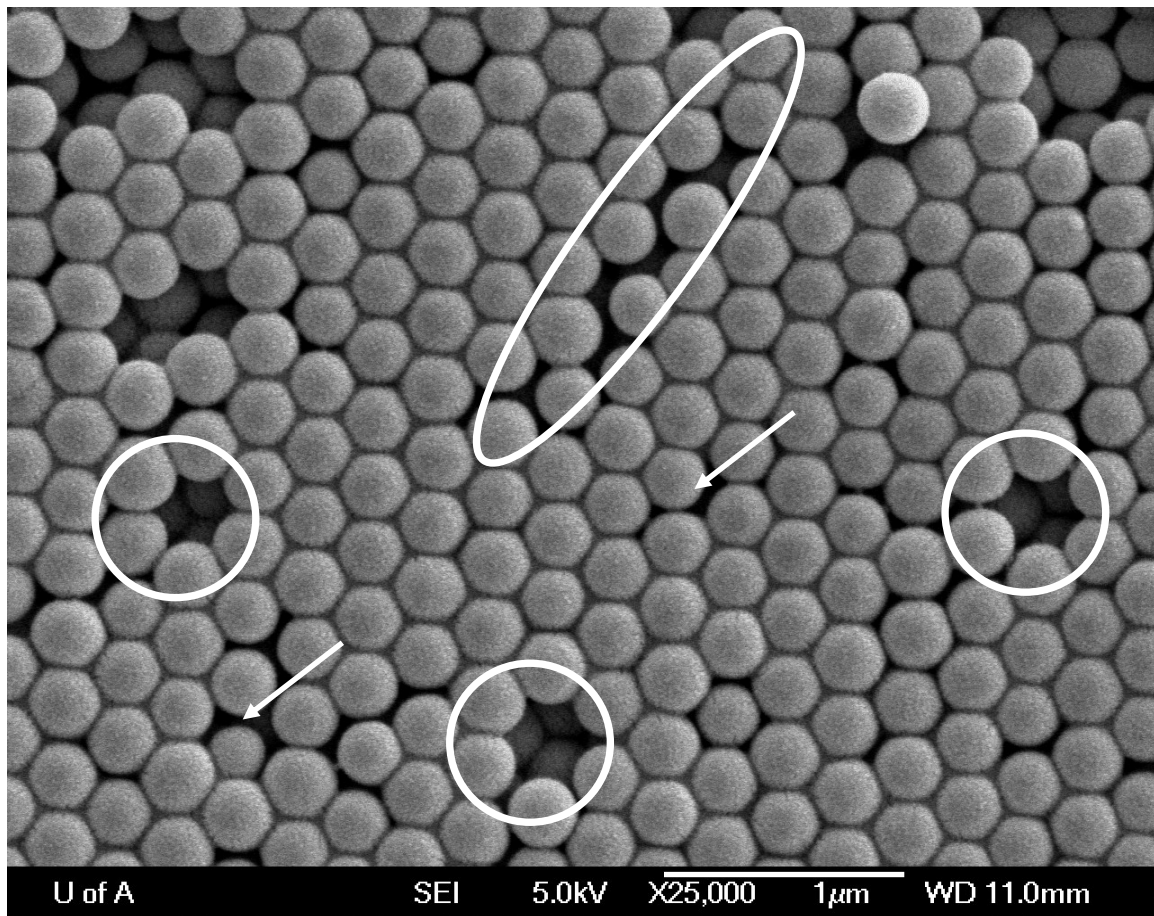


Figure 3-7: SEM image of 300 nm silica particle self-assembly. The vacancies are shown in circles and the phase boundary is shown by the oval shape, while the arrows show the interstitial defects.

To minimize the crystal imperfection and maintain long range order, better than 2% polydispersity of particles is required. In this study, the commercial particles used,

from Bang laboratories or Poly Sciences Inc., are 300 ± 40 nm size, with a polydispersity of more than 13%. A significant amount of interstitial defects or dislocations are present in the structure, due to this level of polydispersity. A large number of plane stacking defects are often present due to a polycrystalline mixture of the FCC and HCP crystals, but these are not easily observed by SEM which images the top layer alone.

3.4.4 Global Orientation Order Parameter

There are several approaches available to quantitatively analyze the degree of order or the crystalline quality.¹³⁴ Among them, a single parameter is quite useful to characterize the two dimensional order of a lattice, known as the global orientation order parameter, ψ . The global orientation parameter is defined as:^{134,135}

$$\psi = \frac{1}{N_p} \sum_{N_p} \frac{\exp(6i\beta)}{6} \quad 3.4$$

where i is a constant, calculated from perfect crystal structure where $\psi = 1$, and β is the angle between the two nearest neighbour of particles in a structure and is calculated using ImageJ software.¹³⁶ N_p is the total number of nearest neighbour particles in the 2-d lattice plane. As all of the colloidal self-assembly in microchannels are hexagonal closed packed, N_p is 6. For any perfect structure the ψ value will be 1.

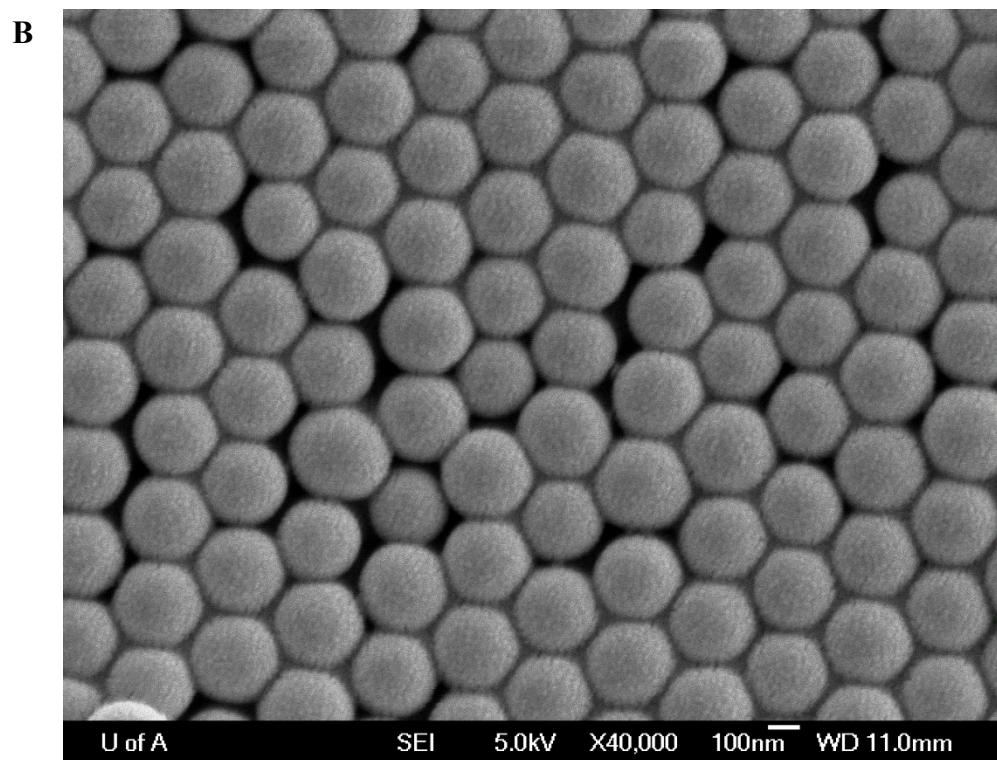
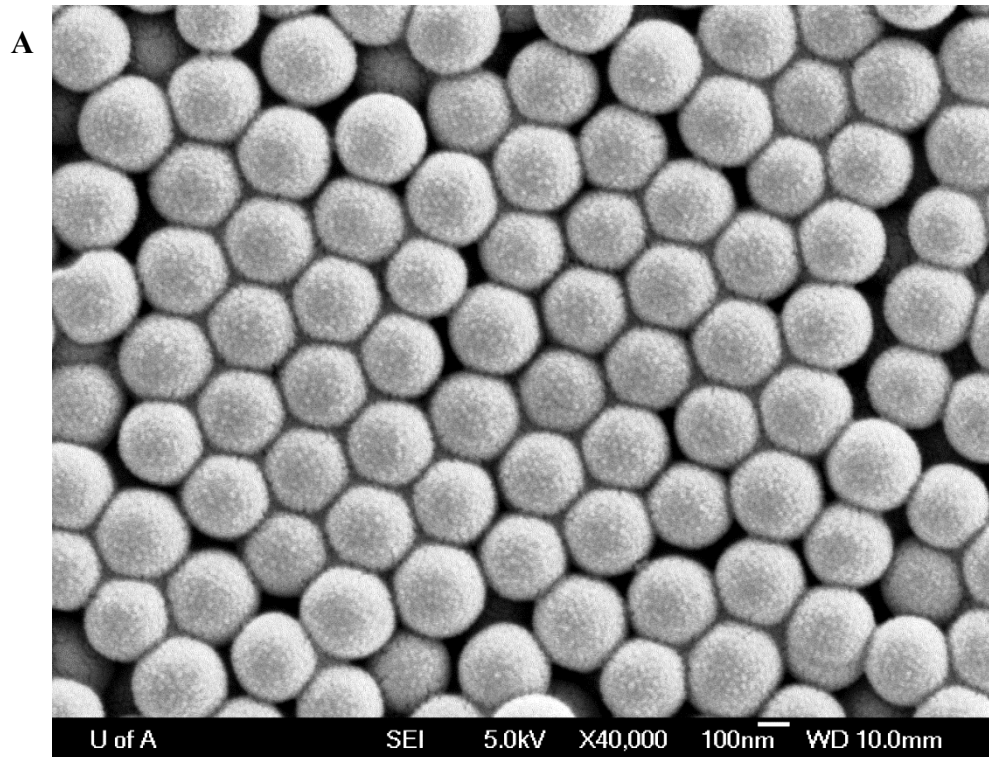


Figure 3-8: SEM image of colloidal self-assembly of 300 nm silica particle surface A) 10 μm thick bed, and B) 4 μm thick bed.

The global orientation parameter values for different thickness CSA beds is given in Table 3-2.

Table 3-2: The global orientation parameter values of different thickness colloidal self-assembled bed

Channel depth, μm	ψ (at cross section)	ψ (5 mm from cross section)	ψ (10 mm from cross section)
20	0.93		
10	0.95		
4	0.97-0.98	0.98	0.99

The ψ value increases from 0.93 to 0.98, measured at the intersection of the channels, as the channel depth decreases from 20 to 4 μm , i.e., the order of crystallinity increases. For a 4 μm thick bed, the ψ value increases slightly along the separation channel. The global orientation parameter values prove that the order of crystalline quality increases with decreasing thickness of the self-assembled nanoparticle bed. The SEM image (Figure 3-8) visually illustrates the 4 μm deep bed has less defects than a 10 μm bed.

3.4.5 Crystal growth studies for narrow bore capillaries

To justify the above discussion of defect formation in colloidal self-assembly, crystal growth rate studies were performed in different thickness microfluidic channels with different silica particles. The crystal growth rate observed by optical microscopy and

measured by slide calipers under a microscope is shown in Figure 3-9 for 50, 100 and 300 nm diameter silica particles. During crystal growth no evidence of crack formation was observed.

The growth rate curve of a colloidal crystal reported by Dufresne et al ^{109,110} obeys a power law:

$$Y \sim t^a \quad 3.5$$

where Y is the growth of colloidal crystal, t is the time of growth and a is the factor depends on the particle size.

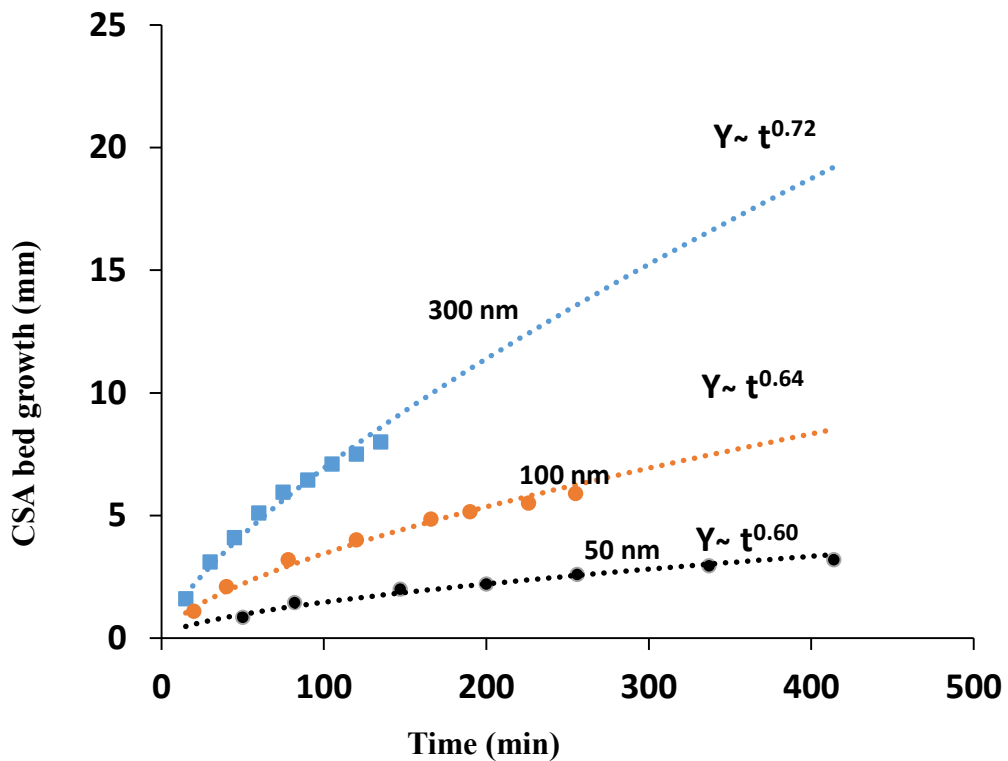


Figure 3-9: Microfluidic monodisperse colloidal crystal (mCC) growth over time for silica particles with different diameter for a 10 μm thick bed

The value of the exponent “a” decreases from 0.72 for 300 nm particles to 0.60 for 50 nm particles. As the particle size decreases, the same length of packing requires more time. This is because, as the pore size reduces with the particle size, the rate of water transport to the drying edge also decreases. Moreover, increased energy is required to evaporate the water from smaller pores. The decreasing trend is very similar to the Dufresne et al.¹⁰⁹ flow and fracture of nano-porous media study. However, the value of the exponential growth factor, 0.60 for 50 nm particles is lower than the value reported by Dufresne et al.¹⁰⁹ They report a value of 0.87 for 52 ± 6 nm particles. The difference is probably due to the presence of defects in their structure, which are evident from their reported bright field images. The presence of higher defects in the Dufresne study can also be deduced from the greater thickness of the bed they studied. In their study they used a 30-100 μm thick bed in a capillary. As the concentration of defects increases with thickness, their structure would be expected to have more defects than the bed (10 μm) of this study.

A quite different type of growth rate trends was reported by Ali et al.⁵¹ for larger silica particles (900-310 nm). They concluded that Dufresne et al.¹⁰⁹ model did not adequately describe the larger silica particle system due to sedimentation, while smaller size silica particles follow almost the same trend as reported by Dufresne.

The growth rate of different thickness beds for the same particle was studied, and the growth rate curve is shown in Figure 3-10. As thickness decreases, the same length of packing requires more time for the same particle size. This is because, the rate of transport and thus evaporation decreases due to fewer defects in the CSA bed. At a lower

evaporation rate, a higher quality crystal is formed, and for slowly grown crystals FCC is favoured over the HCP. The slower growth and fewer particles in the bed ultimately reduce the total number of defects in the lattice structure.

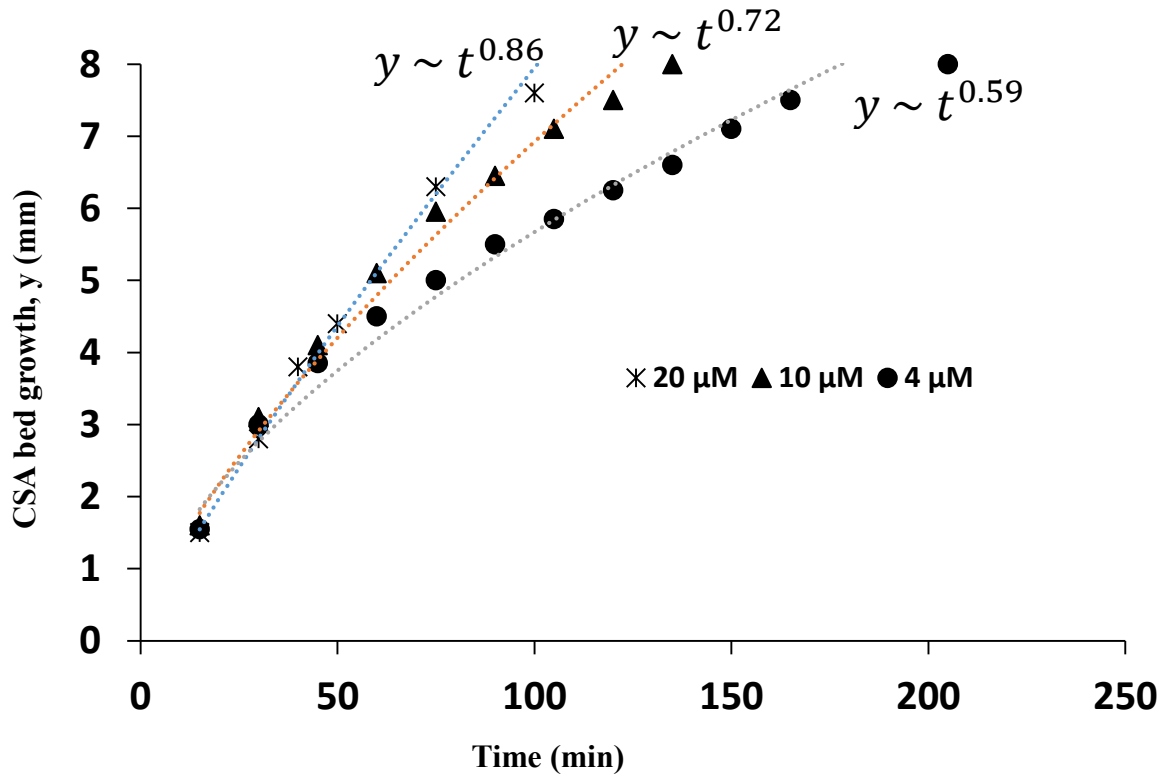


Figure 3-10: Microfluidic monodisperse colloidal crystal (mCC) growth over time for 300 nm silica particles with different thickness microchannels.

3.4.6. Rational for increased stability

The increased stability of colloidal self-assembled nanoparticle beds in narrow bore capillaries is probably due to two reasons 1) less defect or imperfection of the crystal lattice; and 2) an influence of the column wall (wall effect) in stability.

A balance between different attractive and repulsive interactions is required on colloidal particles during their organization into a lattice. The quantification of these forces is an active research field and very difficult to generalize.^{86,137} Among the attractive forces the van der Waals (vdW) force is very important^{86,138}, and in comparison to intermolecular vdW forces, colloidal vdW forces act over a larger distance for two spheres.⁸⁶ The silica particles are negatively charged, so the electrostatic repulsion is the main repulsive force acting on a colloidal system.

When a high electric field is applied to a colloidal self-assembled nanoparticle bed for separation, the electrokinetic force on the charged silica particles can overcome the balance of the attractive force and repulsive forces between particles, causing particles to move towards the positive electrode reservoir. If the particles are located near any void space created due to imperfections of the crystal lattice, they can easily migrate to that space. So defects contribute to initiating motion of the bed, by allowing a pathway for translocation, as illustrated in Figure 3-11. Once particles are migrating into the defects spaces, the bed becomes more unstable.

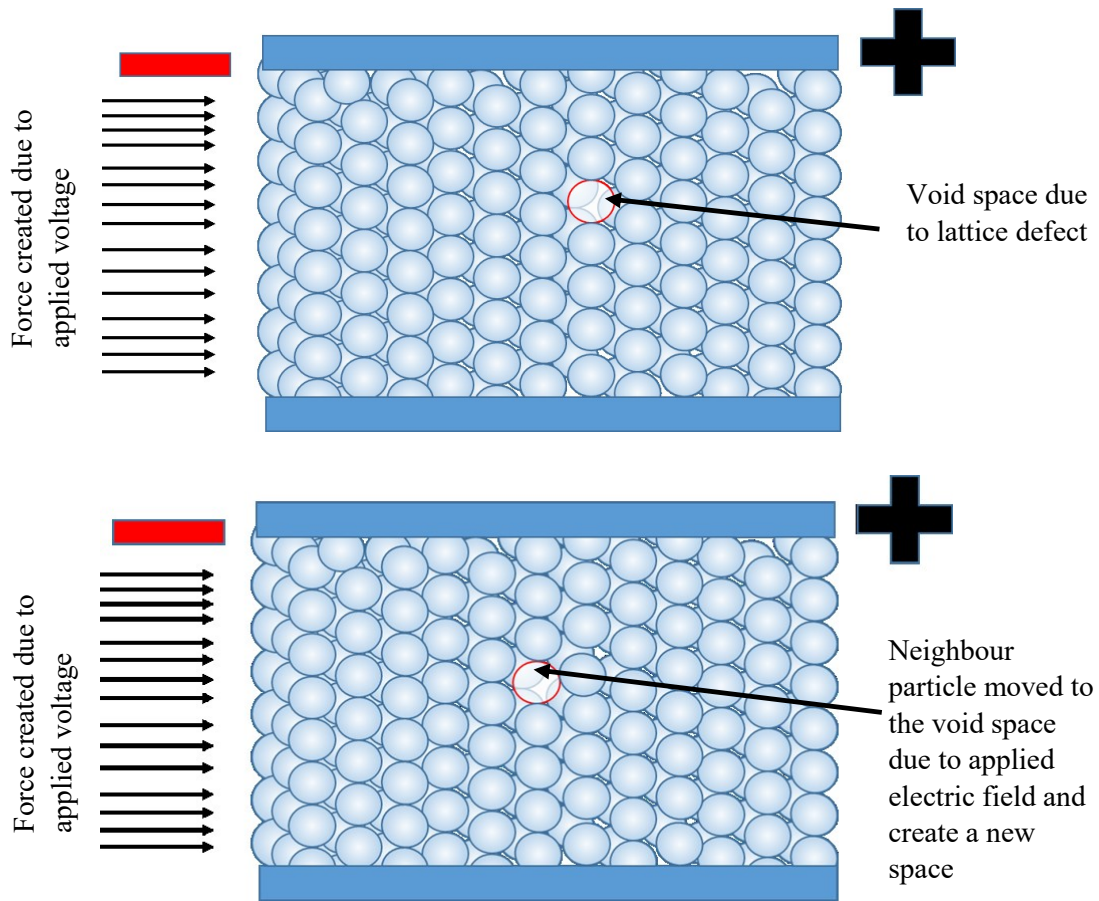


Figure 3-11: Explanation of particle migration to the void space created due to lattice defect in colloidal self-assembly.

For a 20 μm thick bed of 300 nm particles there are approximately 66 layers, whereas for a 4 μm thick bed there are only 13 layers. The microchannel walls will influence a greater percentage of the particles in the narrow channels, and this may enhance durability. However, it could also decrease it, depending on the nature of the interaction. The greater influence of the wall in a thinner channel is suggested in Figure 3-12.

Both the lower number of defects and any wall effect work simultaneously to give a net increase to the stability of narrow beds for high voltage applications. The voltage stability of the beds is shown in Table 3-3.

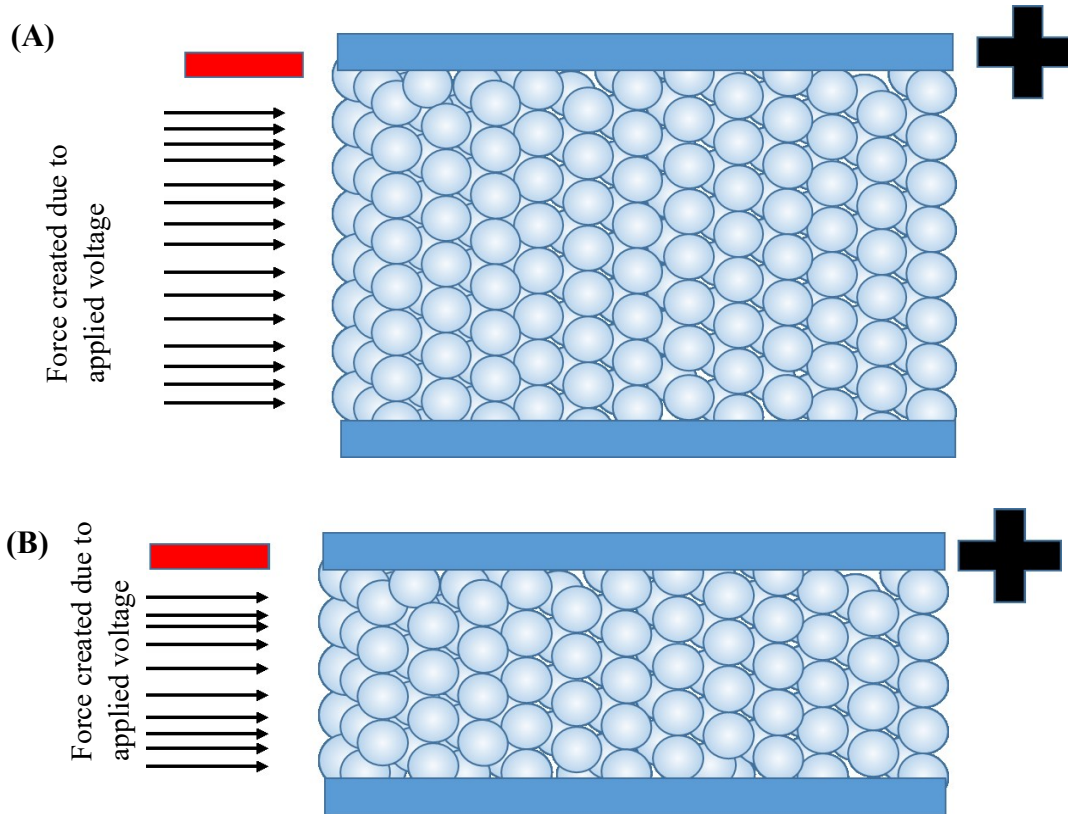


Figure 3-12: Explanation of greater stability in colloidal self-assembly due to wall effect. In the case of a thick bed (A) the wall has less influence on the bed than in the narrow bed (B).

Table 3-3: The voltage stability of nanoparticles bed

Particle diameter, nm	Stability of bed, V/cm		
	20 μm thick bed	10 μm thick bed	4 μm thick bed
300	≤ 320	~1250	~2250
150	≤ 60	450	
100	Hard to work with	320	
50	Hard to work with	Hard to work with	320

Using the narrow bore capillary, the stability of a bed increased many fold. The 300 nm particle, 20 μm thick bed was stable up to 320 V/cm, but for a 10 μm thick bed stability was achieved up to 1250 V/cm, even greater stability (up to 2250 V/cm) was achieved for a 4 μm thick bed. A 150 nm particle, 20 μm thick bed was stable to less than 60 V/cm, but using a 10 μm thick bed up to 450 V/cm could be achieved. In a narrow bore 4 μm thick capillary, we could easily work with 100 nm and 50 nm particle beds, which were almost impossible with a 20 μm thick bed. The stability of beds achieved by narrowing the capillaries in microchip+, are almost comparable to the stability achieved by heating⁴⁵ for larger particles,

3.4.7: High performance protein separations

Electropherograms of a four protein mixture using a 300 nm particle, 10 μm thick bed are shown in Figure 3-13. All four proteins were baseline resolved within 5 mm separation distance. The proteins migrated within 10 s at 950 V/cm and less than 7 s at 1250 V/cm. With the high voltage stability using a narrow bore capillary, extremely fast separations were possible. The maximum resolution was achieved between the two largest proteins in the mixture, ovalbumin (45 kDa) and BSA (66 kDa). The resolution between the peaks should increase with increasing separation voltage. But, when the voltage increased from 950 V/cm to 1250 V/cm, there was no significant increase in the resolution observed. Resolution actually decreased for aprotinin (6.5 kDa) and trypsin inhibitor (20.1 kDa). This decline is probably because the bed started to crack at 1250 V/cm, so the separation performance deteriorated. After a few runs at 1250 V/cm, the bed was completely cracked and no effective separation was possible. The resolution between the peaks at different separation voltages is shown in Table 3-4.

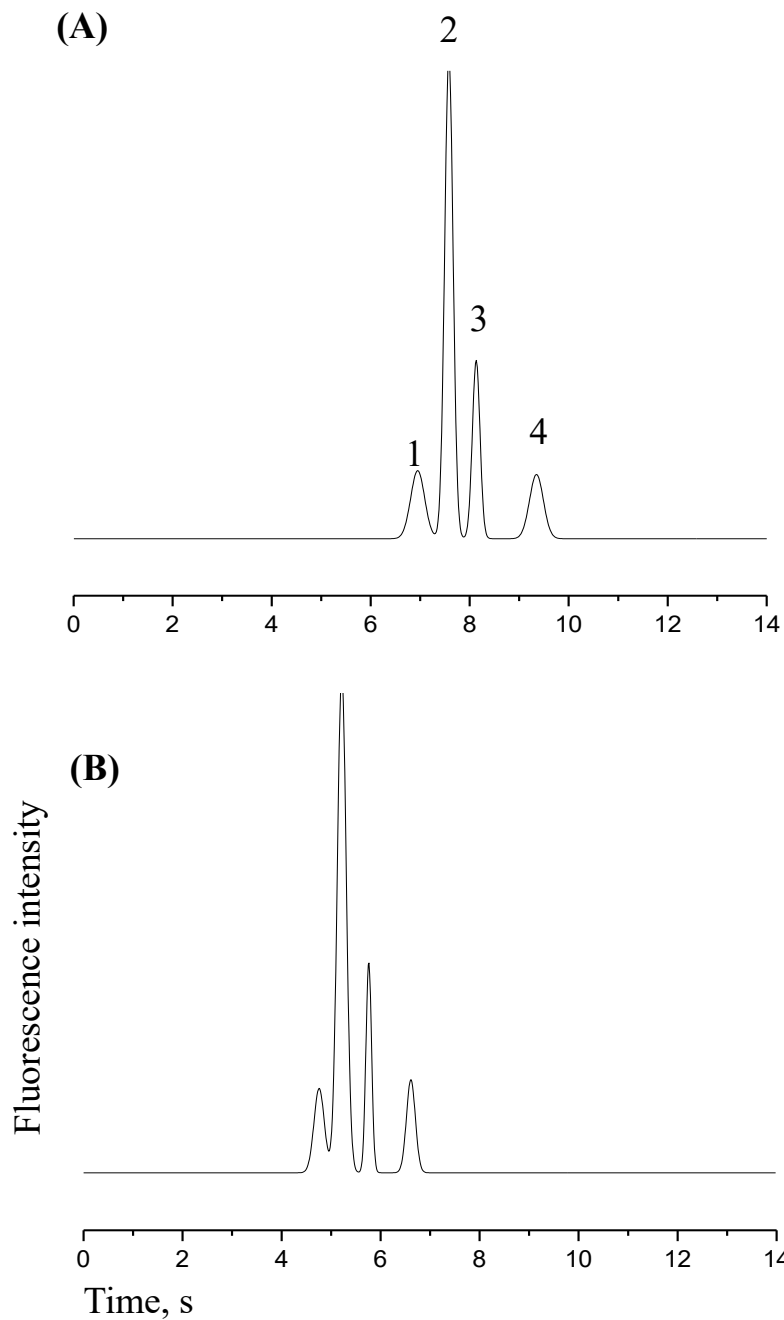


Figure 3-13: Electropherograms of four protein mixture using 300 nm particle 10 μm thick bed at 5 mm detection. (A) at 950 V/cm and (B) 1250 V/cm separation voltage; 1) aprotinin, 6.5 kDa; 2) trypsin inhibitor, 20.1 kDa; 3) ovalbumin, 45 kDa; and 4) BSA, 66 kDa.

Table 3-4: Resolution between the peaks at different separation voltages at 5 mm separation distances

Separation voltage (V/cm)	Resolution between peaks		
	Aprotinin-Trypsin inh.	Trypsin inh.-Ovalbumin	Ovalbumin- BSA
450	1.4	1.6	2.1
650	1.4	1.9	2.8
950	1.5	2.0	3.1
1250	1.3	2.1	3.2

To evaluate the performance of a narrow bore capillary, a 4 μm thick bed of 300 nm particles was prepared in microchannels. Stability of a 4 μm thick bed was seen up to 2250 V/cm. An electropherogram of a four protein mixture at 2250 V/cm voltage is shown in Figure 3-14

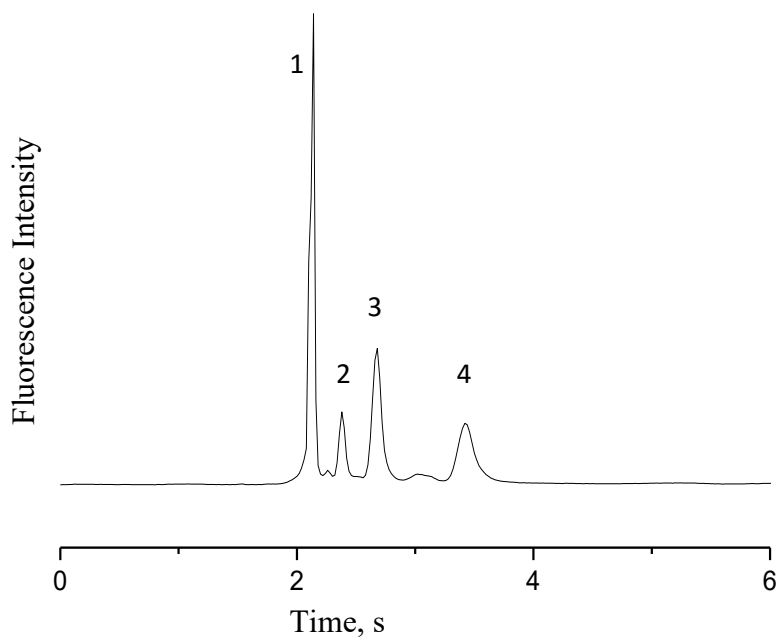
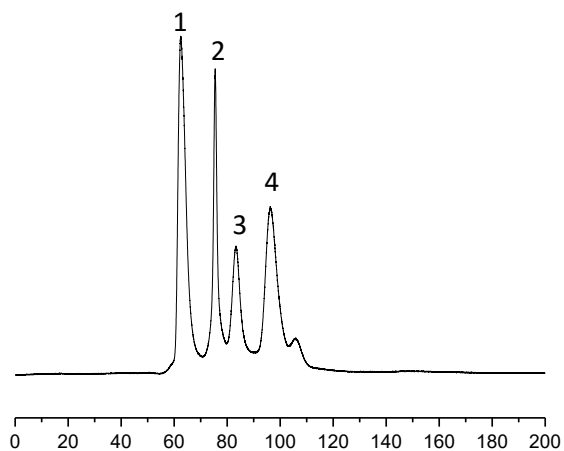


Figure 3-14: An electropherogram of four protein mixture using 300 nm particle 4 μm thick bed at 1250 V/cm at 5 mm separation distance. 1) aprotinin, 6.5 kDa, 2) trypsin inhibitor, 20.1 kDa, 3) ovalbumin, 45 kDa; and 4) BSA, 66 kDa.

The electropherograms of 10 μm thick beds using 100 and 150 nm particles at 320 V/cm are shown in Figure 3-15.

a)



b)

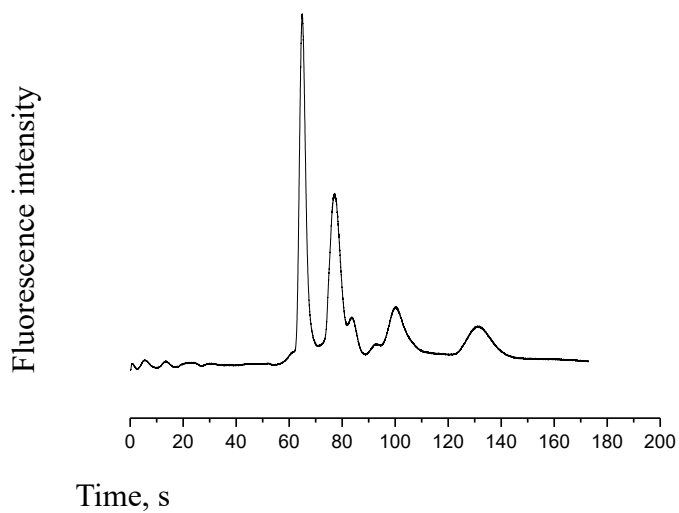


Figure 3-15: Electropherograms of four protein mixture using 10 μm thick bed at 320 V/cm using a) 150 nm particle, and b) 100 nm particle at 8 mm of separation distance. 1) aprotinin, 6.5 kDa, 2) trypsin inhibitor, 20.1 kDa, 3) ovalbumin, 45 kDa; and 4) BSA, 66 kDa.

3.5 Conclusions

The ability to utilize smaller particle beds at higher electric fields, by simply reducing the thickness of the channel has been demonstrated. By reducing the depth of the CSA beds by half, three to four times the electric field stability was achieved. Decreasing particle size in beds greatly improved the separation performance. The separation structure fabrication process is very simple, and much less costly than nano-fabrication methods. Very high separation performance was achieved compared to competing technologies such as conventional gels.

Chapter 4

Evaluation of SDS-Protein Separation Performance of Colloidal Self Assembled Nanoparticle Bed in Narrow Bore Capillaries*

4.1 Introduction

As shown in Chapter 3, the stability of a colloidal self-assembled nanoparticle bed can be increased by simply reducing the thickness of the bed. The elevated stability of a narrow CSA bed makes the microchip suitable for high voltage applications, so the advantages of miniaturization⁶ technology can fully be exploited for size-based protein separations. One of the major advantages of using colloidal self-assembly for separation is that the pore size of the bed can easily be engineered by simply using different sized particles, as shown in Figure 4-1. The estimated pore size of the bed is 15 % of the particle size. Obtaining smaller pores from smaller particle beds is very important for protein separation, as proteins are very small (2-10 nm scale).

* A part of this chapter has been published in the Proceeding of 19th International Conference on Miniaturized Systems for Chemistry and Life Sciences as, "Highly Stabilized Colloidal Self Assembled Nanoparticle bed in Micro-channels for High Performance Size Based Protein Separation" Mohammad Azim, Abebaw B. Jemere and D. Jed Harrison, MicroTAS 2015; Gyeongju, South Korea ; 1978-1980

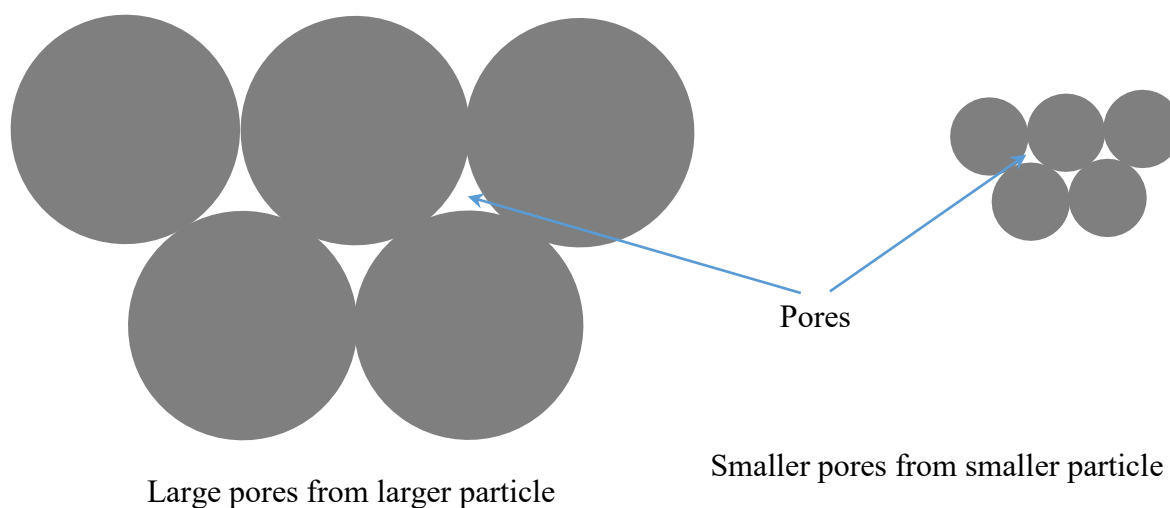


Figure 4-1: An illustration of the comparative pore size of larger and smaller particle assemblies

For example, a 100 nm particle assembly produces a bed with an average pore size of 15 nm. The size of most SDS-protein complexes is below or within this size range. It is important to produce a very stable bed with smaller particles, if we are to achieve very high mass resolution separation. The use of narrow bore capillaries solves this issue.

In this chapter, the SDS-protein complex separation performance of nanoparticle beds made using narrow bore channels is evaluated in detail. The mass resolving capacity of small particle beds have tested by separating small proteins.

4.2 Materials and methods

4.2.1 Protein samples and chemicals

As molecular weight standards, aprotinin (6.5 kDa), lysozyme (14.2 kDa), myoglobin (17.1 kDa), trypsin inhibitor (soybean, 20.1 kDa), ovalbumin (chicken egg, 45 kDa) and bovine serum albumin (BSA, 66 kDa), were from Sigma-Aldrich. In Chapter 2 the detail process of labeling with fluorescent dye, purification and storage is described. The composition of working and sample buffer was also same as described in Chapter 2.

4.2.2 Microchip fabrications and colloidal self-assembly

Microchips were assembled using polydimethylsiloxane (PDMS) with glass support as described in Chapter 2.

An evaporation-induced colloidal self-assembly mechanism was used for nanoparticle bed formation. A 10 % aqueous solution of mono dispersed silica particles (Bang Laboratories, Poly Sciences inc) was used without any modification or treatment, for fabrication of colloidal self-assembled (CSA) structure in the microchips, described in Chapter 2 in details. Before separation, the silica particles/water suspensions were replaced in all the reservoirs with working buffer and the devices were left for about 40 min to equilibrate.

4.2.3 Instrumentation and separation

A confocal epifluorescence microscope¹⁰⁸ was used to monitor the separation as described in Chapter 2.

The working buffer was run for about 20-30 min at 100 V before the separation started, to obtain stable current through the channels. During injection, SDS-protein mixture was loaded from reservoir 2. A 60-80 V potential was applied in sample waste reservoir 3, with all other reservoirs grounded, to form a shaped injection plug which reduced the band broadening during separation. During separation, equal positive and negative potentials were applied between reservoirs 1 and 4, with the other two reservoirs grounded. The negative potential applied in reservoir 1 served as a push back potential to prevent sample leakage from the grounded sample loading arms. The potential at the double T position (red circle position in Figure 3-2A) was calculated by application of Kirchhoff's rules.¹³² The negatively charged SDS-protein complexes migrated towards the anode and the laser spot was located at a fixed distance from the double T position, to excite the FITC labelled SDS-protein complexes.

4.3: Results and discussion

4.3.1: Separation performance of 300 nm particle bed

Narrow bore capillaries impart extremely high voltage stability to colloidal self-assembled beds of nanoparticles. To evaluate the separation performance of colloidal self-assembled nanoparticle beds, SDS-trypsin inhibitor complexes were run through a 300 nm particle bed with 10 μm depth at different separation voltages. The superimposed electropherograms of SDS-trypsin inhibitor complex with varying electric field strengths are shown in Figure 4-2. From Figure 4-2 it is clear that as the separation field strength increases, the peak becomes narrower. There is also a decrease in migration time with increasing applied field strength. The migration rate of trypsin inhibitor is plotted as a

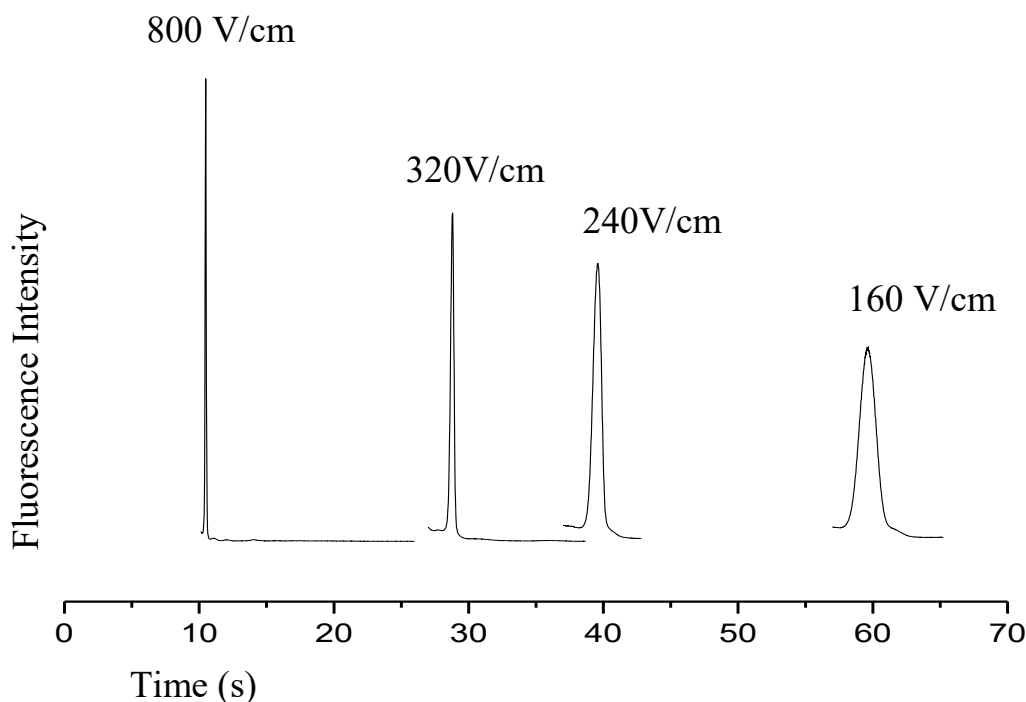


Figure 4-2: Superimposed electropherograms of 1 μM trypsin inhibitor (20.1 kDa) in varying electric fields in running buffer 4xTBE and 0.1% SDS, using 300 nm silica particles with 10 μm depth bed at 5 mm detection.

function of applied voltage and is shown in Figure 4-3A. A linear relationship between migration rates and the applied voltage was achieved with $R^2 = 0.999$, which is expected. At the highest field there may be a slight deviation that could indicate the onset of Joule heating. Error bars are smaller than the symbols in Figure 4-3A.

The efficiency of a separation matrix is usually described by the plate height, H . To calculate the plate height of the nanoparticle bed, the full width at half maximum (FWHM) was calculated for all electropherograms by fitting to a Gaussian distribution. The number of plates in a 5 mm separation distance was calculated using:

$$N = 5.54 \times \left(\frac{t_r}{w_{0.5}} \right)^2 \quad 4-1$$

where t_r is the migration time of SDS-trypsin inhibitor complexes at a particular separation voltage and $w_{0.5}$ is the full width at half maximum of the peak for a corresponding separation voltage.

The plate height is calculated using $H = L/N$, where H is the plate height, N is the number of plates and L is the separation distance. The migration rate is calculated from the time required to reach the detector located at a 5 mm separation distance. A plot of plate height (nm) vs. migration rate (mm/s) is shown in Figure 4-3B. Clearly the plate height depends strongly on the field strength (E), as is reported in the literature.^{15,43,45,139} In this van Deemter relationship, the plate height decreases very fast with the migration rate or field strength and reaches a minimum of 50 nm at 650 V/cm. From 0.265 mm/s (600 V/cm) migration rate, the plate height decreases very slowly, but between 0.375 mm/s (650 V/cm) to 0.480 mm/s (800 V/cm) it is almost constant. After 800 V/cm, the plate

height starts to increase very slowly because of two possible reasons. Firstly, Joule heating may be present to a limited extent, which causes the peak to broaden. Secondly, there may be some nonspecific absorption.

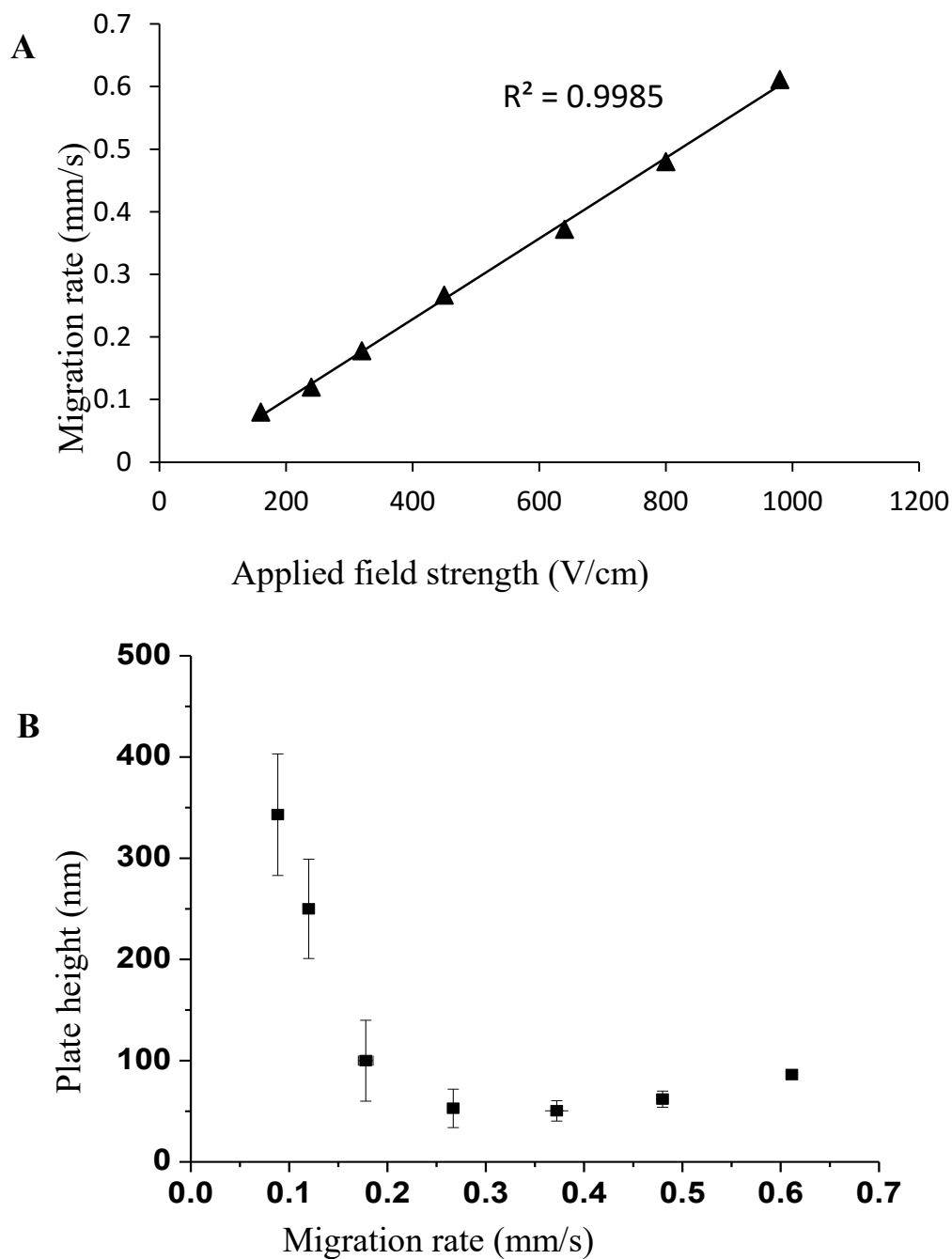


Figure 4-3: (A) Migration rate of SDS-trypsin inhibitor complexes vs. applied electric field, and (B) Plate height vs migration rate plot.

The plot of plate height vs. migration rate in Figure 4-3B is an analog of the van Deemter plot which has the same A, B and C terms as shown in equation 4-2, but plotted as a function of migration rate rather than the velocity of the mobile phase.

$$H = A + \frac{B}{v_x} + C v_x \quad 4-2$$

In the CSA bed, the B term plays the major role as seen in the Figure 4-3B. The A term is a multiple path term, which can be defined as $A = 2\lambda D_p$. The D_p is the particle diameter, while λ depends on particle packing uniformity. The heterogeneity of particle packing increases λ values, while for highly ordered structures of small particles λD_p becomes negligible.¹⁵ The packing of 300 nm particles in 10 μm deep channels is highly ordered (the global orientational order parameter or degree of crystallinity, ψ is 0.95), so the multiple path term A is very close to zero, or at most a few nanometers. Figure 4-3B supports this conclusion. The mass transfer term, C, should be negligible or zero, because the separation is carried out in a single phase, i.e., there is no stationary phase.⁵⁴ However Figure 4-3B shows there may be a modest contribution to mass transfer at higher migration rates, perhaps arising from nonspecific absorption.

The term that contributes to the plate height most significantly is the molecular diffusion term B, which is defined as $B = 2\gamma D$, where γ is the obstruction factor. The obstruction factor is defined as the ratio of diffusion coefficients inside the medium to that in open channel. The γD denotes the effective molecular diffusion. Wirth and co-workers have analyzed the impact of highly ordered, uniform structures on the obstruction factor. They conclude that due to uniformity of the structures, the obstruction factor in the colloidal self-assembled nanoparticle bed is 2 fold lower than other chromatographic

separation matrices, contributing to a lower plate height. So using an ideal CSA, approximately a $\sqrt{2}$ factor lower plate heights should be achieved for separation.¹⁴⁰

The effective molecular diffusion can be calculated from the plot of peak variance vs migration time,¹⁵ as shown in Figure 4-4. To calculate the peak variances, base line peak width, ω , is calculated from the Gaussian fitting of the electropherograms in Figure 4-2. The base line peak width is given by $\omega = 4 \sigma$, where σ^2 is the variance.

The slope of Figure 4-4 is the B term, which is $1.05 \times 10^{-7} \text{ cm}^2/\text{s}$, giving the obstructed diffusion of $\gamma D = 5.2 \times 10^{-8} \text{ cm}^2/\text{s}$, which is the minimum contribution to the plate height. Bingchuan et al.¹⁵ reported, $\gamma D = 0.9 \times 10^{-8} \text{ cm}^2/\text{s}$ for native lysozyme in polymerized CSA beds of 330 nm silica particle. Their lower obstructed diffusion value is probably due to polymerization, which reduced the pore size of the CSA bed. In free solution, the diffusion coefficient of a nanometer sized protein is $> 5.0 \times 10^{-7} \text{ cm}^2/\text{s}$.¹⁴¹ The more than ten times lower obstructed diffusion in a highly ordered bed of nanoparticles is consequently a significant factor in the improved efficiency and lower plate heights in these beds.

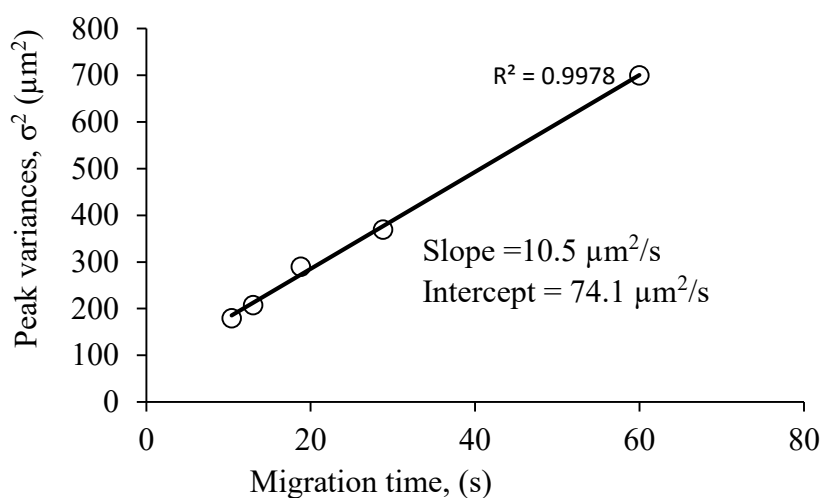


Figure 4-4: A highly linear relationship was achieved between peak variances vs migration time plot

4.3.2 Separation of SDS-protein complexes

A mixture of four proteins were separated with the optimized condition of 650 V/cm separation field. The resultant electropherogram is shown in Figure 4-5. All proteins were baseline separated with high resolution. A comparison of resolution with separation length is shown in Table 4-1.

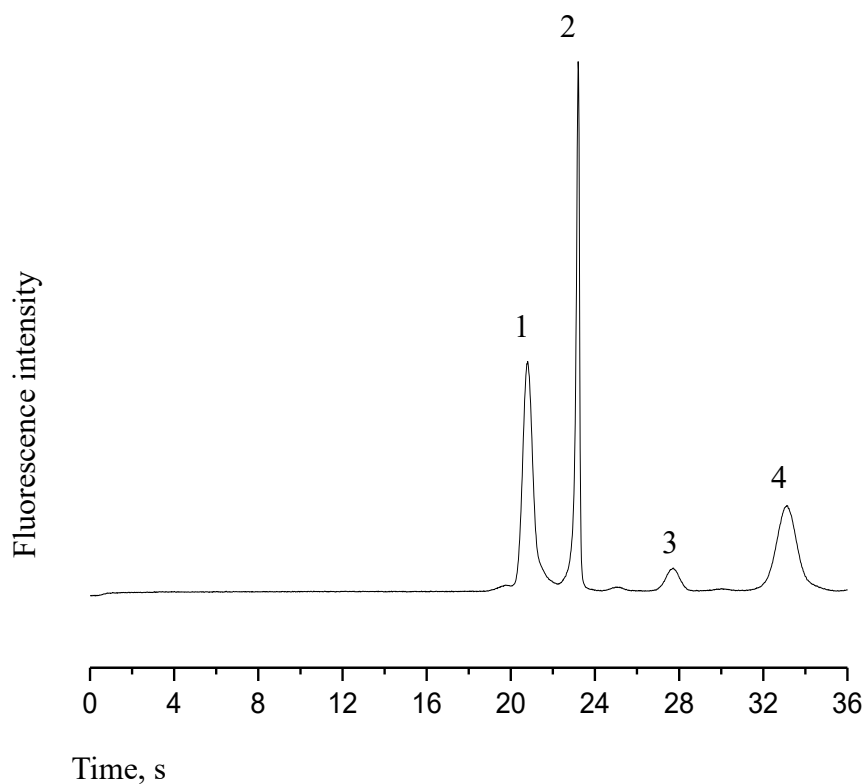


Figure 4-5: Electropherogram of SDS-denatured four-protein mixture at $L = 10$ mm separation distance and 650 V/cm field [1: aprotinin 6.5 kDa, 2: trypsin inhibitor, 20.1 kDa, 3: ovalbumin 45 kDa, and 4: BSA 66 kDa].

Table 4-1: Peak resolution at different separation distances, at 650 V/cm field strength

Detection distance (mm)	Resolution between peaks		
	aprotinin – trypsin inh.	trypsin inh.- ovalbumin	ovalbumin- BSA
5	1.4	1.9	2.8
10	3.9	6.0	4.5

At 5 mm separation distance, all four proteins are baseline separated, with the highest resolution of 2.8 observed between ovalbumin and BSA. These two are the largest proteins in the mixture. When the separation distance was increased to 10 mm, all resolution values increased significantly, though not entirely proportionally. The increase in resolution with distance shows the beds are consistently packed and electric field is uniformly distributed. Using a thermally treated 500 nm particle CSA bed, a minimum plate height for FITC was achieved 300 nm by Tao et al.⁴⁵ Birdsall & coworkers¹⁷ reported minimum plate heights of 0.4 and 1.1 μm for SDS-protein complexes using 350 and 500 nm particle polymerized CSA bed respectively. So the separation efficiency in terms of plate height for narrow bore CSA beds is greatly improved in comparison to reported values in the literature¹¹⁴.

The run-to-run reproducibility of the nanoparticle beds was tested by separating the protein mixture multiple times. The relative standard deviation (RSD) of migration time at 650 V/cm ranged from 0.3% for BSA to 0.9% for aprotinin. Comparatively higher RSD values were observed for the smaller proteins, most likely due to the short separation

distance being more sensitive to errors in measuring migration time. These RSD values validated that the narrow bore capillary beds of nanoparticles are stable for several runs. The run-to-run reproducibility confirms the usability of nanoparticle beds for practical applications at higher voltages.

4.3.3 Separation using smaller particle beds

A set of electropherograms using 100 nm particles in 10 μm thick beds at different separation voltages are shown in Figure 4-6. The 100 nm particle, 10 μm thick bed was initially stable up to 320 V/cm, but better separation performance was achieved at 200 V/cm. At any separation voltage above 160 V/cm, the separation performance degraded, with no effective separation was observed above 320 V/cm. The separation performance in terms of resolution is shown in Table 4-2.

Table 4-2: Separation performance using 100 nm silica particles 10 μm thick beds at different field strengths for 8 mm separation distance

Separation voltage V/cm	Resolution between peaks		
	Aprotinin- Trypsin inh.	Trypsin inh.- Ovalbumin	Ovalbumin- BSA
160	3.5	4.4	4.0
240	2.9	4.2	3.2
320	2.6	3.1	2.6

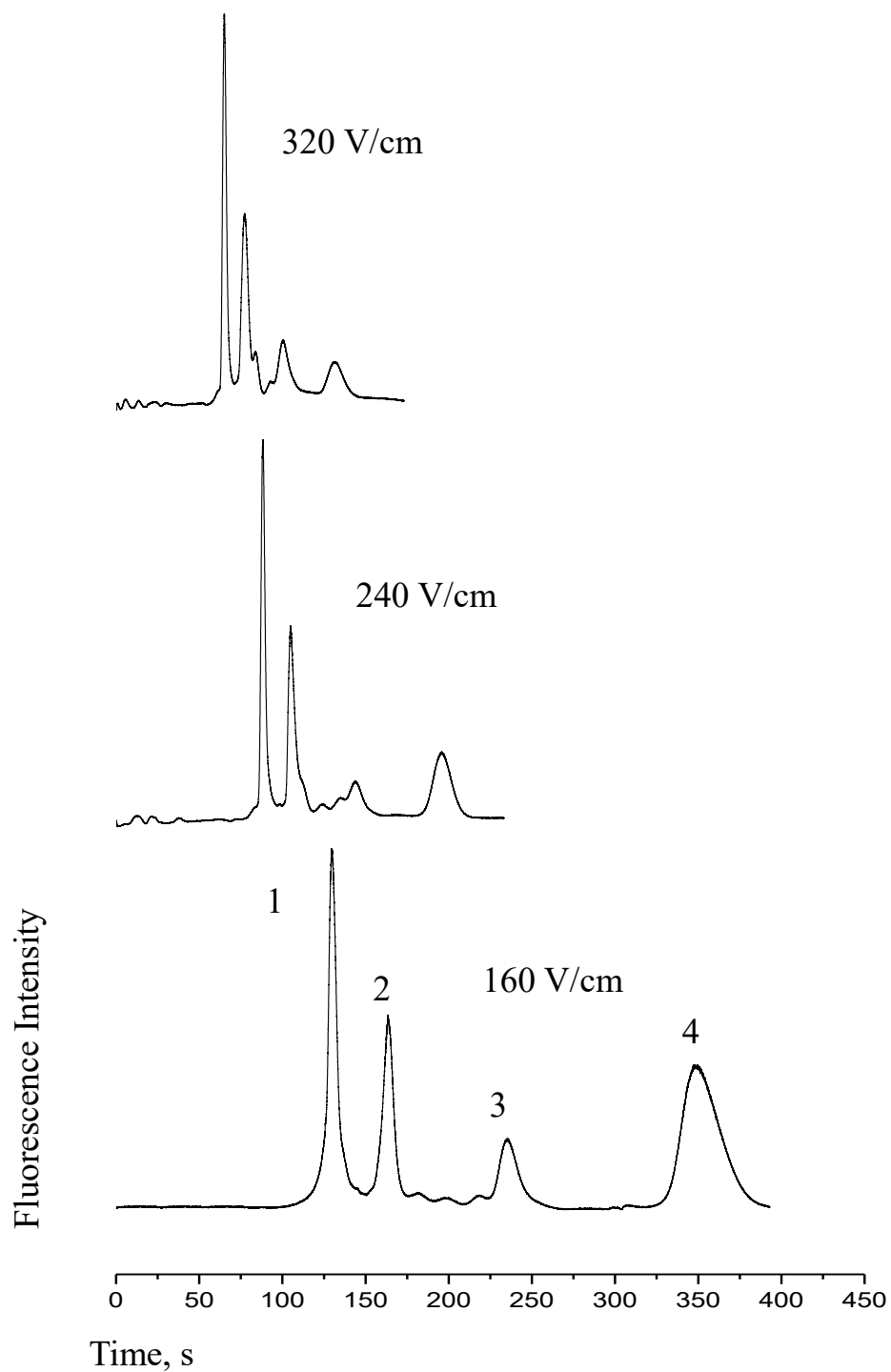


Figure 4-6 : Electropherograms of 4 protein mixtures using 100 nm particle 10 μm thick beds at different separation voltages at 8 mm separation distances. 1: Aprotinin, 6.5 kDa, 2: Trypsin inhibitor, 20.1 kDa, 3) Ovalbumin 45 kDa, and 4) BSA 66 kDa.

Theoretically, smaller particle beds should give better separation. To determine the effect of particle size on separation resolution, a mixture of four proteins was run through different particle beds, using the same separation voltage and same detection length. The resultant electropherograms are shown in Figure 4-7. It is clear that better separation performance was achieved using a smaller particle bed. As usual, the smaller size protein aprotinin, 6.5 kDa, migrated first, but the migration time increased with decreasing particle size. For a 300 nm particle bed, aprotinin required around 80 s to travel the 8 mm separation distance, whereas for the 100 nm particle bed it took ~125 s. The trend of increasing migration time is because protein movement becomes more retarded by the smaller pore size. The migration time for the largest protein in the mixture, BSA (66 kDa), was significantly increased, as expected. The migration time of BSA for a 300 nm particle bed is ~110 s, which increased to ~350 s for a 100 nm particle bed. Due to the effective retardation of the particle beds, the resolution between the proteins also increased significantly. The resolution in different beds is summarized in Table 4-3.

Table 4-3: Resolution of separation using different particle bed at 200 V/cm separation voltage and 8 mm detection length.

Particle size, nm	Resolution between peaks		
	Aprotinin-Trypsin inh.	Trypsin inh.-Ovalbumin	Ovalbumin- BSA
300	2.8	0.9	2.3
150	3.4	1.6	3.0
100	3.5	4.4	4.0

With increasing migration times, the resolution between the proteins also increased with decreasing particle size, as expected. In Figure 4-7, all particle beds resolved the proteins in the mixture. The resolution between the two smallest proteins (aprotinin and trypsin inhibitor) increased from 2.8 for 300 nm particle to 3.6 for 100 nm particle beds. But the resolution between trypsin inhibitor and ovalbumin increased significantly as the particle size changed from 150 nm to 100 nm. Ogston theory predicts that an optimum separation efficiency should be achieved for species that are very close in size to the pores of a sieving matrix.¹⁴ The hydrodynamic diameter of SDS-ovalbumin complex is 13.2 nm,⁶³ which is very close to the 15 nm pore size of the 100 nm particle beds. That is why resolution increased significantly between trypsin inhibitor and ovalbumin. The resolution between ovalbumin and BSA significantly increased as particle sizes decreased from 300 to 100 nm.

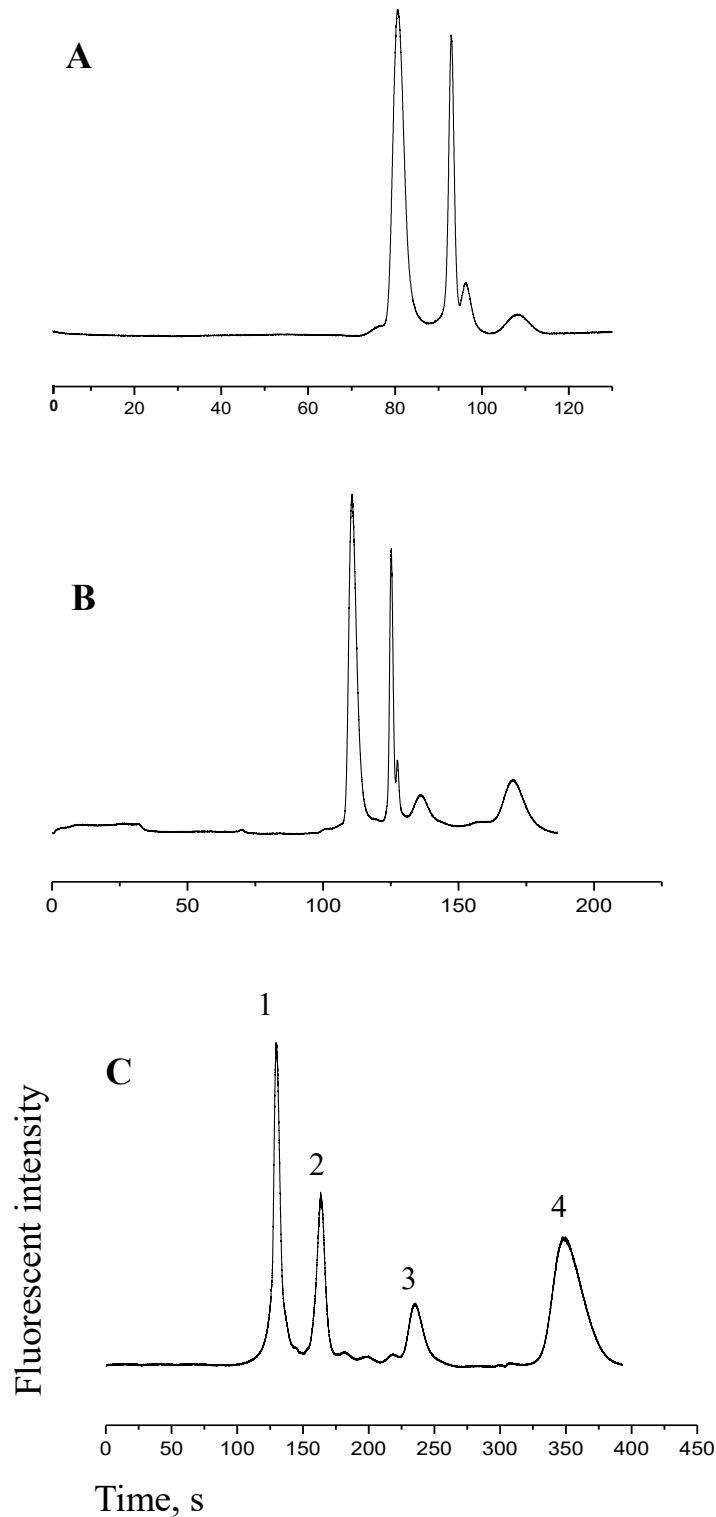


Figure 4-7: Electropherograms of a protein mixture using different particles 10 μm thick bed at 160 V/cm separation voltage at 8 mm detection length. **A)** 300 nm particle **B)** 150 nm particle **C)** 100 nm particle; 1) Aprotinin 6.5 kDa, 2) Trypsin inhibitor 20.1 kDa, 3) Ovalbumin 45 kDa, and 4) BSA 66 kDa.

To test run-to-run reproducibility of a 100 nm particle, 10 μm thick bed, three consecutive separations are shown in Figure 4-8. The relative standard deviation (RSD) of migration time at 160 V/cm varied from 0.5 % for BSA to 2.0 % for aprotinin. Comparatively higher RSD values were observed for smaller proteins, the same trend as was observed for 300 nm particles.

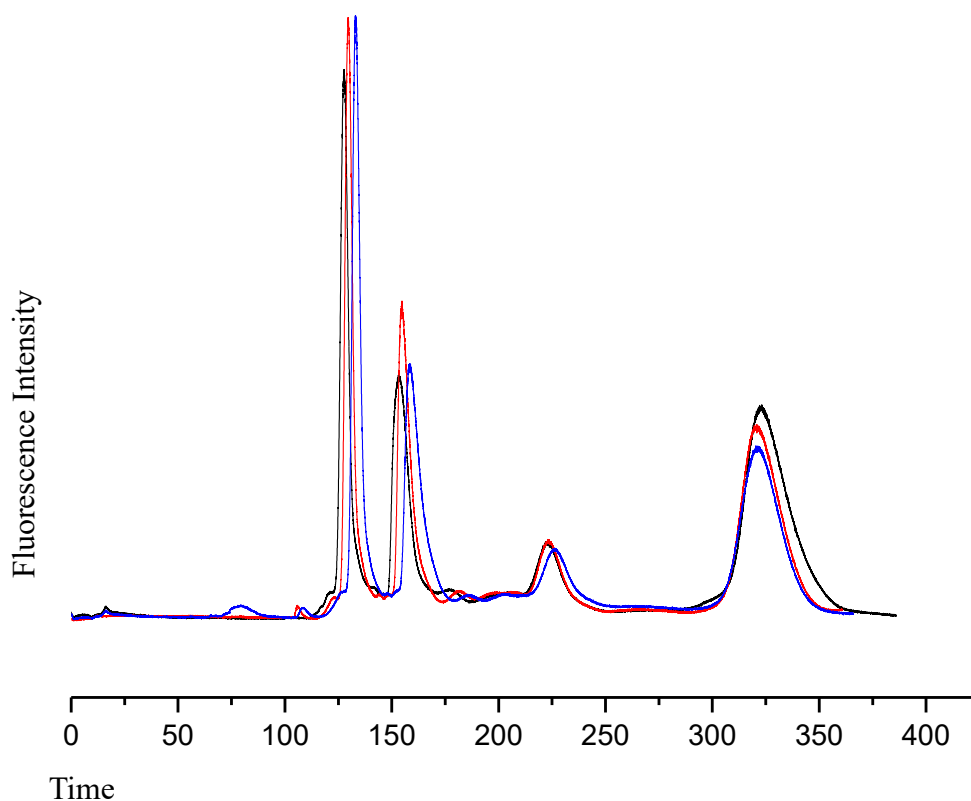


Figure 4-8: Superimposed electropherograms of three consecutive separation runs at 160 V/cm using 100 nm particle 10 μm thick bed.

4.3.4 Separation mechanism of 100 nm particle size CSA bed

Models of separation depend upon the pore size distribution,⁹² so that differences in detail can be expected between gels and CSA beds. To investigate how proteins are moving through the smaller pores, a plot of logarithmic of apparent electrophoretic mobility of proteins vs. the protein molecular weight, and another log-log plot of apparent mobility vs. the protein molecular weight are shown in Figure 4-9A and 4-9B, respectively. A linear relationship between log of apparent mobility vs protein molecular weight was observed, which demonstrates that the separation follows an Ogston-like sieving mechanism⁹¹ while moving through the ~15 nm interstitial pores of the 100 nm particles. The nonlinear relation between log apparent mobility and log molecular weight of proteins confirms this finding.

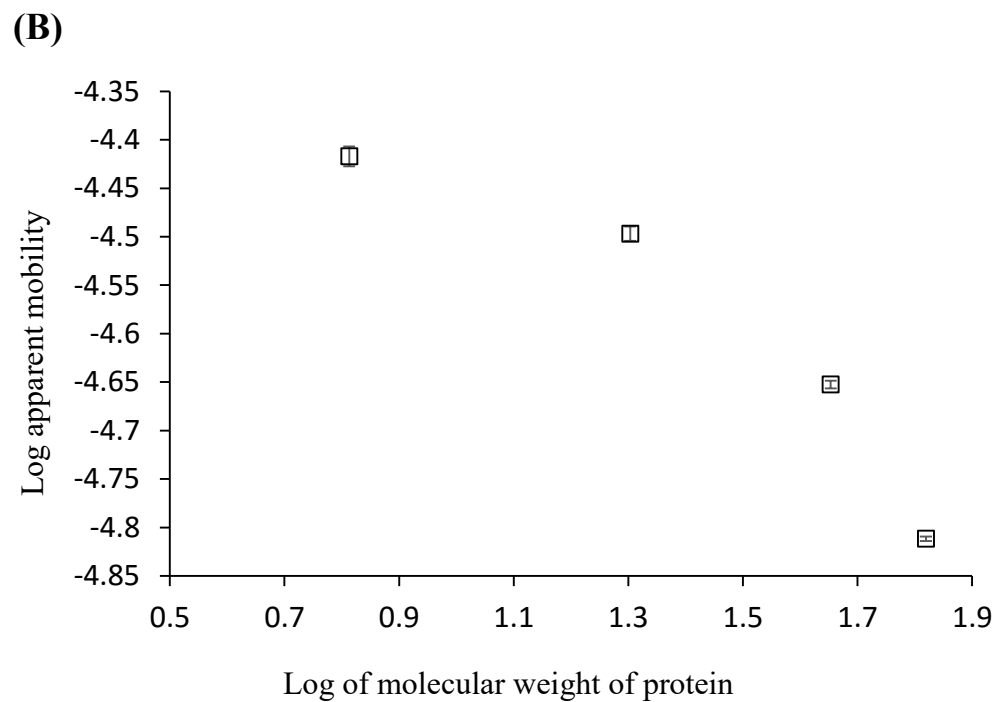
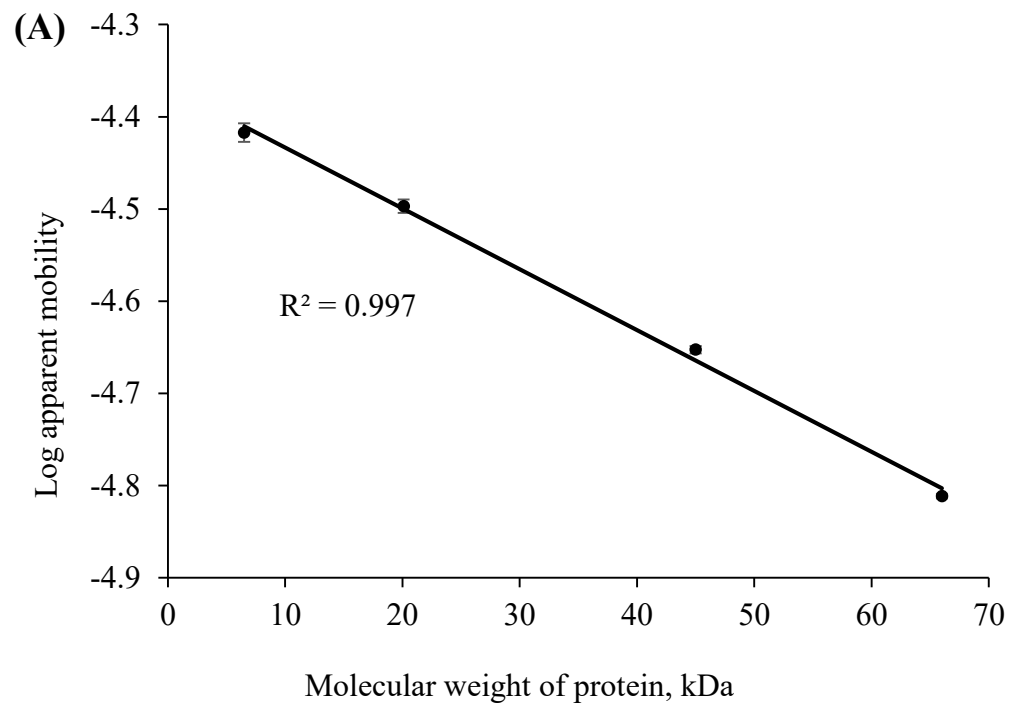


Figure 4-9: Plots of apparent mobility of SDS-protein complex vs protein molecular weight with least square fit using 100 nm particle at 160 V/cm. The error bars are the standard deviation ($n=3$) **(A)** a semi log plot **(B)** a log- log plot

To find out how well the 100 nm particle bed separation data fit with the Giddings model¹⁷ at the much higher field strengths and smaller particle used in these stabilized beds, a plot of $\sqrt{\mu}$ vs. radius of hydration, R_H , of the SDS-proteins, is shown in Figure 4-10. The linear relation between the square root of mobility vs. R_H demonstrates that proteins are following the Wirth/Giddings model for a uniform pore distribution. But the R^2 value of the Wirth/Giddings model is the same as the Ogston model, which means this results can not be used to distinguish between the two models of pore distribution.

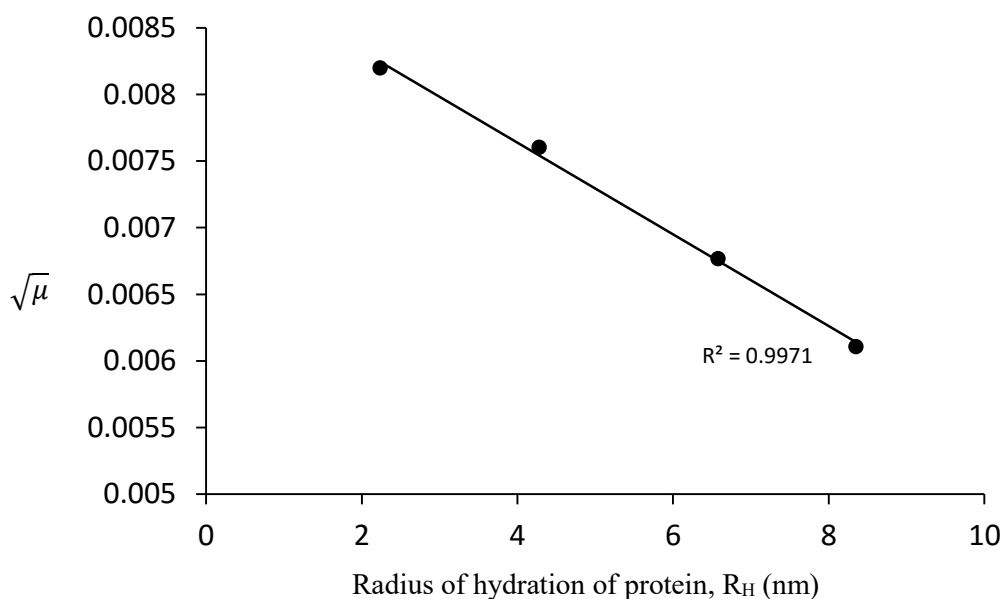


Figure 4-10: A plot of $\sqrt{\mu}$ vs radius of hydration protein, R_H , using 100 nm particle beds. The error bars (smaller than the marker) are the standard deviation ($n=3$)

4.3.5 Mass resolution for smaller particle beds

To characterize the resolving power of smaller particle sieves, the minimum molecular weight difference resolvable was estimated using:¹⁴

$$R_r = \frac{\Delta M}{R_s} \quad 4-3$$

where ΔM is the difference in molecular weight of the proteins which are separated, and R_s is the resolution between those separated proteins.

A resolution of 3.6 (Table 4-3) was achieved between aprotinin, 6.5 kDa, and trypsin inhibitor (20.1 kDa) for an 8 mm separation distance using 100 nm particles. This gives a mass resolving capacity of 3.7 kDa for this separation distance. Two proteins with even closer molecular weights were run at 160 V/cm using a 10 mm separation distance. The electropherogram of this separation is shown in Figure 4-11. The resolution between lysozyme 14.2 kDa, and trypsin inhibitor 20.1 kDa was 2.85 for a 10 mm separation distance. So a mass resolution of ~ 2 kDa is possible. To confirm this finding, two proteins with yet closer molecular weights, lysozyme, 14.2 kDa and myoglobin, 17.1 kDa were separated using a 13 mm separation distance at 160 V/cm. Figure 4-12 shows the electropherogram of this separation. A 1.6 resolution separation was achieved; which yielded a mass resolving power for 100 nm particles with a 13 mm separation distance of 1.8 kDa.

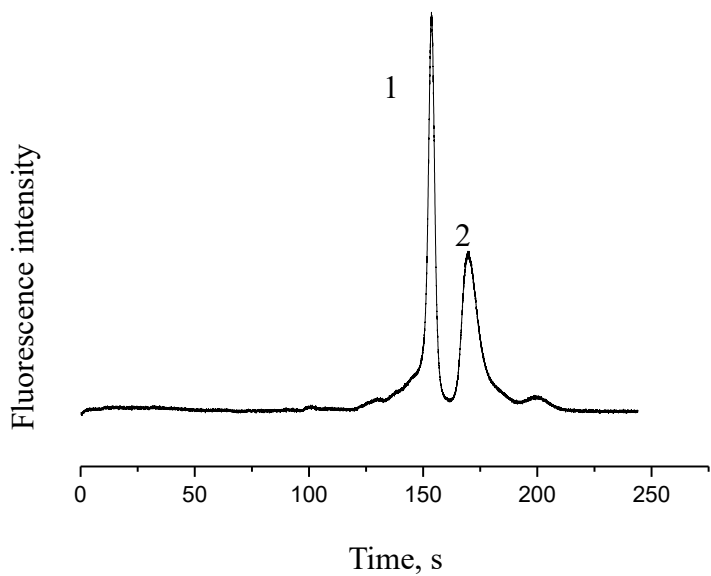


Figure 4-11: Electropherogram of two protein separation at 160 V/cm using 100 nm particle 10 μm thick bed and 10 mm separation distance. 1) lysozyme, 14.2 kDa, 2) trypsin inhibitor, 20.1 kDa.

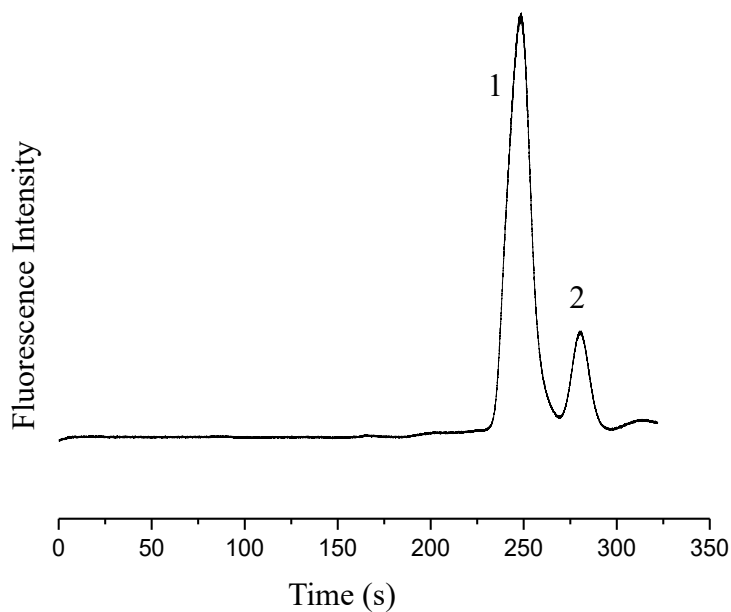


Figure 4-12: Electropherogram of two protein separation at 160 V/cm using 100 nm particle 10 μm thick bed and 13 mm separation distance. 1) lysozyme, 14.2 kDa, 2) myoglobin, 17.1 kDa.

Due to using a narrow bore capillary, stability at 320 V/cm was achieved for 50 nm particles in a 4 μm thick bed. The electropherogram of lysozyme (14.2 kDa) and myoglobin (17.1 kDa) separations using 160 V/cm and 320 V/cm is shown in the Figure 4-13.

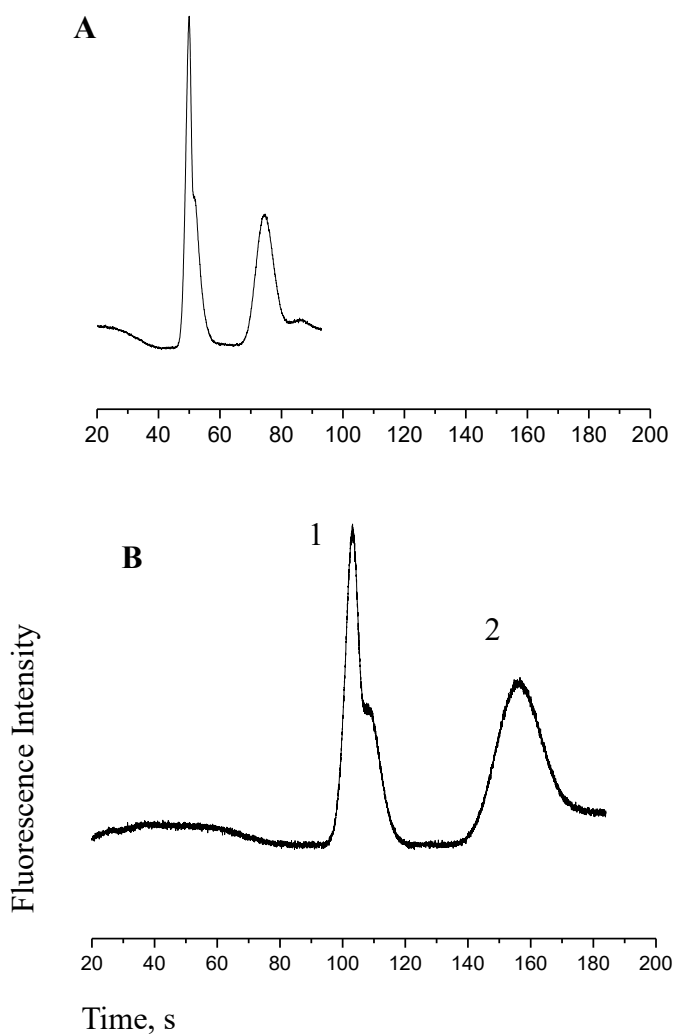


Figure 4-13: Electropherograms of separation at A) 320 V/cm and B) 160 V/cm using 50 nm particles of 4 μm thick bed and 5 mm separation distance.

At 160 V/cm and 320 V/cm separation voltages, a resolution of 2.9 and 3.3 were achieved, respectively. This resolution in the 50 nm particle beds gives mass resolving capacities of 1.0 and 0.86 kDa, respectively. These results are much improved over those reported for gel electrophoresis in a microchip^{16,41,142} for these size ranges of SDS-protein complex separations. The overall findings of mass resolving capacity are summarized in Table 4-4.

Table 4-4: Mass resolving capacity of different separation matrix in microchip

Separation matrix	Mass resolution	Separation distance	Reference
8% Polyacrylamide gel	5.1 kDa	0.4 cm	16
Beckman SDS 14-200 gel	~2-3 kDa	4.5 cm	41
100 nm Silica particle	~1.8 kDa	1.3 cm	This work
50 nm Silica particle	~0.87 kDa	0.5 cm	This work

4.4 Conclusions

We have evaluated the separation performance of narrow bore capillaries in terms of resolution and mass resolving capacity of different sized particle beds. Narrowing the capillary bore greatly stabilized the particle beds even for smaller particle assemblies. The 50 nm plate height at 650 V/cm is valuable for a miniaturized separation. The 0.87 kDa mass resolving capacity of 50 nm particle bed within a 5 mm separation distance increases the scope of particle beds in protein separation. The results demonstrate that this simple and inexpensive fabrication process for microchips with a CSA bed has high potential in improving protein analysis.

Chapter 5

Ortho Silicate Cross Linking (Sol-Gel) between the Particles of CSA Bed for Highly Stabilized Bed*

5.1 Introduction

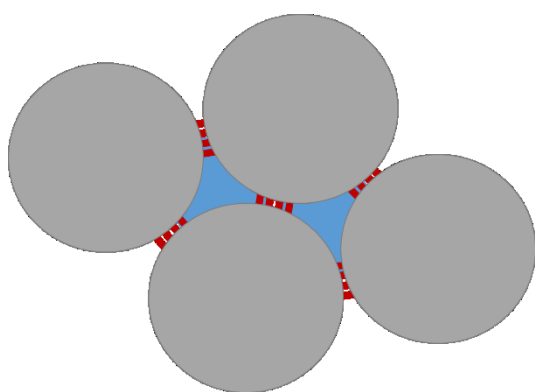
The stability of colloidal self-assembly of nanoparticle beds is very important for high performance SDS-protein separation. The reasons for instability of CSA beds have been discussed in Chapter 3. A few processes have been reported in the literature to stabilize the CSA bed.^{15,45} Chapters 3 and 4 demonstrate the stability of narrow bore capillary beds for high performance SDS-protein separation. Unfortunately, the narrow bore chips are still not stable for more than a few days at high fields.

Polymers inside the CSA bed increase the stability,^{15,43} but they complicate true electrophoresis due to possible chromatographic effects. Thermal stabilization could be a possible alternative, but it is very challenging to prepare crack free beds by thermal treatment, especially with nanoparticles.^{116,117} Cracks are the most unwanted phenomena in CSA beds used for separation. So an alternative approach is required, which would not interfere with electrophoresis yet provide stable CSA beds for long term repetitive use.

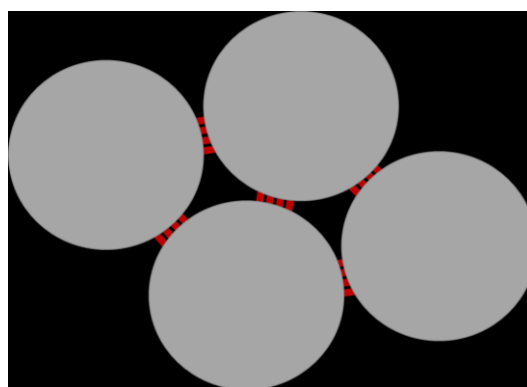
* A part of this chapter has been published in Proceeding of 18th International Conference on Miniaturized Systems for Chemistry and Life Sciences as, "Colloidal self-assembled nanoparticles sieves with orthosilicate cross linking for protein separation in microchips and retardation coefficient for on chip protein sizing", Mohammad Azim, Abebaw B. Jemere and D. Jed Harrison, MicroTAS 2014; San Antonio, USA; 2387-2389

Silica gel formation inside pores of a CSA bed using sol-gel chemistry is a possible alternative bonding method. Silica gel is prepared from the same starting materials as silica nanoparticles, so similar surface chemistry, surface charge and electroosmotic flow (EOF) is expected.

During silica gel formation inside the packed bed, two possible alternative phenomena may happen. The gel may form inside the pores and block them, making the chip unusable for separation. Alternatively, a gel could be formed to crosslink the particles to stabilize the CSA bed.



Gel formation inside the pores



Cross linking between the particles

Figure 5-1: Two possible alternative where gel could be formed.

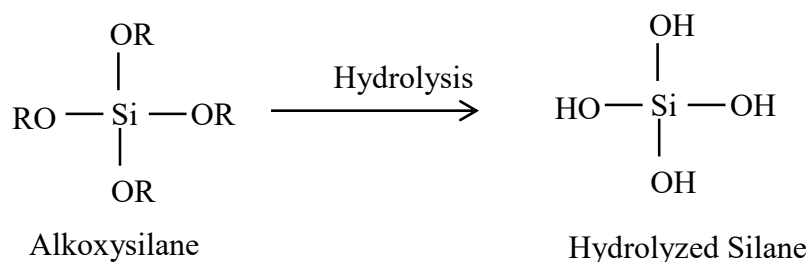
In this chapter we report the use of silica gel to entrap particles in CSA beds. As a result, the beds can be suitable for high voltage separation and show stability for long term repetitive use. The effect of catalyst (acid or base) on gel formation inside the pores is reported here. The stabilization was evaluated by separation of SDS-protein complexes at

various voltages, while the long term stability of chips was tested by running SDS-protein complexes over several days.

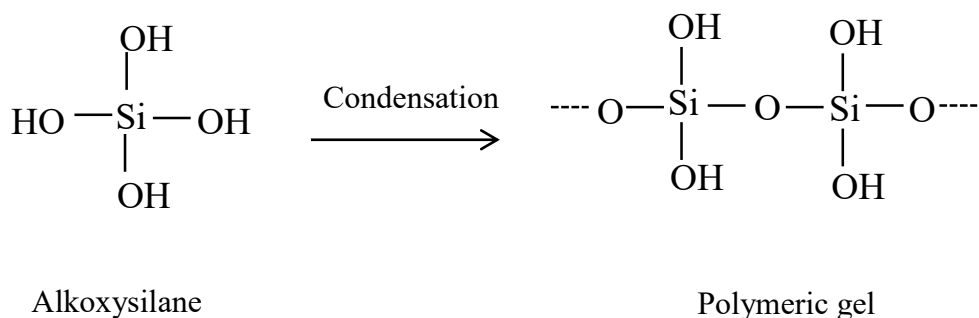
5.2 Sol Gel chemistry

In the sol-gel polymerization process,^{143,144} silica gel is prepared from silicon alkoxides eg Si(OR)₄. The reaction has two steps:

- 1) First step: alkoxy silane is hydrolyzed



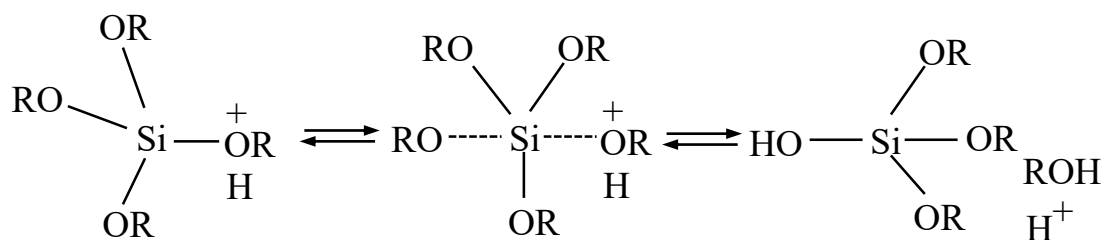
- 2) Second step: hydrolyzed silane is condensed to polymeric silica gel



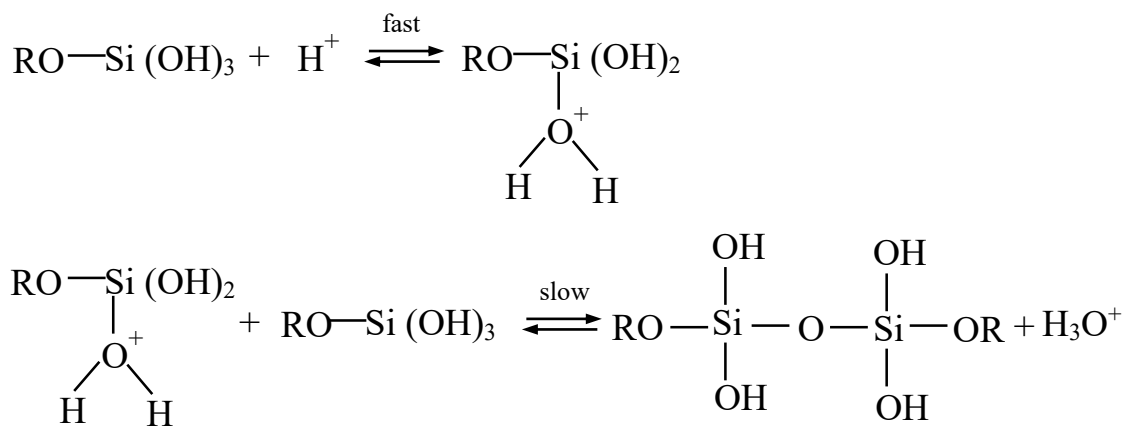
Different silicon alkoxides are used for gel formation. In this study, tetraethyl orthosilicate (TEOS) was used. When TEOS and water are mixed in a mutual solvent, e.g., ethanol, hydrolysis occurs. Both hydrolysis and condensation reactions occur by nucleophilic substitution reactions¹⁴³ in the presence of acid or base catalysis. The overall mechanism of gel formation is describe below:

The mechanisms¹⁴³

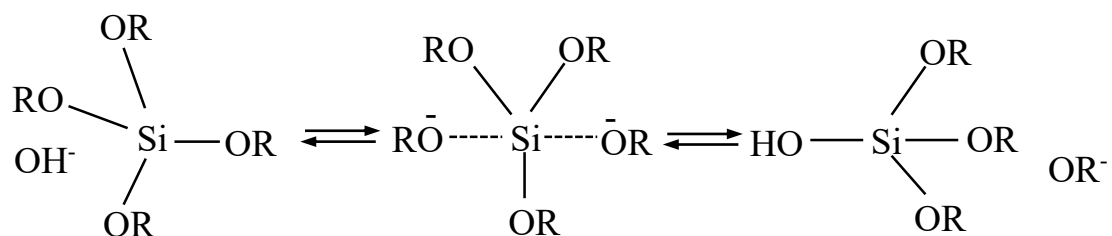
Acid Catalyzed Hydrolysis



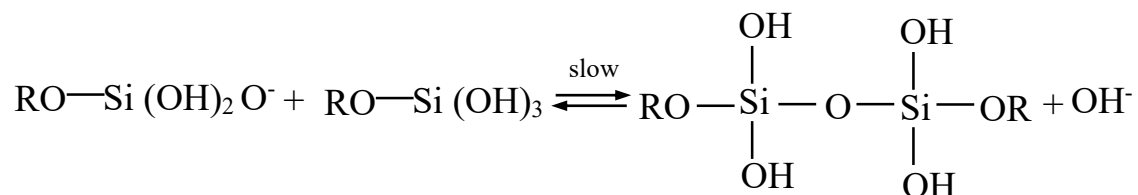
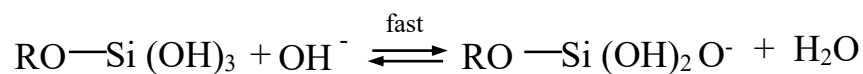
Acid Catalyzed Condensation



Base-Catalyzed Hydrolysis



Base-Catalyzed Condensation



Under acidic conditions,¹⁴³ hydrolysis is very slow and the silica tends to form linear molecules with some cross linking. These chains entangle and form additional branches during gelation. As a result, high-density low-pore volume gels are formed. As polymers impinge on one another, the gels formed by acid catalysis deform readily to create a dense gel structure.

In basic conditions, hydrolysis is more rapid. Highly branched clusters of molecules are formed which are not inter-penetrable. Gelation occurs by linking of the clusters.

The stoichiometric molar ratio of TEOS:Ethanol:H₂O for the gel formation reaction is 1:4:4. For completely hydrolyzed TEOS, 4 moles of water are required. But excess water is used to drive the reaction to the right.¹⁴³ So, the actual optimum molar ratio of the reaction is TEOS:Ethanol:H₂O = 1:4:16.

5.3 Materials and methods

5.3.1 Protein samples and chemicals

As molecular weight standards, aprotinin (6.5 kDa), lysozyme (14.2 kDa), myoglobin (17.1 kDa), trypsin inhibitor (soybean, 20.1 kDa), ovalbumin (chicken egg, 45 kDa) and bovine serum albumin (BSA, 66 kDa), were from Sigma-Aldrich. The detail process of labeling with fluorescent dye, purification and storage is described in Chapter 2. The composition of working and sample buffer was also same as the described in Chapter 2.

5.3.2 Microchip fabrications and colloidal self-assembly

Microchips were assembled using polydimethylsiloxane (PDMS) with glass support as described in Chapter 2.

An evaporation-induced colloidal self-assembly mechanism was used for nanoparticle bed formation. A 10 % aqueous solution of mono dispersed silica particles (Bang Laboratories, Poly Sciences Inc) was used without any modification or treatment,

for fabrication of colloidal self-assembled (CSA) structure in the microchips which is described in Chapter 2 in detail. Before gel formation the silica particles/water suspensions in reservoirs were replaced with water.

5.3.3 Gel formation inside the packed bed

Sol-gel polymerization was used to form the gel inside the CSA structure. Tetra ethyl ortho silicate (TEOS) (Sigma-Aldrich), ethanol and water were used as starting materials, and hydrochloric acid (HCl) and ammonia solution (NH₄OH) was used as catalyst. A mixture of TEOS, ethanol and water was prepared in a molar ratio of TEOS:EtOH:H₂O = 1:4:16, to form monolithic gel within a reasonable time.¹⁴³

The mixture of TEOS, ethanol and water was vortexed for about 2 min to mix properly. Before adding the TEOS/ethanol/water mixture in the reservoir, the packed bed was conditioned with a 1:1 mixture of ethanol and water for about 2 h (depending on the length of the chip). After conditioning, the ethanol/water mixture remained in reservoir 4 and reservoirs 1, 2 and 3 were replaced with the TEOS/ethanol/water mixture. The mixture were kept in all the reservoir for about 5-6 h at room temperature to disperse properly throughout the CSA structure. Then the TEOS mixture was replaced with 1:1 ethanol/water in reservoirs 1, 2 & 3. At the same time, either 0.1 M HCl or 0.1 M NH₄OH solution was added in reservoir 4 as a catalyst, and left in the chip for ~5 h. After that, all the reservoirs were washed with the ethanol and water mixture two times. Then the ethanol/water was mixture run through the CSA bed in microchip at 100 V/cm for about 20-25 min to remove unreacted TEOS. After this first run of cleaning, fresh ethanol/ water

mixture was added and run again at the same voltage, for the same time. Then all reservoirs were rinsed with water several times and filled with water for storage.

5.3.4 Instrumentation and separation

A confocal epifluorescence microscope¹⁰⁸ was used to monitor the separation as described in Chapter 2.

Before separation, the water was replaced with working buffer and left in the devices for about 30 min to equilibrate with the working buffer inside the CSA structure. The working buffer was run for about 20-30 min at 100 V/cm. After this first run, the fresh working buffer was added and run again at the same voltage and for the same time to remove any trace ethanol from the chip.

The working buffer was run for about 20-30 min at 100 V before the separation started, to obtain stable current through the channels. During injection, SDS-protein mixture was loaded from reservoir 2. A 60-80 V potential was applied to sample waste reservoir 3, with all other reservoirs grounded, to form a shaped injection plug which reduced the band broadening during separation. During separation, equal positive and negative potentials were applied between reservoirs 1 and 4, with the other two reservoirs grounded. The negative potential applied in reservoir 1 served as a push back potential to prevent sample leaking from the grounded sample loading arms. The potential at the double T position (red circle position in figure 1A) was calculated by application of Kirchhoff's rules.¹³² The negatively charged SDS-protein complexes migrated towards the

anode and the laser spot was located at a fixed distance from the double T position, to excite the FITC labelled SDS-protein complexes.

5.4 Results and discussion

5.4.1 Conditioning CSA bed

Before starting gel formation, the particle packed chip was conditioned with a 1:1 mixture of ethanol and water. To determine the conditioning time, FITC solution was added to the reservoirs and monitored. The diffusion of FITC in the bed was about 1 mm/10 min. From this observation, depending on the channel length, the conditioning time was optimized. The effect of conditioning is shown in Figure 5-2. A good quality chip after conditioning and gel formation is shown in Figure 5-2a. Without conditioning, if the TOES mixture was added in the reservoir, the portion of the packed bed in the separation channel became dried (Figure 5-2c), which was impossible to rewet and the chip became unusable for separation. This problem was solved by simply conditioning the chip with an ethanol/water mixture. To visually differentiate between a dried out and a good chip, a completely dried chip is also shown in Figure 5-2b.

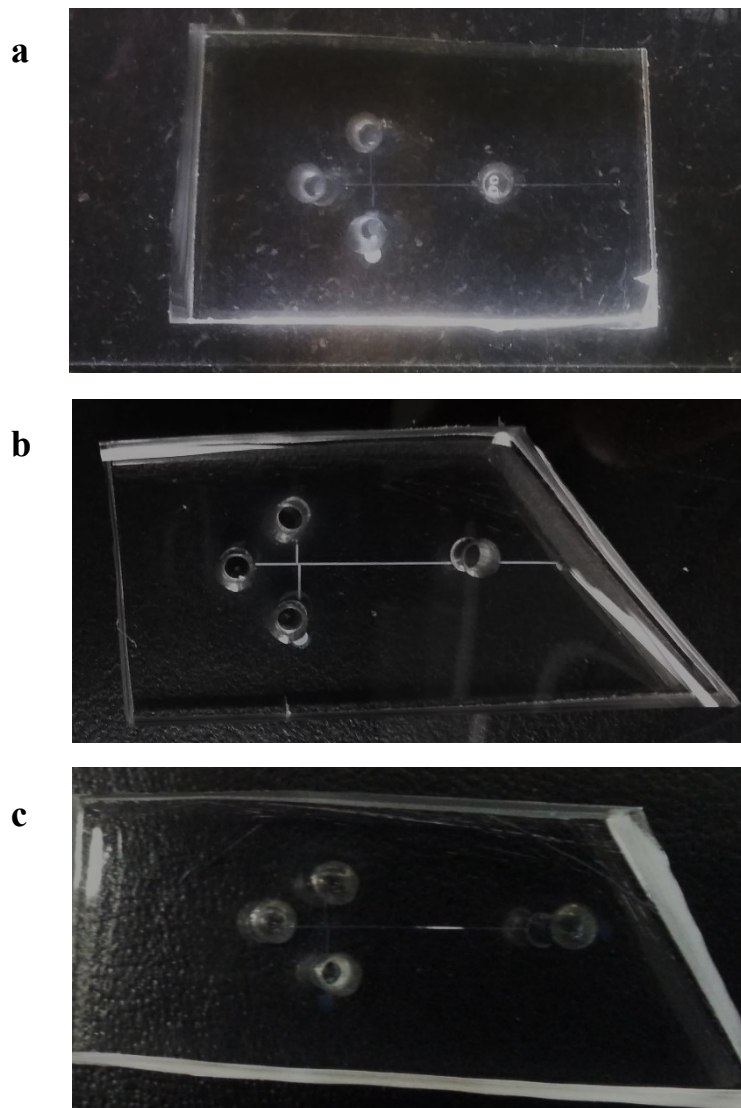


Figure 5-2: Photograph of chips a) a good quality packed gel-chip in water after conditioning with alcohol, b) a packed gel-chip completely dried condition, and c) a chip without conditioning became dried from the middle.

5.4.2 Effect of catalyst on the orthosilicate cross linking

The main objective of gel formation was to use the gel as a glue between the particles. When acid (HCl) was used as catalyst, the formed gel clogged all the pores of the CSA structure and even injection of sample was not possible. The SEM images in Figure 5-3 show both acid catalyzed and base catalyzed gel formation inside the CSA bed. From the SEM images it is clear that the gel form by acid catalysis filled all the pores of CSA bed (Figure 5-3b) and made the CSA bed unusable for separation. On the other hand, base (NH₄OH) catalyzed gel (Figure 5-3a) just acted like glue to hold the particles together, leaving the interstitial pores open, and made the CSA bed suitable for high voltage separation. The results are consistent with the known behavior of acid versus base catalysis.¹⁴³

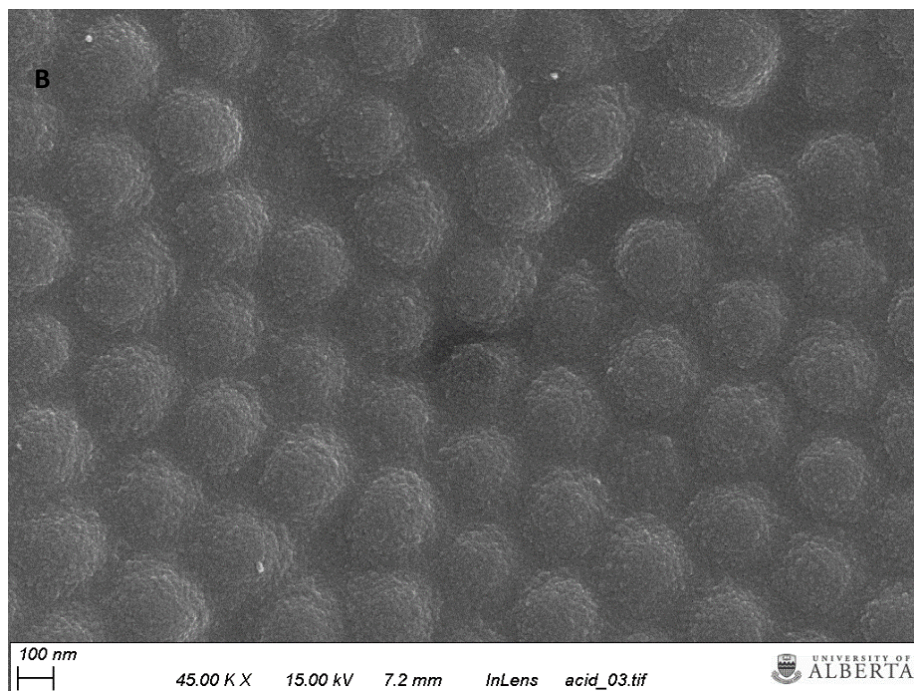
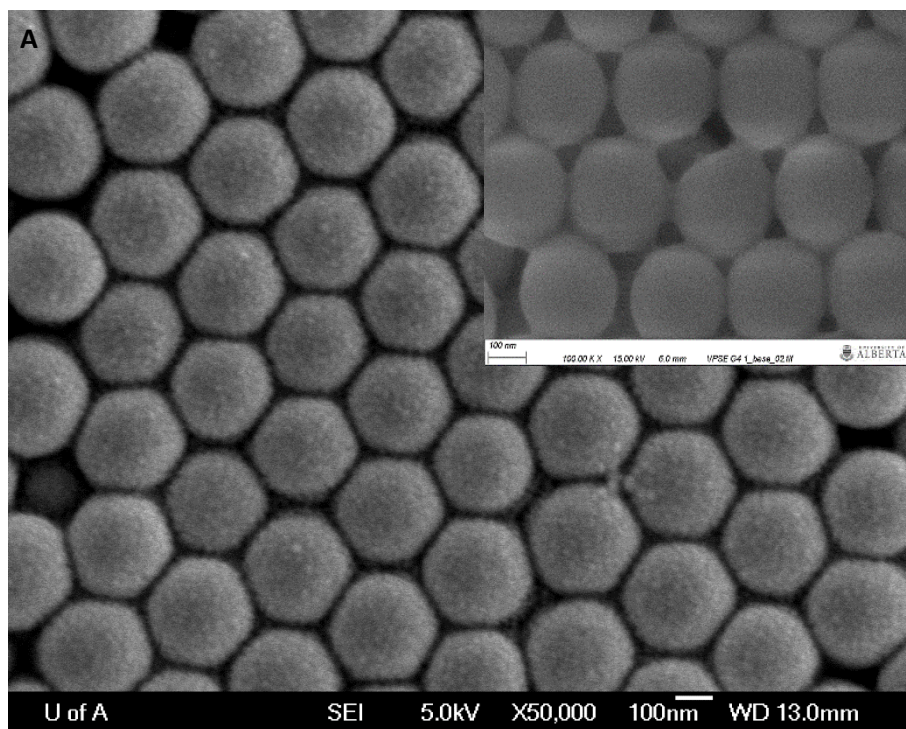


Figure 5-3: SEM image of a) base catalyzed gel formation inside the CSA bed of chip (highly magnified image is shown inset), and b) acid catalysed gel block all pores inside the CSA bed of nano particles

5.4.3 Separation performance of 300 nm particle bed with base catalyzed gel

The electropherograms of mixtures of four SDS-protein complexes at 1280 and 1600V/cm using a stabilized 300 nm silica particle bed are shown in Figure 5-4. The chip was stable up to 1600 V/cm, and all the proteins were baseline separated with good resolution (Table 5-1). A plot of migration rate of SDS-aprotinin complex with applied voltage is shown in Figure 5-5. The migration rate was linearly ($R^2 = 0.996$) dependent on the applied voltage. At the highest voltage (1600 V/cm), there was a slight deviation, probably due to Joule heating.

The number of plates for aprotinin was calculated using equation 4-1, and the plate height was calculated ($L = 4$ mm). The plot of plate height as a function of migration rate is shown in Figure 5-6. The plate height is highly dependent on the separation field strength. The minimum plate height was achieved at 1280 V/cm (240 nm) at a migration rate of 0.82 mm/s, after that it starts to increase slowly.

The maximum resolution (R_s) of 3.0 was achieved between ovalbumin (45 kDa) and BSA (66 kDa) with a 4.0 mm separation distance. All the separation performance parameters are shown in Table 5-1.

The minimum plate height of 240 nm was achieved at 1280 V/cm for aprotinin (6.5 kDa), and is highly dependent on separation voltage. At higher fields, the plate height started to increase slowly. This result is a good improvement for separation in terms of plate height for SDS-protein complexes reported in the literature for polymerized and thermal treated CSA beds in chip (Lin et al reported 0.78-3.88 μm for capillary gel

electrophoresis in microchips¹⁴⁵ and Birdsall et al.¹⁴⁶ reported 0.4 to 1.1 μm for electrophoresis using a polymerized CSA structure¹⁴⁶). However, the results in narrow bore capillary of ~ 50 nm is better.

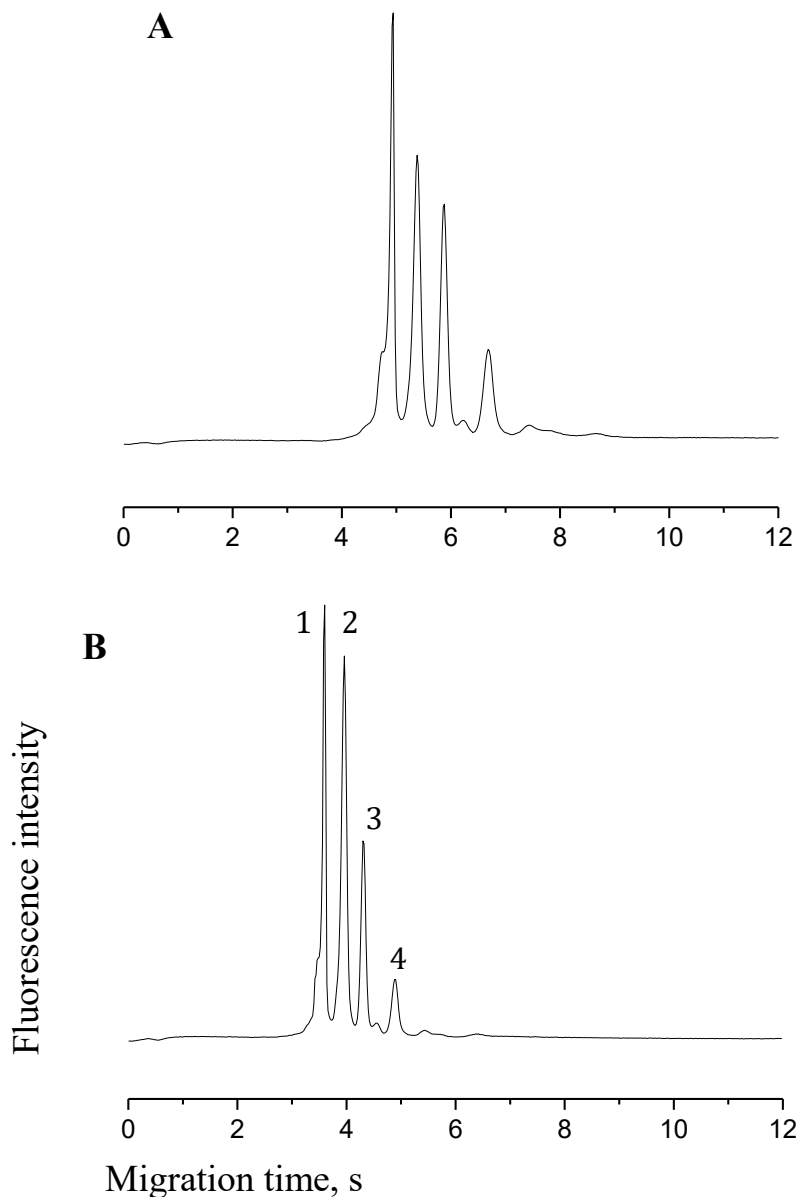


Figure 5-4: Electropherograms of four protein mixture using 300 nm particle bed stabilized with basic gel formation at 4 mm separation distance A) at 1280 V/cm, and B) 1600 V/cm separation voltage. 1) aprotinin, 6.5 kDa; 2) trypsin inhibitor, 20.1 kDa; 3) ovalbumin, 45 kDa; and 4) BSA, 66 kDa.

Table 5-1: Resolution between different proteins and plate numbers at different separation voltage

Separation Voltage (V/cm)	Resolution between			Efficiency	
	Aprotinin-Try. Inhi.	Try. Inhi.-Ovalbumin	Ovalbumin-BSA	Minimum plate height (nm)	Plate number, $N/m \times 10^6$
960	2.2	1.2	2.7	305	1.38-3.27
1280	2.3	1.8	2.9	240	1.54-4.13
1600	2.5	2.0	3.0	242	1.69-4.13

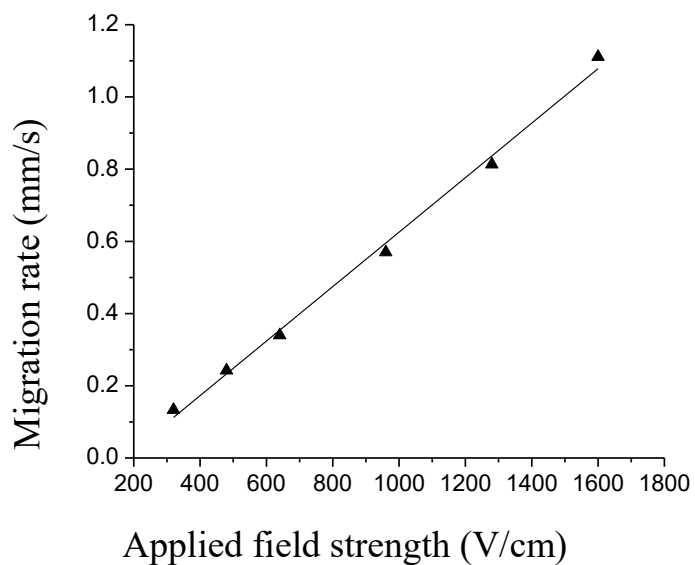


Figure 5-5: A linear relationship between migration rates of SDS-aprotinin complexes vs. applied electric field.

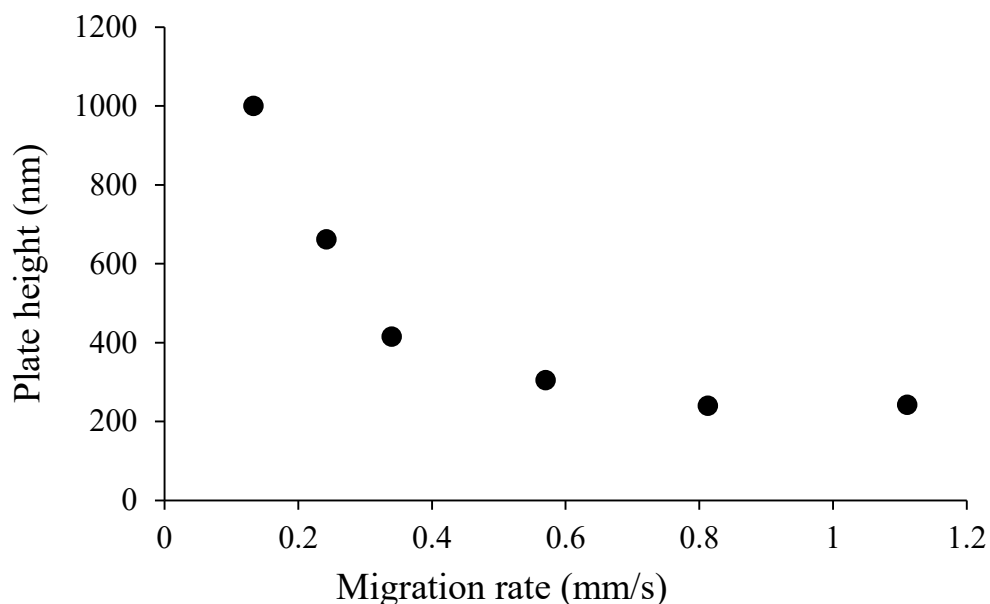


Figure 5-6: A nonlinear relationship between migration rates of SDS-aprotinin complexes vs. plate height.

5.4.4 Stability and reproducibility

The stability of a bed at high voltage and reproducibility of bed fabrication are crucial for routine use of the chips in analytical applications. To test the stability and reproducibility of a chip at high voltage, three consecutive runs are shown in Figure 5-7. The relative standard deviation (RSD) of migration time at 1280 V/cm varied from 0.8 to 2 % for different proteins.

To test chip to chip fabrication reproducibility and day to day reproducibility, trypsin inhibitor was run at 960 V/cm. The RSD of the migration time of 5 different chips was ~2.5 %. The day to day RSD value for up to 7 days with the same chip was ~3.0 %. The RSD confirmed the chip could be used at least a week without significant deviation in performance.

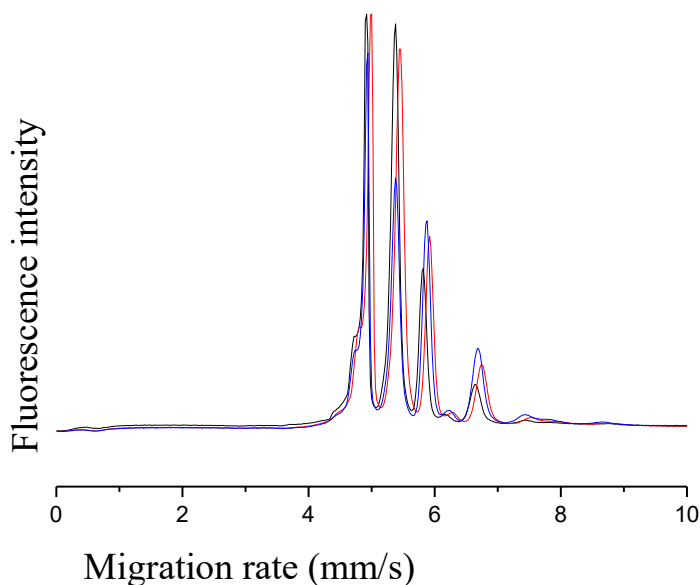


Figure 5-7: Superimposed electropherograms of three consecutive separation runs at 1280 V/cm using base catalyzed chip.

5.5 Conclusions

We have demonstrated another method to stabilize the CSA bed of nanoparticles in microchip. The base catalyzed sol-gel polymerization introduces cross links between the particles to entrap them, and gave the bed stability up to 1600 V/cm. The acid catalyzed gel filled the pores and made the microchip unusable. The minimum plate height achieved at 1280 V/cm was 240 nm. This plate height is higher than the plate height achieved using narrow bore capillary (50 nm). This is probably because of random gel formation in the pores, which increases the A term of the van Deemter equation. However, the CSA bed

entrapped by gel can be used for at least a week and the reproducibility of fabrication is high. This study demonstrates that gel entrapped particles bed can be used for high performance SDS-protein separation up to several days without significant deviation of chip performances.

Chapter 6

Conclusions and Future work

6.1 Conclusions

Colloidal self-assembly of nanoparticles is a very simple and inexpensive way to prepare molecular sieves in comparison to conventional microfabrication. These highly ordered, uniform pores are very suitable for biomolecular separation. However, the CSA beds in microchips are not stable for high performance separation. To exploit all the benefits of miniaturization, a CSA bed needs to be stable for high voltage separation. In this research, focus was given mainly in two areas: 1) understanding how the SDS-protein complexes move through the highly ordered CSA bed of nanoparticles; and 2) determining how to make CSA beds stable for high voltage separation. The findings are summarized below:

The stability of native CSA beds is highly dependent on the size of nanoparticle. As size decreases, stability of the bed also decreases. For 20 μm thickness, the 300 nm particle beds are stable up to 320 V/cm whereas for 150 nm stability was found up to 60 V/cm. Better separation is achieved using smaller sized particles. The migration behaviour

of SDS-protein complexes through a colloidal self-assembled particle bed was analyzed by the classical, modified Ogston sieving model for protein separation in a porous media, and by the Wirth/Giddings modified expression for separation in a single pore size medium. The results showed improved fits and better predictive interpolation of the molecular weight on unknowns using the Wirth/Giddings model for a uniform pore structure. The better predictive interpolation of the single pore size model indicates that it is meaningful to characterize these structures as having a predominantly single pore size. The simple manipulation of the Wirth/Giddings equation gives a convenient method to generate calibration curves for a function of mobility versus molecular weight of protein standards, as is commonly done in gel electrophoresis.

By reducing the depth of the CSA beds, three to four times the electric field stability is achieved. Fewer numbers of defects and the increasing influence of the PDMS wall to the CSA bed are the main reasons for the stability increase. The stability of a 300 nm particle bed, 20 μm thick, was only ≤ 320 V/cm, but for a 10 μm thick bed, stability was achieved up to 1250 V/cm, while a 4 μm thick bed was stable up to 2250 V/cm. A 150 nm particle, 20 μm thick bed gave stability to less than 60 V/cm, but using a 10 μm thick bed up to 450 V/cm could be achieved. In a narrow bore 4 μm thick capillary, we could easily work with 100 nm and 50 nm particle beds, which was almost impossible with a 20 μm thick bed. Decreasing particle size in beds greatly improves the separation performance. The separation structure fabrication process is very simple, and much less costly than nanofabrication methods. Very high separation performance was achieved compared to competing technologies such as conventional gels.

The separation performance of narrow bore capillaries in terms of resolution and mass resolving capacity of different sized particle beds has been evaluated. A 50 nm plate height was achieved for trypsin inhibitor using 300 nm particles in a 10 μm thick bed at 650 V/cm. A minimum plate height for FITC of 300 nm was achieved, using a thermally treated 500 nm particle CSA bed, and a minimum plate heights of 0.4 and 1.1 μm for SDS-protein complexes using 350 and 500 nm particle polymerized CSA beds, respectively. So in terms of plate height, the separation efficiency for narrow bore CSA beds of native silica is greatly improved. The mass resolving capacity for 100 nm particle beds at 13 mm distance was 1.8 kDa at 160 V/cm. Resolution of 0.87 kDa was obtained for 50 nm particle beds within a 5 mm separation distance. The separation efficiency in terms of mass resolution is also greatly improved in comparison to gel in a microchip. Using 8% polyacrylamide gel in microchip, 5.1 kDa, and using Beckman SDS 14-200 gel, 2-3 kDa mass resolution was reported. So, our findings are almost 3-6 time better than the reported results. Though highly efficient separation was achieved using narrow bore CSA beds, the stability of these native silica bed was not that high. These kind of chips were stable up to 5-6 run at highest stable field strength. But if the separation voltage was maintained 50-100 V/cm below the highest stable voltage, 12-15 runs were possible.

Gel formation inside the particle beds is another way to increase the stability of a CSA bed. The base catalyzed sol-gel polymerization, cross linked between the particles to entrap them and gave stability up to 1600 V/cm for 300 nm particle 10 μm thick bed, which was 1250 V/cm without gel formation. Acid catalyzed gel filled the pores and made the microchip unusable. For 300 nm particle beds, the minimum plate height was achieved at 1280 V/cm, which is 240 nm. In compare to plate height of native 300 nm silica particle

using narrow bore capillary ($H = 50 \text{ nm}$ at 650 V/cm), gel chip plate height is much higher even though higher separation voltage was used. This is probably because of random gel formation in the pores, which increases the A term of the van Deemter equation and also could be from nonspecific absorption. But the CSA bed entrapped by gel was suitable to use at least for a week, (10-15 runs/day) which was not possible using narrow bore capillary. The reproducibility of fabrication of CSA-gel chip (yield = 85-90 %) was comparable with narrow bore capillary CSA (yield = 95 %) chip. This study demonstrated that gel entrapped particles bed can be used for high performance SDS-protein separation up to a few days without significant deviation of chip performances.

The competing technology of CSA based chip for protein separation is gel electrophoresis. Gel is a very well established and popular technology for protein separation. So, to make CSA based microchips popular and commercially success, few barriers need to be considered including bulk production facilities, on-chip detection system and also cost. If these barriers could overcome, CSA-microchips have high potential as a LOC devices for everyday protein analysis.

6.2 Future work

From the discussion of the research presented in this thesis, there are a few thoughts presented in this section as a reference for future perspective of this research.

In Chapter 2, the sieving mechanism for proteins ranging from 6.5-66 kDa has been explored. The radius of hydration of the protein across this range is lower than the nominal size of the pores of the smallest particles (150 nm) used in this study. This places the expected performance in Ogston sieving regime, as was observed. Westerhuis et al.¹⁰⁶ evaluated that larger proteins separated through higher gel concentrations could not appropriately be described by the Ogston sieving model. If the pore size of the gel networks size is similar or significantly smaller than the analyte, then the analyte migrates through the gel in a head first, snake like mechanism, which is called a reptation mechanism. To determine how larger proteins migrate through smaller pore CSA beds, experiments can be designed using smaller particle assemblies and larger sized proteins.

In Chapter 3 and 4, the separation performance of narrow bore capillaries has been described. But all the experiments were designed using model proteins. The SDS-PAGE method is commonly used for quality control and stability monitoring of monoclonal antibodies or therapeutic proteins.^{147,148} Capillary electrophoresis has very high potential in this field.¹⁴⁷⁻¹⁴⁹ So microchip electrophoresis can play a very important role in this area. To explore the usability of microchip electrophoresis in quality control application of therapeutic proteins and to evaluate separation performance, studies should be undertaken using narrow bore capillaries.

In Chapter 5, gel formation inside the CSA bed has been studied. But only the role of catalyst has been explored using 300 nm particles. So the role of other alkoxides as starting materials and the role of solvent in gel formation can be studied. This area can be extended to gel formation in 150, 100 and 50 nm particle assemblies.

Western blotting is an indispensable tool for clinical diagnosis.⁴⁷ The present state of Western blotting is very time consuming and tedious. To improve this technique and overcome the present shortcomings, Herr and coworkers reported microfluidic based micro chamber Western blotting technique.⁴⁹ They used polyacrylamide gel inside the micro chamber and intergraded separation, transfer, blocking and immune-detection, all steps in a single chip. As a CSA bed of nano particles provides more uniform pores than gel, a micro chamber filled with the CSA bed instead of gel could give improved efficiency of this technique. So, experiments can be design to evaluate the CSA bed based western blotting performances in micro chamber.

References

- 1 Manz, A., Graber, N. & Widmer, H. M. Miniaturized total chemical analysis systems: A novel concept for chemical sensing. *Sensors and Actuators B: Chemical* **1**, 244-248, (1990).
- 2 Castro, E. R. & Manz, A. Present state of microchip electrophoresis: State of the art and routine applications. *Journal of Chromatography A* **1382**, 66-85, (2015).
- 3 Haddad, P. R. Editorial on “Present state of microchip electrophoresis: State of the art and routine applications” by Eric R. Castro and Andreas Manz. *Journal of Chromatography A* **1382**, 65, (2015).
- 4 Manz, A. *et al.* Micromachining of monocrystalline silicon and glass for chemical analysis systems A look into next century's technology or just a fashionable craze? *TrAC Trends in Analytical Chemistry* **10**, 144-149, (1991).
- 5 Manz, A. *et al.* Planar chips technology for miniaturization and integration of separation techniques into monitoring systems. *Journal of Chromatography A* **593**, 253-258, (1992).
- 6 Whitesides, G. M. The origins and the future of microfluidics. *Nature* **442**, 368-373 (2006).
- 7 Duffy, D. C., McDonald, J. C., Schueller, O. J. A. & Whitesides, G. M. Rapid Prototyping of Microfluidic Systems in Poly(dimethylsiloxane). *Analytical Chemistry* **70**, 4974-4984, (1998).
- 8 Weinberger, S. R., Morris, T. S. & Pawlak, M. Recent trends in protein biochip technology. *Pharmacogenomics* **1**, 395-416, (2000).
- 9 Macounová, K., Cabrera, C. R. & Yager, P. Concentration and Separation of Proteins in Microfluidic Channels on the Basis of Transverse IEF. *Analytical Chemistry* **73**, 1627-1633, (2001).

- 10 Khandurina, J. & Guttman, A. Bioanalysis in microfluidic devices. *Journal of Chromatography A* **943**, 159-183, (2002).
- 11 Lion, N., Reymond, F., Girault, H. H. & Rossier, J. S. Why the move to microfluidics for protein analysis? *Current Opinion in Biotechnology* **15**, 31-37, (2004).
- 12 Dou, Y.-H., Bao, N., Xu, J.-J., Meng, F. & Chen, H.-Y. Separation of proteins on surface-modified poly(dimethylsiloxane) microfluidic devices. *ELECTROPHORESIS* **25**, 3024-3031, (2004).
- 13 Zeng, Y. & Harrison, D. J. Confinement effects on electromigration of long DNA molecules in an ordered cavity array. *ELECTROPHORESIS* **27**, 3747-3752, (2006).
- 14 Zeng, Y. & Harrison, D. J. Self-Assembled Colloidal Arrays as Three-Dimensional Nanofluidic Sieves for Separation of Biomolecules on Microchips. *Analytical Chemistry* **79**, 2289-2295, (2007).
- 15 Wei, B., Malkin, D. S. & Wirth, M. J. Plate Heights below 50 nm for Protein Electrochromatography Using Silica Colloidal Crystals. *Analytical Chemistry* **82**, 10216-10221, (2010).
- 16 Herr, A. E. & Singh, A. K. Photopolymerized Cross-Linked Polyacrylamide Gels for On-Chip Protein Sizing. *Analytical Chemistry* **76**, 4727-4733, (2004).
- 17 Birdsall, R. E., Koshel, B. M., Hua, Y., Ratnayaka, S. N. & Wirth, M. J. Modeling of protein electrophoresis in silica colloidal crystals having brush layers of polyacrylamide. *ELECTROPHORESIS* **34**, 753-760, (2013).
- 18 Han, J. & Singh, A. K. Rapid protein separations in ultra-short microchannels: microchip sodium dodecyl sulfate–polyacrylamide gel electrophoresis and isoelectric focusing. *Journal of Chromatography A* **1049**, 205-209, (2004).
- 19 Volkmuth, W. D. & Austin, R. H. DNA electrophoresis in microlithographic arrays. *Nature* **358**, 600-602 (1992).

- 20 Kaji, N. *et al.* Separation of Long DNA Molecules by Quartz Nanopillar Chips under a Direct Current Electric Field. *Analytical Chemistry* **76**, 15-22, (2004).
- 21 Nazemifard, N., Bhattacharjee, S., Masliyah, J. H. & Harrison, D. J. DNA Dynamics in Nanoscale Confinement under Asymmetric Pulsed Field Electrophoresis. *Angewandte Chemie International Edition* **49**, 3326-3329, (2010).
- 22 King, S. B. & Dorfman, K. D. Role of Order during Ogston Sieving of DNA in Colloidal Crystals. *Analytical Chemistry* **85**, 7769-7776, (2013).
- 23 Dittrich, P. S. & Manz, A. Lab-on-a-chip: microfluidics in drug discovery. *Nat Rev Drug Discov* **5**, 210-218 (2006).
- 24 Lombardi, D. & Dittrich, P. S. Advances in microfluidics for drug discovery. *Expert Opinion on Drug Discovery* **5**, 1081-1094, (2010).
- 25 Pihl, J., Karlsson, M. & Chiu, D. T. Microfluidic technologies in drug discovery. *Drug Discovery Today* **10**, 1377-1383, (2005).
- 26 Wheeler, A. R. *et al.* Microfluidic Device for Single-Cell Analysis. *Analytical Chemistry* **75**, 3581-3586, (2003).
- 27 Andersson, H. & van den Berg, A. Microfluidic devices for cellomics: a review. *Sensors and Actuators B: Chemical* **92**, 315-325, (2003).
- 28 Fortier, M.-H., Bonneil, E., Goodley, P. & Thibault, P. Integrated Microfluidic Device for Mass Spectrometry-Based Proteomics and Its Application to Biomarker Discovery Programs. *Analytical Chemistry* **77**, 1631-1640, (2005).
- 29 Yager, P. *et al.* Microfluidic diagnostic technologies for global public health. *Nature* **442**, 412-418 (2006).
- 30 Myers, F. B. & Lee, L. P. Innovations in optical microfluidic technologies for point-of-care diagnostics. *Lab on a Chip* **8**, 2015-2031, (2008).
- 31 Chin, C. D., Linder, V. & Sia, S. K. Commercialization of microfluidic point-of-care diagnostic devices. *Lab on a Chip* **12**, 2118-2134, (2012).

- 32 Sorger, P. K. Microfluidics closes in on point-of-care assays. *Nat Biotech* **26**, 1345-1346 (2008).
- 33 Govindarajan, A. V., Ramachandran, S., Vigil, G. D., Yager, P. & Bohringer, K. F. A low cost point-of-care viscous sample preparation device for molecular diagnosis in the developing world; an example of microfluidic origami. *Lab on a Chip* **12**, 174-181, (2012).
- 34 Marle, L. & Greenway, G. M. Microfluidic devices for environmental monitoring. *TrAC Trends in Analytical Chemistry* **24**, 795-802, (2005).
- 35 Volpatti, L. R. & Yetisen, A. K. Commercialization of microfluidic devices. *Trends in Biotechnology* **32**, 347-350, (2014).
- 36 <http://www.medgadget.com/2016/04/point-of-care-diagnostics-market-is-poised-to-reach-32-billion-revenue-by-the-year-2022.html>. Point of Care Diagnostics Market is poised to reach \$32 billion revenue by the year 2022.
- 37 Gomez, F. A. The future of microfluidic point-of-care diagnostic devices. *Bioanalysis* **5**, 1-3, (2012).
- 38 Wirth, M. J. Separation Media for Microchips. *Analytical Chemistry* **79**, 800-808, (2007).
- 39 Egas, D. A. & Wirth, M. J. Fundamentals of Protein Separations: 50 Years of Nanotechnology, and Growing. *Annual Review of Analytical Chemistry* **1**, 833-855, (2008).
- 40 Zhu, Z., Lu, J. J. & Liu, S. Protein separation by capillary gel electrophoresis: A review. *Analytica chimica acta* **709**, 21-31 (2012).
- 41 Yao, S. *et al.* SDS capillary gel electrophoresis of proteins in microfabricated channels. *Proceedings of the National Academy of Sciences of the United States of America* **96**, 5372-5377 (1999).
- 42 Bousse, L. *et al.* Protein Sizing on a Microchip. *Analytical Chemistry* **73**, 1207-1212, (2001).

- 43 Malkin, D. S., Wei, B., Fogiel, A. J., Staats, S. L. & Wirth, M. J. Submicrometer Plate Heights for Capillaries Packed with Silica Colloidal Crystals. *Analytical Chemistry* **82**, 2175-2177, (2010).
- 44 Njoya, N. K., Birdsall, R. E. & Wirth, M. J. Silica Colloidal Crystals as Emerging Materials for High-Throughput Protein Electrophoresis. *The AAPS Journal* **15**, 962-969, (2013).
- 45 Liao, T., Guo, Z., Li, J., Liu, M. & Chen, Y. One-step packing of anti-voltage photonic crystals into microfluidic channels for ultra-fast separation of amino acids and peptides. *Lab on a Chip* **13**, 706-713, (2013).
- 46 Adam, T., Unger, K. K., Dittmann, M. M. & Rozing, G. P. Towards the column bed stabilization of columns in capillary electroendosmotic chromatography: Immobilization of microparticulate silica columns to a continuous bed. *Journal of Chromatography A* **887**, 327-337, (2000).
- 47 Hughes, A. J. & Herr, A. E. Microfluidic Western blotting. *Proceedings of the National Academy of Sciences* **109**, 21450-21455, (2012).
- 48 Tia, S. Q., He, M., Kim, D. & Herr, A. E. Multianalyte On-Chip Native Western Blotting. *Analytical Chemistry* **83**, 3581-3588, (2011).
- 49 Chung, M., Kim, D. & Herr, A. E. Microchamber Western Blotting Using Poly-l-Lysine Conjugated Polyacrylamide Gel for Blotting of Sodium Dodecyl Sulfate Coated Proteins. *Analytical Chemistry* **85**, 7753-7761, (2013).
- 50 Rahong, S. *et al.* Three-dimensional Nanowire Structures for Ultra-Fast Separation of DNA, Protein and RNA Molecules. *Scientific Reports* **5**, 10584, (2015).
- 51 Malekpourkoupaei, A., Kostiuik, L. W. & Harrison, D. J. Fabrication of Binary Opal Lattices in Microfluidic Devices. *Chemistry of Materials* **25**, 3808-3815, (2013).
- 52 Ceriotti, L., de Rooij, N. F. & Verpoorte, E. An Integrated Fritless Column for On-Chip Capillary Electrochromatography with Conventional Stationary Phases. *Analytical Chemistry* **74**, 639-647, (2002).

- 53 http://www.agilent.com/cs/library/primers/Public/5990_3777EN.pdf.
- 54 Harris, D. C. & Lucy, C. A. *Quantitative chemical analysis*. Ninth edition. edn, (W. H Freeman & Company, 2015).
- 55 Jorgenson, J. W. & Lukacs, K. D. Zone electrophoresis in open-tubular glass capillaries. *Analytical Chemistry* **53**, 1298-1302, (1981).
- 56 Amikura, K. & Kiga, D. The number of amino acids in a genetic code. *RSC Advances* **3**, 12512-12517, (2013).
- 57 Reynolds, J. A. & Tanford, C. Binding of Dodecyl Sulfate to Proteins at High Binding Ratios. Possible Implications for the State of Proteins in Biological Membranes. *Proceedings of the National Academy of Sciences* **66**, 1002-1007 (1970).
- 58 Grabski, A. C. & Novagen, R. R. B. Preparation of protein samples for SDS-polyacrylamide gel electrophoresis: procedures and tips. (2010).
- 59 He, Y. & Yeung, E. S. Rapid Determination of Protein Molecular Weight by the Ferguson Method and Multiplexed Capillary Electrophoresis. *Journal of Proteome Research* **1**, 273-277, (2002).
- 60 Guo, X.-H. & Chen, S.-H. The structure and thermodynamics of protein—SDS complexes in solution and the mechanism of their transports in gel electrophoresis process. *Chemical Physics* **149**, 129-139, (1990).
- 61 Turro, N. J., Lei, X.-G., Ananthapadmanabhan, K. P. & Aronson, M. Spectroscopic Probe Analysis of Protein-Surfactant Interactions: The BSA/SDS System. *Langmuir* **11**, 2525-2533, (1995).
- 62 Patterson, J. P., Robin, M. P., Chassenieux, C., Colombani, O. & O'Reilly, R. K. The analysis of solution self-assembled polymeric nanomaterials. *Chemical Society Reviews* **43**, 2412-2425, (2014).
- 63 Wilkins, D. K. *et al.* Hydrodynamic Radii of Native and Denatured Proteins Measured by Pulse Field Gradient NMR Techniques. *Biochemistry* **38**, 16424-16431, (1999).

- 64 Narang, P., Bhushan, K., Bose, S. & Jayaram, B. A computational pathway for bracketing native-like structures for small alpha helical globular proteins. *Physical Chemistry Chemical Physics* **7**, 2364-2375, (2005).
- 65 Cohen, A. S. & Karger, B. L. SIXTH INTERNATIONAL SYMPOSIUM ON HIGH-PERFORMANCE LIQUIDHigh-performance sodium dodecyl sulfate polyacrylamide gel capillary electrophoresis of peptides and proteins. *Journal of Chromatography A* **397**, 409-417, (1987).
- 66 Schägger, H. & von Jagow, G. Tricine-sodium dodecyl sulfate-polyacrylamide gel electrophoresis for the separation of proteins in the range from 1 to 100 kDa. *Analytical Biochemistry* **166**, 368-379, (1987).
- 67 Weber, K. & Osborn, M. The reliability of molecular weight determinations by dodecyl sulfate-polyacrylamide gel electrophoresis. *Journal of Biological Chemistry* **244**, 4406-4412 (1969).
- 68 Hames, B. D. *Gel Electrophoresis of Proteins: A Practical Approach: A Practical Approach*. Vol. 197 (Oxford University Press, 1998).
- 69 Rodbard, D. & Chrambach, A. Estimation of molecular radius, free mobility, and valence using polyacrylamide gel electrophoresis. *Analytical biochemistry* **40**, 95-134 (1971).
- 70 Shi, Q. & Jackowski, G. One-dimensional polyacrylamide gel electrophoresis. *Gel electrophoresis of proteins: A practical approach, 3rd ed. Oxford University Press, Oxford*, 1-52 (1998).
- 71 Dunn, M. J. *Gel electrophoresis of proteins*. (Elsevier, 2014).
- 72 Shapiro, A. L., Viñuela, E. & V. Maizel Jr, J. Molecular weight estimation of polypeptide chains by electrophoresis in SDS-polyacrylamide gels. *Biochemical and Biophysical Research Communications* **28**, 815-820, (1967).
- 73 Plieva, F., Huiting, X., Galaev, I. Y., Bergenstahl, B. & Mattiasson, B. Macroporous elastic polyacrylamide gels prepared at subzero temperatures: control of porous structure. *Journal of Materials Chemistry* **16**, 4065-4073, (2006).

- 74 Guttman, A. & Nolan, J. Comparison of the Separation of Proteins by Sodium Dodecyl Sulfate-Slab Gel Electrophoresis and Capillary Sodium Dodecyl Sulfate-Gel Electrophoresis. *Analytical Biochemistry* **221**, 285-289, (1994).
- 75 Wu, D. & Regnier, F. E. Sodium dodecyl sulfate-capillary gel electrophoresis of proteins using non-cross-linked polyacrylamide. *Journal of Chromatography A* **608**, 349-356, (1992).
- 76 Shieh, P. C. H., Hoang, D., Guttman, A. & Cooke, N. Capillary sodium dodecyl sulfate gel electrophoresis of proteins I. Reproducibility and stability. *Journal of Chromatography A* **676**, 219-226, (1994).
- 77 Guttman, A. Capillary sodium dodecyl sulfate-gel electrophoresis of proteins. *ELECTROPHORESIS* **17**, 1333-1341, (1996).
- 78 Guttman, A. Effect of temperature on separation efficiency in capillary gel electrophoresis. *TrAC Trends in Analytical Chemistry* **15**, 194-198, (1996).
- 79 Manabe, T. Capillary electrophoresis of proteins for proteomic studies. *ELECTROPHORESIS* **20**, 3116-3121, (1999).
- 80 Schomburg, G., Lux, J. A. & Yin, H. F. (Google Patents, 1992).
- 81 Hu, S. *et al.* Capillary sodium dodecyl sulfate-DALT electrophoresis with laser-induced fluorescence detection for size-based analysis of proteins in human colon cancer cells. *ELECTROPHORESIS* **23**, 3136-3142, (2002).
- 82 Ganzler, K. *et al.* High-performance capillary electrophoresis of SDS-protein complexes using UV-transparent polymer networks. *Analytical Chemistry* **64**, 2665-2671, (1992).
- 83 Widhalm, A., Schwer, C., Blaas, D. & Kenndler, E. Capillary zone electrophoresis with a linear, non-cross-linked polyacrylamide gel: separation of proteins according to molecular mass. *Journal of Chromatography A* **549**, 446-451, (1991).
- 84 Fu, J., Mao, P. & Han, J. Artificial molecular sieves and filters: a new paradigm for biomolecule separation. *Trends in Biotechnology* **26**, 311-320, (2008).

- 85 Bezuidenhout, L. W., Nazemifard, N., Jemere, A. B., Harrison, D. J. & Brett, M. J. Microchannels filled with diverse micro- and nanostructures fabricated by glancing angle deposition. *Lab on a Chip* **11**, 1671-1678, (2011).
- 86 Vogel, N., Retsch, M., Fustin, C.-A., del Campo, A. & Jonas, U. Advances in Colloidal Assembly: The Design of Structure and Hierarchy in Two and Three Dimensions. *Chemical Reviews* **115**, 6265-6311, (2015).
- 87 Wang, W. & Gu, B. Self-Assembly of Two- and Three-Dimensional Particle Arrays by Manipulating the Hydrophobicity of Silica Nanospheres. *The Journal of Physical Chemistry B* **109**, 22175-22180, (2005).
- 88 Ogston, A. G. The spaces in a uniform random suspension of fibres. *Transactions of the Faraday Society* **54**, 1754-1757, (1958).
- 89 Morris, C. J. O. R. *Protides of the Biological Fluids* **14**, 543-561 (1966).
- 90 Rodbard, D. & Chrambach, A. Unified Theory for Gel Electrophoresis and Gel Filtration. *Proceedings of the National Academy of Sciences* **65**, 970-977 (1970).
- 91 Guttman, A. On the separation mechanism of capillary sodium dodecyl sulfate-gel electrophoresis of proteins. *ELECTROPHORESIS* **16**, 611-616, (1995).
- 92 Giddings, J. C., Kucera, E., Russell, C. P. & Myers, M. N. Statistical theory for the equilibrium distribution of rigid molecules in inert porous networks. Exclusion chromatography. *The Journal of Physical Chemistry* **72**, 4397-4408, (1968).
- 93 Nazemifard, N. *et al.* A systematic evaluation of the role of crystalline order in nanoporous materials on DNA separation. *Lab on a Chip* **12**, 146-152, (2012).
- 94 Righetti, P. G. & Candiano, G. Recent advances in electrophoretic techniques for the characterization of protein biomolecules: A poker of aces. *Journal of Chromatography A* **1218**, 8727-8737, (2011).
- 95 Ben-Moshe, M., Alexeev, V. L. & Asher, S. A. Fast Responsive Crystalline Colloidal Array Photonic Crystal Glucose Sensors. *Analytical Chemistry* **78**, 5149-5157, (2006).

- 96 Vlasov, Y. A., Bo, X.-Z., Sturm, J. C. & Norris, D. J. On-chip natural assembly of silicon photonic bandgap crystals. *Nature* **414**, 289-293 (2001).
- 97 Kim, S.-H., Lee, S. Y., Yang, S.-M. & Yi, G.-R. Self-assembled colloidal structures for photonics. *NPG Asia Mater* **3**, 25-33 (2011).
- 98 Xia, Y., Gates, B., Yin, Y. & Lu, Y. Monodispersed Colloidal Spheres: Old Materials with New Applications. *Advanced Materials* **12**, 693-713, (2000).
- 99 Mezzenga, R. *et al.* Templating Organic Semiconductors via Self-Assembly of Polymer Colloids. *Science* **299**, 1872-1874, (2003).
- 100 Hua, Y., Koshel, B. M. & Wirth, M. J. Field-Free Remobilization of Proteins after Isoelectric Focusing in Packed Capillaries. *Analytical Chemistry* **82**, 8910-8915, (2010).
- 101 Jemere, A. B., Oleschuk, R. D., Ouchen, F., Fajuyigbe, F. & Harrison, D. J. An integrated solid-phase extraction system for sub-pico (2002).
- 102 Jemere, A. B., Oleschuk, R. D. & Harrison, D. J. Microchip-based capillary electrochromatography using packed beds. *ELECTROPHORESIS* **24**, 3018-3025, (2003).
- 103 Zeng, Y., He, M. & Harrison, D. J. Microfluidic Self-Patterning of Large-Scale Crystalline Nanoarrays for High-Throughput Continuous DNA Fractionation. *Angewandte Chemie International Edition* **47**, 6388-6391, (2008).
- 104 Nykypanchuk, D., Strey, H. H. & Hoagland, D. A. Brownian Motion of DNA Confined Within a Two-Dimensional Array. *Science* **297**, 987-990, (2002).
- 105 Zheng, S., Ross, E., Legg, M. A. & Wirth, M. J. High-Speed Electro-separations Inside Silica Colloidal Crystals. *Journal of the American Chemical Society* **128**, 9016-9017, (2006).
- 106 Westerhuis, W. H. J., Sturgis, J. N. & Niederman, R. A. Reevaluation of the Electrophoretic Migration Behavior of Soluble Globular Proteins in the Native and Detergent-Denatured States in Polyacrylamide Gels. *Analytical Biochemistry* **284**, 143-152, (2000).

- 107 Oliver, G., Simpson, C., Kerby, M. B., Tripathi, A. & Chauhan, A. Electrophoretic migration of proteins in semidilute polymer solutions. *ELECTROPHORESIS* **29**, 1152-1163, (2008).
- 108 Ocvirk, G., Tang, T. & Jed Harrison, D. Optimization of confocal epifluorescence microscopy for microchip-based miniaturized total analysis systems. *Analyst* **123**, 1429-1434, (1998).
- 109 Dufresne, E. R. *et al.* Flow and Fracture in Drying Nanoparticle Suspensions. *Physical Review Letters* **91**, 224501 (2003).
- 110 Dufresne, E. R. *et al.* Dynamics of Fracture in Drying Suspensions. *Langmuir* **22**, 7144-7147, (2006).
- 111 Ferguson, K. A. Starch-gel electrophoresis; Application to the classification of pituitary proteins and polypeptides. *Metabolism - Clinical and Experimental* **13**, 985-1002, (1958)
- 112 Yates, J. R., Ruse, C. I. & Nakorchevsky, A. Proteomics by Mass Spectrometry: Approaches, Advances, and Applications. *Annual Review of Biomedical Engineering* **11**, 49-79, (2009).
- 113 Billen, J. & Desmet, G. Understanding and design of existing and future chromatographic support formats. *Journal of Chromatography A* **1168**, 73-99, (2007).
- 114 Park, J. *et al.* Fully Packed Capillary Electrochromatographic Microchip with Self-Assembly Colloidal Silica Beads. *Analytical Chemistry* **79**, 3214-3219, (2007).
- 115 Behnke, B., Grom, E. & Bayer, E. Evaluation of the parameters determining the performance of electrochromatography in packed capillary columns. *Journal of Chromatography A* **716**, 207-213, (1995).
- 116 Kim, J. Y., Cho, K., Ryu, S.-a., Kim, S. Y. & Weon, B. M. Crack formation and prevention in colloidal drops. *Scientific Reports* **5**, 13166, (2015).
- 117 Zhang, Y., Qian, Y., Liu, Z., Li, Z. & Zang, D. Surface wrinkling and cracking dynamics in the drying of colloidal droplets. *Eur. Phys. J. E* **37**, 84 (2014).

- 118 Boulogne, F., Pauchard, L. & Giorgiutti-Dauphiné, F. Annular cracks in thin films of nanoparticle suspensions drying on a fiber. *EPL (Europhysics Letters)* **102**, 39002 (2013).
- 119 Jing, G. & Ma, J. Formation of Circular Crack Pattern in Deposition Self-Assembled by Drying Nanoparticle Suspension. *The Journal of Physical Chemistry B* **116**, 6225-6231, (2012).
- 120 Ma, H. *et al.* Radially aligned microchannels prepared from ordered arrays of cracks on colloidal films. *Physical Chemistry Chemical Physics* **15**, 9808-9811, (2013).
- 121 Singh, K. B. & Tirumkudulu, M. S. Cracking in Drying Colloidal Films. *Physical Review Letters* **98**, 218302 (2007).
- 122 Teh, L. K., Tan, N. K., Wong, C. C. & Li, S. Growth imperfections in three-dimensional colloidal self-assembly. *Appl. Phys. A* **81**, 1399-1404, (2005).
- 123 Koh, Y. K., Teh, L. & Wong, C. C. Defects in self assembled colloidal crystals. (2005).
- 124 O'Mahony, C. T., Holmes, J. D., Morris, M. A., Farrell, R. A. & Goshal, T. *The thermodynamics of defect formation in self-assembled systems*. (INTECH Open Access Publisher, 2011).
- 125 Wong, S., Kitaev, V. & Ozin, G. A. Colloidal Crystal Films: Advances in Universality and Perfection. *Journal of the American Chemical Society* **125**, 15589-15598, (2003).
- 126 Manoharan, V. N. Colloidal matter: Packing, geometry, and entropy. *Science* **349**, (2015).
- 127 Woodcock, L. V. Entropy difference between the face-centred cubic and hexagonal close-packed crystal structures. *Nature* **385**, 141-143 (1997).
- 128 Ye, Y.-H., LeBlanc, F., Haché, A. & Truong, V.-V. Self-assembling three-dimensional colloidal photonic crystal structure with high crystalline quality. *Applied Physics Letters* **78**, 52-54, (2001).

- 129 Bruce, A. D., Wilding, N. B. & Ackland, G. J. Free Energy of Crystalline Solids: A Lattice-Switch Monte Carlo Method. *Physical Review Letters* **79**, 3002-3005 (1997).
- 130 Dux, C. & Versmold, H. Light Diffraction from Shear Ordered Colloidal Dispersions. *Physical Review Letters* **78**, 1811-1814 (1997).
- 131 Pusey, P. N. *et al.* Structure of crystals of hard colloidal spheres. *Physical Review Letters* **63**, 2753-2756 (1989).
- 132 Seiler, K., Fan, Z. H., Fluri, K. & Harrison, D. J. Electroosmotic Pumping and Valveless Control of Fluid Flow within a Manifold of Capillaries on a Glass Chip. *Analytical Chemistry* **66**, 3485-3491, (1994).
- 133 Manz, A. *et al.* Planar chips technology for miniaturization and integration of separation techniques into monitoring systems: Capillary electrophoresis on a chip. *Journal of Chromatography A* **593**, 253-258, (1992).
- 134 Bevan, M. A., Lewis, J. A., Braun, P. V. & Wiltzius, P. Structural Evolution of Colloidal Crystals with Increasing Ionic Strength. *Langmuir* **20**, 7045-7052, (2004).
- 135 Halperin, B. I. & Nelson, D. R. Theory of Two-Dimensional Melting. *Physical Review Letters* **41**, 121-124 (1978).
- 136 <http://rsb.info.nih.gov/ij/>.
- 137 Li, Q., Jonas, U., Zhao, X. S. & Kappl, M. The forces at work in colloidal self-assembly: a review on fundamental interactions between colloidal particles. *Asia-Pacific Journal of Chemical Engineering* **3**, 255-268, (2008).
- 138 Norris, D. J., Arlinghaus, E. G., Meng, L., Heiny, R. & Scriven, L. E. Opaline Photonic Crystals: How Does Self-Assembly Work? *Advanced Materials* **16**, 1393-1399, (2004).
- 139 Ericson, C., Holm, J., Ericson, T. & Hjertén, S. Electroosmosis- and Pressure-Driven Chromatography in Chips Using Continuous Beds. *Analytical Chemistry* **72**, 81-87, (2000).

- 140 Rogers, B. J. & Wirth, M. J. Obstructed Diffusion in Silica Colloidal Crystals. *The Journal of Physical Chemistry A* **117**, 6244-6249, (2013).
- 141 Zareh, Shannon K., DeSantis, Michael C., Kessler, Jonathan M., Li, J.-L. & Wang, Y. M. Single-Image Diffusion Coefficient Measurements of Proteins in Free Solution. *Biophysical Journal* **102**, 1685-1691, (2012).
- 142 Nagata, H., Tabuchi, M., Hirano, K. & Baba, Y. High-speed separation of proteins by microchip electrophoresis using a polyethylene glycol-coated plastic chip with a sodium dodecyl sulfate-linear polyacrylamide solution. *ELECTROPHORESIS* **26**, 2687-2691, (2005).
- 143 Buckley, A. M. & Greenblatt, M. The Sol-Gel Preparation of Silica Gels. *Journal of Chemical Education* **71**, 599, (1994).
- 144 Neville, F., Mohd. Zin, A., Jameson, G. J. & Wanless, E. J. Preparation and Characterization of Colloidal Silica Particles under Mild Conditions. *Journal of Chemical Education* **89**, 940-942, (2012).
- 145 Lin, Q.-H. *et al.* High-speed separation of proteins by sodium dodecyl sulfate-capillary gel electrophoresis with partial translational spontaneous sample injection. *ELECTROPHORESIS* **32**, 2898-2903, (2011).
- 146 Birdsall, R. E., Koshel, B. M., Hua, Y., Ratnayaka, S. N. & Wirth, M. J. Modeling of protein electrophoresis in silica colloidal crystals having brush layers of polyacrylamide. *ELECTROPHORESIS* **34**, 753-760, (2013).
- 147 Felten, C. & Solano, O. S. Capillary Electrophoresis in Quality Control: PART I: Application for Therapeutic Proteins. *Beckman Coulter*, 1-8 (2010).
- 148 Zhang, J., Burman, S., Gunturi, S. & Foley, J. P. Method development and validation of capillary sodium dodecyl sulfate gel electrophoresis for the characterization of a monoclonal antibody. *Journal of Pharmaceutical and Biomedical Analysis* **53**, 1236-1243, (2010).

- 149 Tamizi, E. & Jouyban, A. The potential of the capillary electrophoresis techniques for quality control of biopharmaceuticals—A review. *ELECTROPHORESIS* **36**, 831-858, (2015).